RADIAL PROFILE STUDIES IN METAL VAPOUR LASER DISCHARGES

Alan L. McKenzie

A Thesis Submitted for the Degree of PhD
at the
University of St Andrews

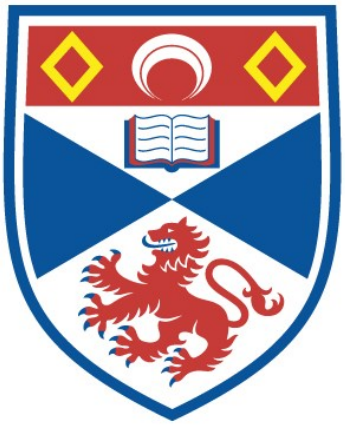

1976

Abstract from

Radial profile studies in metal vapour laser discharges

A thesis presented by

A. L. McKenzie, B.Sc

to the University of St. Andrews
in application for the degree
of Doctor of Philosophy

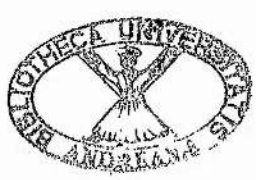

Positive-column metal-vapour lasers are important because of the many visible and ultra-violet c.w. wavelengths attainable. In many such systems population inversion among the metal ion states is produced in charge-exchange reactions with helium ions. Although the power of such lasers should apparently increase linearly with the helium ion density and, hence, with the discharge current, several observers have noted a power saturation. This work describes a phenomenon which will account for this.

The spontaneous emission from laser states in a helium-selenium discharge is observed across the tube, and the radial profiles of intensity show a central dip which deepens with discharge current and helium pressure. This axial depletion of laser states sets a limit to the achievable power. The dip effect is shown to be due to the removal of metal atoms from the centre of the tube by ionisation followed by a build-up of the vapour at the walls where the metal is neutralised. States excited from the axially reduced neutral population will reflect the depletion to some extent in their own distribution.

The helium-cadmium discharge is selected as representative of metal-vapour systems for further study using the dip effect. By comparing the radial profiles of different excited states under the same discharge conditions, it is shown that electron collisions probably contribute to the excitation of levels which are normally assumed to result from charge-exchange and Penning collisions. Radial profiles of helium and cadmium metastables are examined. The behaviour of the helium profiles at high cadmium partial pressures is consistent with an electron temperature which depends upon the local cadmium concentration. The shape of the cadmium metastable profile indicates that this species is being destroyed in the discharge - either by electron collision or collisional mixing with the cadmium neutral resonance state.

Observations of cadmium ion profiles at various cadmium partial pressures indicate that electron collisions are the principal source of cadmium ionisation. From the magnitude of the radial dip, the ionisation rate constant is calculated ($1 - 5 \times 10^{-8}$ cm^3 s^{-1}). This varies with E/N, the reduced axial electric field. The ionisation rate is found another way, by modulating the discharge current and observing the phase lag of the profile dip. This experiment yields a value similar to the above.

RADIAL PROFILE STUDIES IN METAL VAPOUR LASER DISCHARGES

A THESIS

PRESENTED BY

A. L. McKENZIE, B.Sc.,

TO THE

UNIVERSITY OF ST. ANDREWS

IN APPLICATION FOR THE DEGREE OF

DOCTOR OF PHILOSOPHY

DECLARATION

I hereby certify that this thesis has been composed by me, and is a record of work done by me, and has not previously been presented for a Higher Degree.

This research was carried out in the School of Physical Sciences, in the University of St. Andrews under the supervision of Dr. M. H. Dunn and Dr. A. Maitland.

A. L. McKenzie

CERTIFICATE

We certify that Alan L. McKenzie, B.Sc., has spent nine terms at research work in the School of Physical Sciences, in the University of St. Andrews, under our direction, that he has fulfilled the conditions of the Resolution of the University Court, 1967, No. 1, and that he is qualified to submit the accompanying thesis in application for the degree of Doctor of Philosophy.

M.H. Dunn

A. Maitland

CAREER

A.L. McKenzie began school in Nicosia, Cyprus and completed his secondary education in Peterhead Academy, Aberdeenshire. He was awarded a bursary to study for the degree of B.Sc. at Aberdeen University and graduated with first class honours in June 1972. Since October 1972 he has been a Carnegie Scholar at the University of St. Andrews.

ACKNOWLEDGEMENTS

I am grateful to Dr. M. H. Dunn for many lively and useful discussions about metal vapour laser discharges and to Dr. A. Maitland for his interest and encouragement and to them both for their advice to put pen to paper at a sufficiently early stage in my work. I am indebted to Mr. F. Akerboom for his skill and patience in constructing for me the laser discharge tubes necessary for my experiments. I thank the Carnegie Trust for the Universities of Scotland for financial support during this work and Mrs. Catherine Evans-Smith for typing the manuscript. Finally I thank Rosie, my wife, for sharing me with the Physics Department for the past three years.

ABSTRACT

Radial profiles have been measured of emission from upper laser levels in the positive columns of He-Se and He-Cd discharges. In both systems the lasing states show an axial depletion which is aggravated at higher currents and pressures.

The process responsible for this effect - diffusion of metal vapour from the discharge tube walls to replace atoms lost by ionisation - should be a feature common to all such metal-vapour lasers.

The He-Cd discharge is selected as representative of such systems for a more detailed study of the radial profiles of some of the states, including the helium and cadmium metastable states and the cadmium ion ground and excited states. From the radial profiles and cross-section calculations it is apparent that some states, pumped by cascade from levels excited by charge-exchange and Penning reactions with helium ions and metastable atoms respectively, are also excited, in part, from the metal ion ground state by electron collision. About a third of the pumping of the 4f states is shown to arise from such a process.

The cadmium ionisation rate constant is deduced by two separate techniques. The first involves observing the dip behaviour with varying discharge conditions and the other uses current modulation of the discharge to determine how quickly, in effect, the neutral cadmium can diffuse inwards from the tube walls.

The principal cadmium ionisation mechanism seems to be electron ionisation from the neutral ground and metastable states, rather than by Penning or charge-transfer collisions, with an ionisation rate constant of $1 - 5 \times 10^{-8}$ cm^3 s^{-1}. The phase behaviour of the signals from excited states in the current - modulated discharge is also explained in terms of the excitation mechanisms of the states.

The significance of the dip phenomenon is that the power output of positive column metal vapour lasers may not be raised indefinitely by increasing the discharge current, even if the laser levels are pumped by Penning or charge-transfer reactions.

TABLE OF CONTENTS

CHAPTER I

INTRODUCTION

Since the first demonstration of c.w. laser light in a helium-cadmium discharge in 1968 [1] much effort has been directed towards the development of positive-column metal-vapour lasers. This work describes a power-limiting effect in which there is a depletion of the lasing species along the axis of the laser tube. This is shown to be a property of the discharge configuration of such lasers.

In these devices the active medium is the positive column of a discharge in a binary mixture of a buffer gas, such as helium or neon at several Torr, and a metal vapour at a partial pressure of a few milli-Torr. Among the attractions of these systems are the many visible and ultra-violet laser wavelengths attainable, and the simplicity of the design and construction of the discharge tubes. Output powers of the order of tens of milliwatts are typical.

Most metal-vapour lasers today follow the design proposed independently by Sosnowski [2] and Goldsborough [3] in 1969. Their idea was to introduce the metal vapour into the anode end of the positive column, the process of cataphoresis [4] then driving it along the tube towards the cathode, so building up a reasonably uniform vapour concentration.

Excited laser levels of the metal ions are generally populated by one of two mechanisms, Penning ionisation or charge-exchange. For example, in the He-Cd [1], He-Sn [5], He-Zn [5] and

He-Mg [6] systems, excited states arise from the Penning ionisation process,

$$X^* + M_g \rightarrow (M^+)^* + X_g + e^- + \Delta E$$

Here X and M are the buffer gas and metal vapour atoms. The subscript g denotes the ground state, the asterisk * represents an excited state (often a metastable level in the case of the buffer gas) and ΔE is the excess kinetic energy of the reaction.

Alternatively the laser levels may be excited by charge exchange with, for example, helium ions as in the He-Se [7], He-Zn [8] and He-Hg [9] systems:

$$(X^+)_g + M_g \rightarrow X_g + (M^+)^* + \Delta E$$

(This reaction may be referred to as a Duffendack reaction following Green and Webb [10].)

In the Penning-excited lasers it is not expected that powers will increase monotonically with discharge current - for example, in the He-Cd system the observations of Browne and Dunn [11] have shown that the helium metastable populations (and, hence, the laser-level pumping rate) saturate with increasing current. (The term "saturation" is used throughout this work to indicate that a quantity ceases to be explicitly dependent on a given parameter, such as current in this case.) On the other hand, in the case of Duffendack-pumped lasers, since the helium ion density increases with current, the power output should rise with current.

This latter behaviour was not observed either in the He-Hg [9] or in the He-Se system [7].

We have observed a power saturation with respect to current and a sub-linear current dependence of the sidelight emission in a He-Se laser. These effects were also noted by Klein and Silfvast [12] and were attributed by them to cataphoretic sweep-out of the selenium vapour and suppression of the helium ion population by increased fractional ionisation of the metal atom population. However, using a He-Se laser, we found that power was not fully restored by increasing the oven temperature, the remedy suggested by the cataphoresis argument, and the sublinearity with current of the upper laser level sidelight emission persisted even at very low selenium partial pressures, which suggests that competition of selenium ions with helium ions does not completely explain the noted behaviour.

In an attempt to examine more fully the power saturation, we have examined the radial distributions of the upper laser level ions in two helium-metal-vapour discharges.

Chapter II describes observations of an axial dip in the upper-laser-level profiles in a He-Se discharge and proposes a model to explain this power limiting phenomenon. The profile dip of the laser states is due to a dip in the metal neutral ground-state density. This arises from the relatively high ionisation rate of the metal in the discharge : to balance the loss of neutral atoms in the centre

of the tube, metal atoms must flow inwards from the walls down a diffusion gradient. The metal atom population is replenished at the walls by the recombination of metal ions which have drifted to the wall under the influence of the radial electric field. The dip should be a feature of any metal - rare-gas discharge where the metal ionisation potential is far enough below that of the rare gas to provide a sufficiently high metal ionisation rate.

The subsequent chapters deal in greater detail with the study of the spatial population distributions in a He-Cd discharge. This system was selected because it is well documented and because a comparison is afforded between states excited by the two different pumping mechanisms. The general features of the system are common to all positive-column metal-vapour lasers.

Using emission and absorption techniques, radial profiles are obtained of excited cadmium ion states, cadmium metastable and ion ground states and helium metastable states. From the different degrees to which the various cadmium states are dipped under similar discharge conditions, the nature of the different pumping mechanisms is investigated. An important result is that, apart from cascade from Duffendack or Penning-pumped levels, many of the excited ion states are pumped by electron excitation from the cadmium ion ground state.

From the behaviour of the dip with cadmium partial pressure it is shown in Chapter V that cadmium is ionised principally by electron processes, rather than by Duffendack or Penning reactions. From a detailed study of the dip behaviour at 6360Å with changing discharge

parameters, the ionisation rate constant is found in Chapter VI to be typically $1 - 5 \times 10^{-8}$ cm^3 s^{-1}.

Chapter VII describes an experiment in which the discharge current is modulated and the phase of excited cadmium ion states on the axis is compared with the current phase. Cadmium which is driven to the wall in a high-current half of a cycle has less time to diffuse back to the centre in the low current half as the modulation frequency is increased, which introduces a phase shift between the cadmium signal and the current. The observed behaviour of different cadmium lines is explained in terms of the different pumping mechanisms. From the phase behaviour of the 5378Å signal the above ionisation rate is confirmed to within a factor of 2.

Appendix I lists a computer program to evaluate the instrumental distortion of the radial profiles observed with the optics described in Chapter III. Appendices II - V describe the computation of the absorption curves required in Chapter III, and Appendix VI gives an example of a calculation to find the fractional contribution to the 5378Å transition of pumping by electron excitation from the cadmium ion ground state. Finally, Appendix VII explains the computer program used to predict the behaviour of the cadmium states in the current-modulation experiments.

CHAPTER II

RADIAL PROFILES OF EMISSION IN A HELIUM-SELENIUM DISCHARGE

Abstract

A dip has been observed in the radial profiles of upper-laser-level emission in a He - Se discharge. Possible complications in interpreting the profiles are discussed. A model to explain the dip phenomenon is proposed. It is shown by a physical argument and by comparison with the case of a flat ionisation profile that the dip is not strongly dependent on the detailed shape of the electron density distribution.

2.1 Introduction

This chapter describes the investigation of the radial distribution of upper-laser-level populations in a helium-selenium laser discharge. The population densities are determined by emission spectroscopy, the densities at any point being taken as proportional to the light emitted from the states in question at that point [13]. A model is proposed which explains the observed axial depletion of the metal ion species.

2.2 Apparatus and Experiment

Experience of typical lasing conditions was gained through the use of the laser mentioned in Chapter I. This had an active medium of length 50 cm and diameter 2.4mm. An optimum power of 15 mW for 6 lines was achieved using mirrors coated for 98% reflectivity at 5000 Å. The system lased at currents above 100 mA with an oven temperature of 150°C at helium pressures of between 5 and 20 Torr.

In order to examine the radial profiles under these conditions a 5mm bore quartz capillary discharge tube of active length 10 cm was built with a tungsten rod anode and a 3cm diameter, 15cm long cylindrical aluminium cathode. A quartz side-arm containing selenium pellets (5N purity) was heated by passing current through "Nichrome" ribbon wire wound around it and the temperature was stabilised to $\pm 1C^{O}$ by an Ether "Digi" temperature controller. The fused silica end-windows of the discharge tube were seated on rubber "O" rings on stainless steel mounts and held in place by atmospheric pressure so that they could be removed and cleaned when necessary.

The filling pressure of the helium (4N5 purity) was monitored with a Wallace and Tiernan capsule gauge which had been calibrated against a McLeod gauge. A 10kV, 1A smoothed power supply provided the discharge current.

The end-light from the capillary discharge was focused by a UV achromatic lens in the plane of a 35μm diameter pinhole set at the entrance slit of a prism monochromator (Carl Zeiss SPM2). Scanning was effected by moving the lens with a micrometer screw perpendicularly to the tube axis, so tracking the image across the pinhole (see Fig. 2.1).

The output of the monochromator was detected by a photo-multiplier (either EMI type 9594 QUB or type 9558 QB) which was operated so that its response was linear to within 5%.

The apparatus was aligned at first coarsely with a He-Ne laser and then finely with a collimating telescope with a focal range from zero to infinity. The optical parameters of the lens focal length (150mm) , lens diaphragm width (1.5mm) and pinhole diameter were chosen so that the radius of the field of view in the discharge determined by ray optics was about the same size as the radius of the Airy disc in the discharge. The pinhole was conjugate with an image of 76μm radius in the near-end of the discharge (see Fig. 2.2). Light is accepted from a circle of 180μm radius at the far end of the capillary tube. Moving the lens off-centre when scanning inclines the axis of the acceptance cone to the tube axis introducing a parallax of up to 280μm in the discharge. Thus any point in the radial profile receives contributions to the signal from other points up to (180 + 230/2)μm = 300μm distant. Since the Airy disc radius in the discharge is 320μm it may be seen that 300μm represents the lower limit to the effective field of view of the system. A 50μm illuminated slit situated in the discharge space produced a profile with a half-width equivalent to less than 350μm in agreement with the above calculation.

2.3 Results

Radial profiles were taken of the emission from the upper levels of the six strongest selenium laser transitions [7] which

are pumped by Duffendack reactions with helium ions [7, 12, 17] at 5305Å ($5p\ ^2D_{3/2} \rightarrow 5s\ ^2P_{1/2}$), 5227Å ($5p\ ^4D_{7/2} \rightarrow 5s\ ^4P_{5/2}$), 5176Å ($5p\ ^4D_{5/2} \rightarrow 5s\ ^4P_{3/2}$), 5069Å ($5p\ ^4P_{5/2} \rightarrow 5s\ ^4P_{5/2}$), 4993Å ($5p\ ^4P_{3/2} \rightarrow 5s\ ^4P_{3/2}$) and 4976Å ($5p\ ^2D_{5/2} \rightarrow 4s\ 4p^4\ ^2P_{3/2}$). The filling pressures of helium ranged from 2 Torr to 20 Torr, discharge currents of up to 600 mA were used and the sidearm temperature was set at 150°C which had been found appropriate to optimum lasing conditions for the 50cm laser (see Section 2.2).

For helium pressures above about 6 Torr a significant central dip appears in the radial profiles. The ratio of the maximum intensity to the axial intensity for 5227Å emission is presented in graphical form in Figs. 2.3 and 2.4 and complete profiles for some discharge conditions appear in Figs. 2.5 and 2.6. Since the intensity of the selenium lines exhibited a long-term drift after a change of current (caused, perhaps by a combination of the wall-temperature change and the change in the cataphoretic sweep-out rate of ions down the tube) it is not useful to compare absolute intensities and so the profiles have been normalised at the centre to facilitate comparison of the dip. The symmetry of the profiles showed the system was well aligned. The "kink" on the right side of the profiles is attributed to reflection from the tube walls. The corresponding reflection from the opposite wall is obscured by a slight constriction at the end of the capillary tube.

From the graphs it may be seen that, at constant current, the dip deepens with increasing pressure and at constant pressure it deepens with increasing current. All six lines investigated showed a similar behaviour.

2.4 Possible Complications in Profile Interpretation

We wish to be able to say that the emission at any point across the profile is proportional to the pumping rate at that point. No detectable distortion of the profiles should occur due to gain on the transition as this will be only 10% per metre [7]. The contribution to the observed profiles of the light from the end-stubs of the discharge tube is very small, the stubs totalling only 10% of the capillary discharge length and being 16 times greater in cross-sectional area. Also, the metal ion profile may be expected to be very low and flat in the centre of a wide discharge tube. The signal detected by scanning outside the capillary diameter was only a few percent of the average signal inside the capillary. Distortion of the capillary discharge profiles is therefore considered negligible within the errors of the experiment.

No complication is introduced by the motion of the ions in the radial electric field. Taking an electron mean-free-path of 0.05mm and an electron temperature of 4eV the potential difference between the axis and the wall sheath is about 14V [16] which sets an upper limit to the average ion radial velocity of 3×10^{5} cm s^{-1}. Thus, in a typical lifetime of 10^{-8} s the ion travels only 1% of the tube radius.

In view of the high radiative loss-rate reported by Ferrario [15], it is assumed that electron collisional destruction of the laser states is negligible. This assumption is consistent with the observations of Green & Webb [75] for cadmium states of similar lifetimes.

2.5 Discussion

It was proposed by Silfvast and Klein [7, 12] and confirmed by Turner-Smith, Green and Webb [17] that the upper laser levels of selenium are pumped by charge-transfer collisions with helium ions. Turner-Smith [18] points out that some selenium laser levels may be excited as a result of three-body collisions with a neutral helium atom as the third body. However, as the helium atom concentration must be uniform across the tube apart from a slight depletion at the centre due to heating caused by elastic collisions with electrons, the pumping rate of the upper laser levels may be written

$$\text{Pump rate} \sim N_{He+} N_{Se}$$

where N_{He+} and N_{Se} are the concentrations of helium ions and selenium atoms respectively. Assuming that the selenium is ionised by charge-exchange and electron collision then the ionisation rate is given by

$$\text{Ionisation Rate} = N_{Se} N_{He+} \langle \sigma_+ C_+ \rangle + N_{Se} N_e \langle \sigma_e C_e \rangle$$

where N_e and N_{He+} are the electron and helium ion density, σ_+ and σ_e are the cross-sections for charge-transfer and electron collisional ionisation and C_+, C_e are the appropriate relative velocities. Assuming that the helium ion density and electron density are equal, this becomes

$$\text{Ionisation Rate} = N_e N_{Se} f$$

where

$$f = \langle \sigma_+ C_+ \rangle + \langle \sigma_e C_e \rangle$$

If there is no volume recombination (see section 4.2.4), the diffusion rate of selenium atoms towards any point in the discharge will be balanced solely by their rate of loss by ionisation. It is assumed, following section 4.3.7, that conditions for ambipolar diffusion hold. Thus we have

$$\frac{\partial N_{Se}}{\partial t} = - \nabla . J - N_e N_{Se} f$$

where the vector J is the selenium particle current density given by

$$J = - D \nabla N_{Se}$$

with D as the diffusion coefficient of selenium atoms in helium. Thus, in steady state,

$$D \nabla^2 N_{Se} - N_e N_{Se} f = 0 \qquad (2.1)$$

Since the selenium sidelight intensity is approximately constant along the length of the tube only the radial variation of the vapour density need be considered. Thus we have

$$\frac{d^2 N_{Se}}{dr^2} + \frac{1}{r} \frac{d N_{Se}}{dr} - \frac{N_{Se} N_e f}{D} = 0 \qquad (2.2)$$

Following Schottky [4], with an ambipolar-diffusion-controlled discharge, N_e is described by a zero-order Bessel function with the first zero at r = R (the tube radius). Hence, expanding the Bessel function, we have

$$N_e = N_{eo}\left(1 - \frac{\frac{1}{4}(2.4\,\frac{r}{R})^2}{(1!)^2} + \frac{\frac{1}{16}(2.4\,\frac{r}{R})^4}{(2!)^2} - \ldots\right)$$

where N_{eo} is the axial electron density. With this substitution the series solution of equation (2.2) is

$$N_{Se} = N_{Seo}\,(1 + \frac{\alpha}{4}\,\frac{r^2}{R^2} + \frac{1}{16}\,(\frac{\alpha^2}{4} - 1.44\alpha)\,\frac{r^4}{R^4} + \ldots) \qquad (2.3)$$

where N_{Seo} is the axial selenium neutral concentration and α is given by

$$\alpha = (N_{eo}\, f\, R^2)D^{-1} \qquad (2.4)$$

Thus the model predicts that the selenium vapour concentration increases monotonically outwards from the axis.

Now it is important in later discussion that the magnitude of the dip in the neutral population can be assumed fairly insensitive to the detailed shape of the electron density profile. That this is so may be made physically plausible by the following argument. The destruction term in equation (2.1) which describes the destruction of neutrals is $N_e f$. This term may be thought of as comprising a neutral destruction term ϕ_1 which has a flat profile and a neutral creation term ϕ_2 which is zero at the axis but rises towards the walls. In this way we may construct any ionisation function (regarded as destruction of neutrals) which decreases towards the walls, including a zero-order Bessel function. It will now be shown that the dip resulting from the flat-profile part of the ionisation is not seriously modified by the competing neutral creation process.

Assume for the moment that the neutral ground state selenium profile has been dipped by the process ϕ_1 and is described by a

constant term plus a term varying as r^2. (In general there will also be a dependence on higher order powers but the essence of the argument is unchanged by truncating the series). Now if $N_e f$ is a parabolic function decreasing to zero at the walls, then ϕ_2 varies as r^2. For large dips in the selenium density profile the constant term in the series expansion for the selenium profile may be neglected as a first approximation and so the total creation rate, $\phi_2 N_{Se}$, will be proportional to r^4. Hence most of the selenium "created" by ϕ_2 appears near the tube walls - for an r^4 dependence half of the selenium is produced within 0.1 R of the tube walls. Even if the selenium profile has such a small dip that its radial dependence is entirely neglected, half of the metal vapour comes from within 0.15R of the walls. There is no source term in equation (2.1) as this is implicit in the solution - the source of the metal vapour is at the tube walls. The boundary conditions affect the total amount of metal vapour in the system, but not the profile shape. Thus, inasmuch as the creation term ϕ_2 merely increases the flux of metal atoms from around the wall, the shape of the profile is unchanged from that established by ϕ_1.

While the foregoing argument merits closer treatment of the higher powers of r in the ionisation process, this second-order argument shows that deviation from a flat-profile ionisation process does not greatly distort the metal vapour profiles, justifying the claim that the dip is fairly independent of the detailed shape of the electron density profiles.

It is interesting to compare equation (2.3) with the solution to equation (2.2) derived for a flat ionisation profile. Equation (2.2) becomes

$$r^2 \frac{d^2 N_{Se}}{dr^2} + r \frac{dN_{Se}}{dr} - r^2 \frac{N_{Se} N_{eo} f}{D} = 0$$

The solution is a modified Bessel function:

$$N_{Se} = N_{Seo} \, I_o \left(\frac{r}{R} \sqrt{\alpha}\right)$$

which may be expanded:

$$N_{Se} = N_{Seo} \left(1 + \frac{1}{4} \alpha \frac{r^2}{R^2} + \frac{1}{64} \alpha^2 \frac{r^4}{R^4} + \ldots\right)$$

This differs from (2.3) only in small terms of the fourth order upwards.

The profiles of upper-laser-level emission will be less dipped than those of the neutral ground state density because the pumping species, helium ions, is less concentrated at the walls than at the axis. However, multiplication of the zero-order Bessel function assumed to describe the helium ion density (if the selenium ion density is small in comparison) by the expression for the ground-state dip described by (2.3) shows the dip will still be evident at high enough values of α.

To calculate a typical value of α, equation (2.4) is used. We will assume here that only electron ionisation contributes to f. At a current of 400mA and a helium pressure of 10 Torr the axial electron density is taken to be $10^{13} cm^{-3}$ and the energy-averaged cross section for the electron ionisation of selenium is taken to be $10^{-16} cm^2$. With an electron random velocity of $10^8 cm\ s^{-1}$ and a

diffusion coefficient of 300 $cm^2 s^{-1}$ (see, for example, Table 6.1), α is about 20 which means the ratio of the intensity of emission from excited states observed at 0.7R divided by the axial intensity is about 2. This is of the order of the size of dip observed (see Fig. 2.5 or Fig. 2.6).

From the model the "hole" will be deeper at larger values of N_e, corresponding to greater discharge currents, and at smaller D corresponding to greater pressures. Thus the model predicts the observations both in magnitude and in dependence on discharge parameters.

There are limitations to this simple model. An increase in the metal atom concentration at the sides of the tube will lower the electron temperature so reducing the value of f. Similarly at the walls the metal ion concentration may become comparable with the helium ion concentration which would affect the shape of the upper-laser-level pumping profiles.

2.6 Conclusion

The dip phenomenon depends, in the final analysis, on the high fractional ionisation of the metal which arises because of the relatively low ionisation potential of selenium compared with that of helium. If the metal were only slightly ionised the neutral diffusion gradient would not need to be high to balance the small radial ion flux. Since the buffer gases tend to have much higher ionisation potentials than the metal atoms in metal-rare-gas mixtures, the dip should be a feature of such discharges in general and not confined to helium-selenium systems.

The implications of the model and the experimental observations are that the power output of both Duffendack-and Penning-pumped positive - column metal-vapour lasers will saturate with current because, as the electron density is increased, a greater fraction of the metal is found near the walls where a smaller fraction of rare gas ions or metastables exists to populate the upper laser levels. Hence the total number of laser level ions increases sublinearly with current and the axial concentration, in the most sensitive region of the tube for zero-order mode laser oscillation, will saturate and even decrease at sufficiently high α. The onset of this sidelight sublinearity and laser power saturation with current was found to be coincident by Klein and Silfvast (12) which is in accordance with the model.

Unfortunately the efficacy of the solution of increasing the oven temperature is limited because the axial density of metal vapour will be maintained only at the expense of creating a very dense metal-vapour sheath. Since electrons ionise more easily in the sheath, the axial electric field will decrease so reducing the overall production rate of rare-gas ions or metastable atoms near the axis. A similar situation will exist for any such positive-column system where a radial electric field can drive the highly ionised metal vapour to the wall.

Owing to the complicating effect of molecular selenium which probably exists in such discharges [7], the possible involvement of selenium metastable levels in He-Se Duffendack reactions[17] and the incomplete spectroscopic literature available on selenium, the remainder of this work describes a more detailed investigation

of the hole effect using a helium-cadmium discharge. Cadmium was selected because the system is simple in design and construction and is well-documented and because a comparison is afforded between the Penning and the Duffendack pumped levels. (There is no disadvantage in observing charge-exchange levels which have not in fact been made to lase in the positive column because the general features of such a discharge are common to all such systems, and so He-Cd serves as a model for all positive-column metal-vapour lasers.)

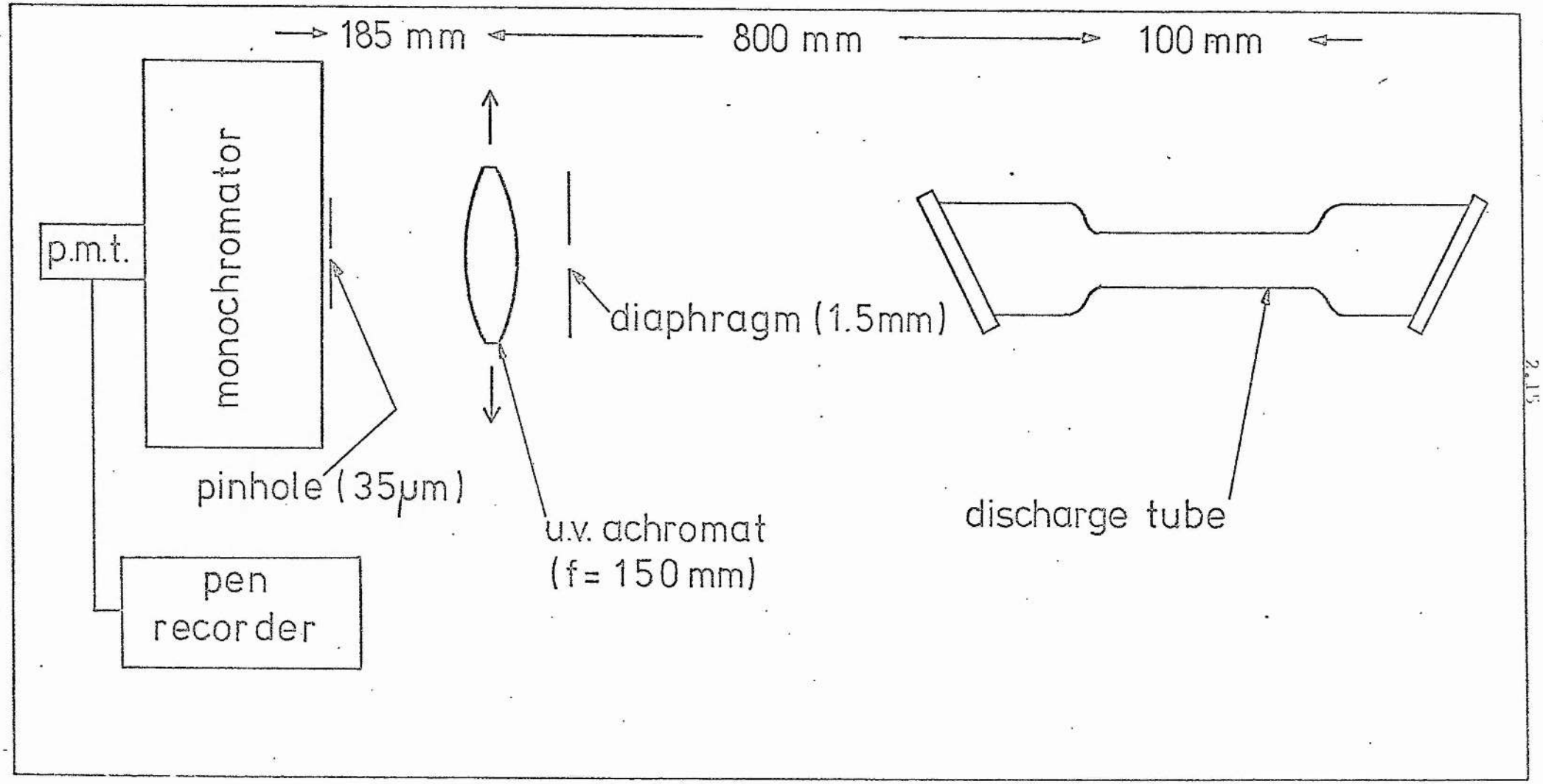

Fig. 2.1 · Diagram of the Apparatus

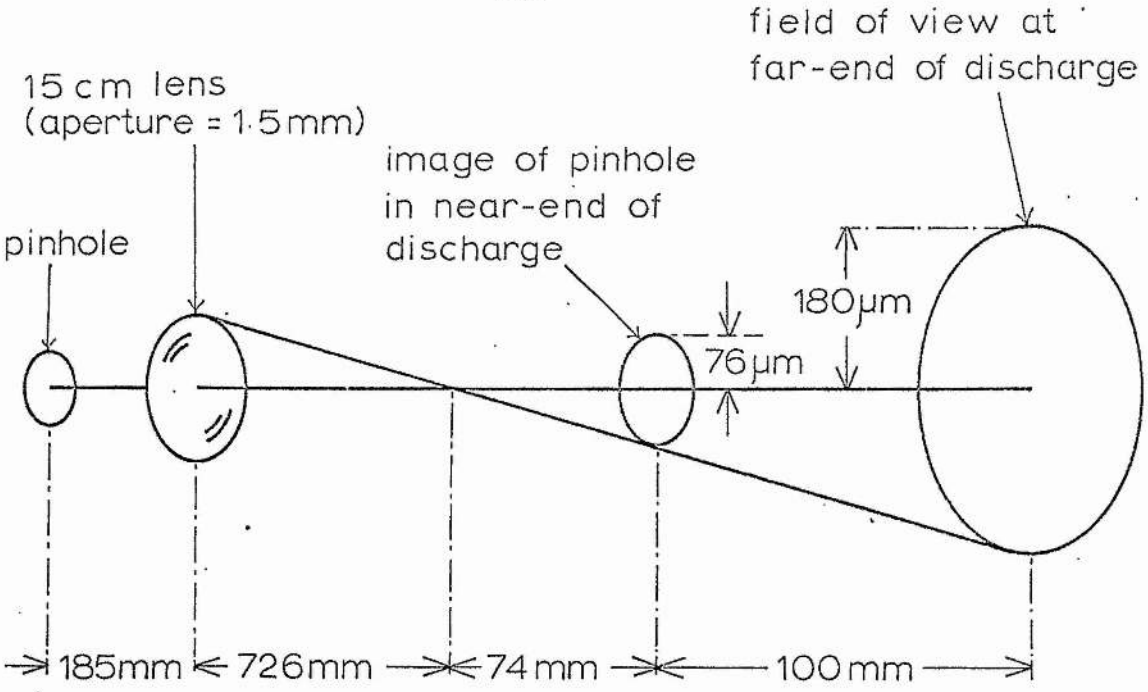

Field of view determined by ray optics

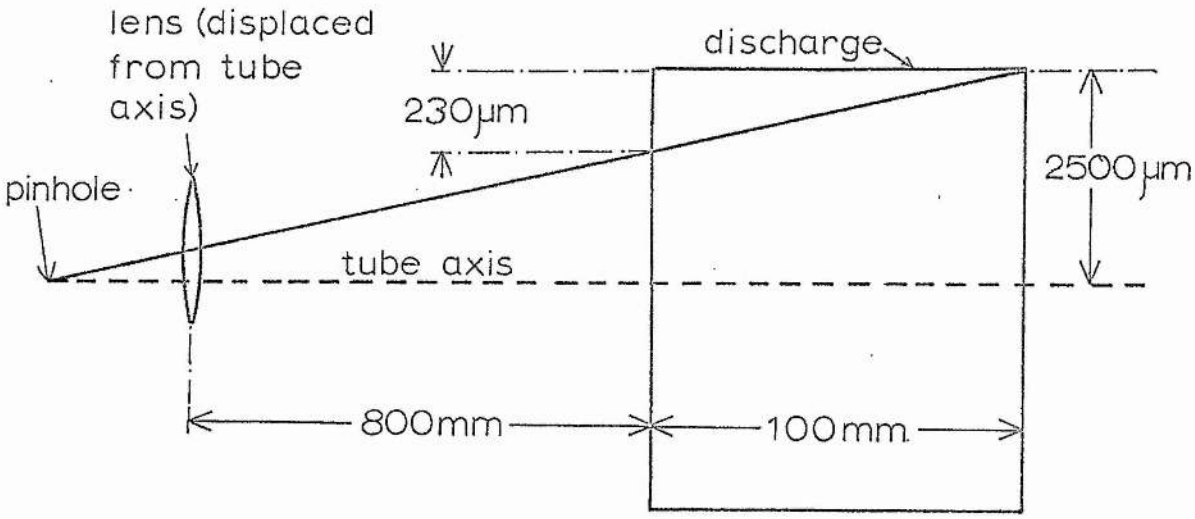

Field of view determined by parallax

Fig. 2.2

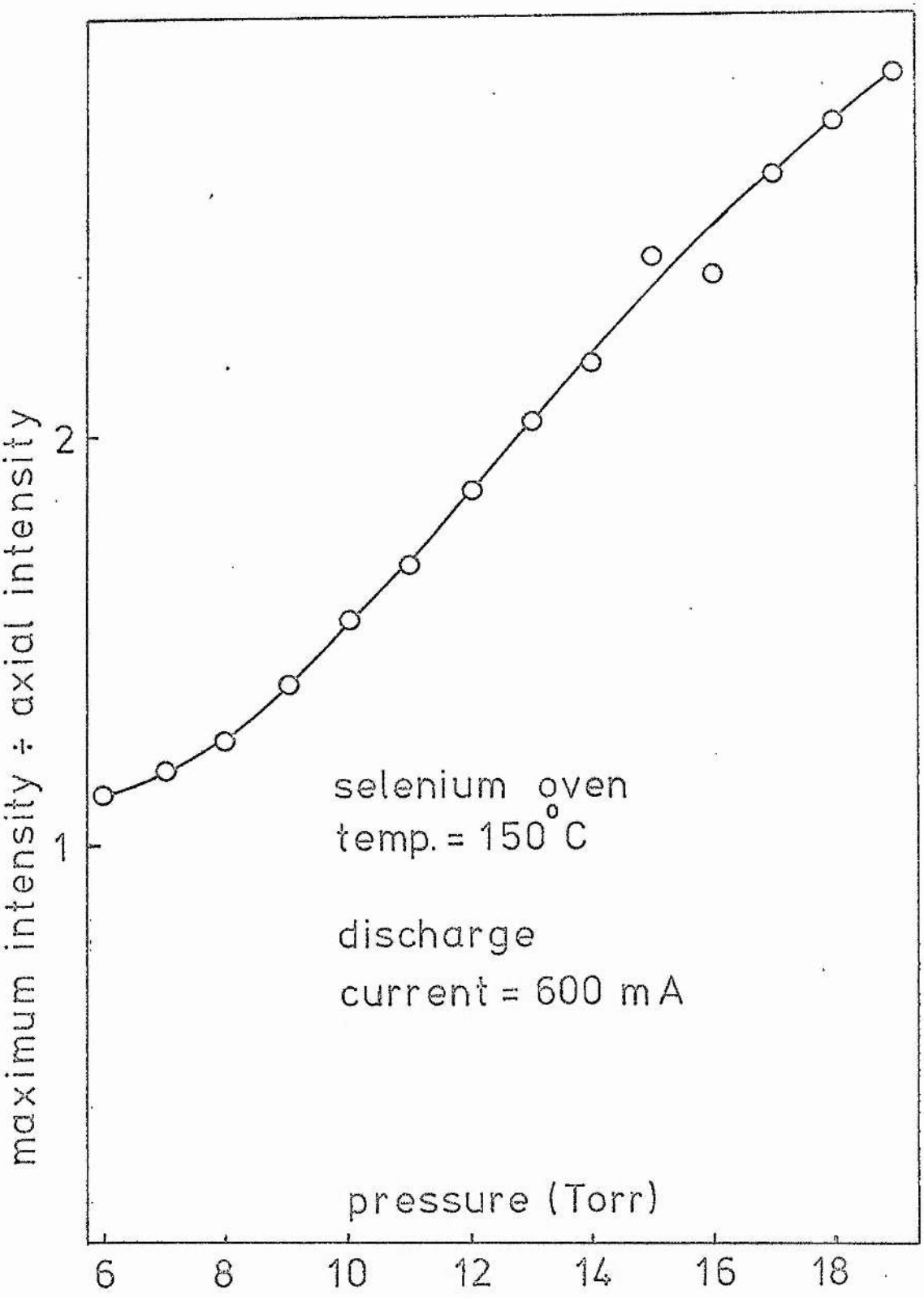

Fig. 2.3 Ratio of maximum intensity to axial intensity for 5227Å radial profiles.

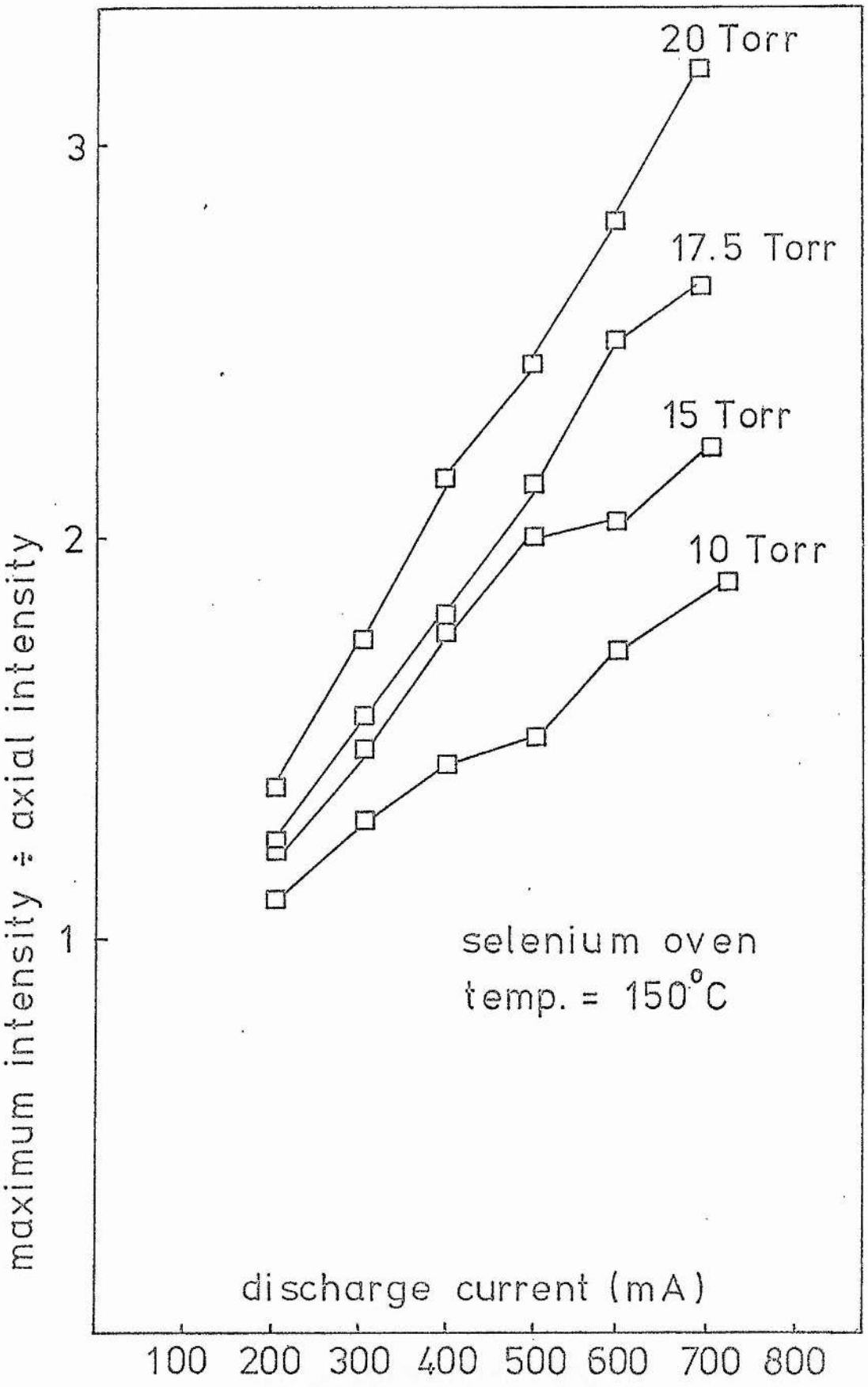

Fig. 2.4 Ratio of maximum intensity to axial intensity for 5227Å profiles.

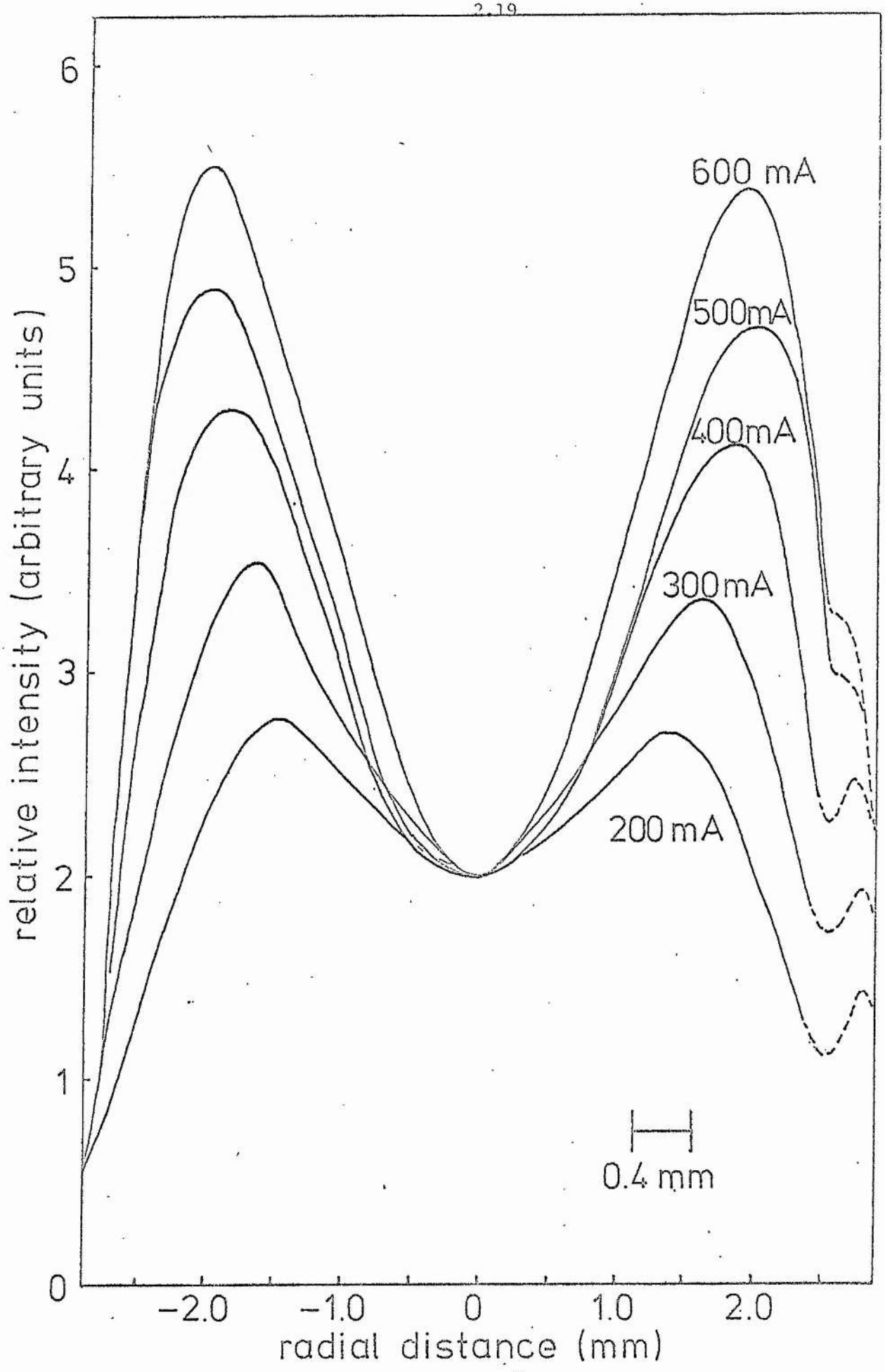

Fig. 2.5 Radial profiles at 5227Å

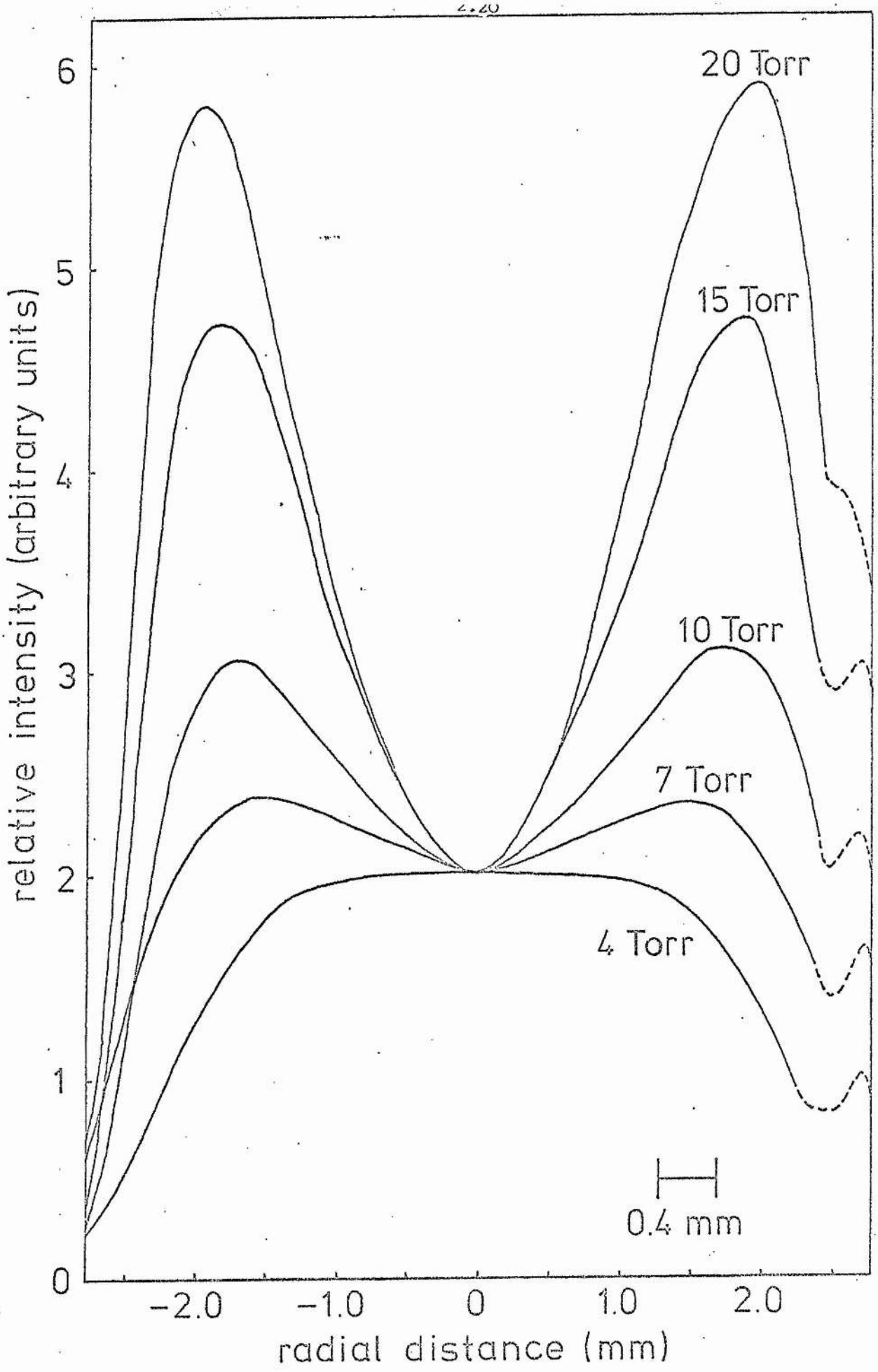

Fig. 2.6 Radial profiles at 5227Å

CHAPTER III

DESCRIPTION OF EMISSION AND ABSORPTION EXPERIMENTS TO OBTAIN RADIAL PROFILES IN A HELIUM-CADMIUM DISCHARGE

Abstract

The apparatus used to measure radial profiles by emission and absorption techniques is described. The axial dependence of cadmium vapour density is investigated.

3.1 Introduction

This chapter outlines the principal techniques used in this work to obtain radial profiles. The first part describes the optical system used to examine emission from the capillary discharge. The second part describes the additional apparatus required to perform absorption measurements. The final section deals with an experiment to test the variation of cadmium vapour density down the tube.

3.2 Emission Experiments

Two main features of the optical system described in Chapter II require improving. To reduce the effective field of view the discharge tube may be moved relative to the complete optical system hence eleminating the parallax incurred by tracking the lens perpendicularly to the optic axis. Secondly, the light collected, and, hence, the system sensitivity, for a given field of view may be increased by using the technique employed by Webb[19] to measure radial profiles of excited species in an argon capillary discharge.

3.3 Apparatus

In this arrangement, the essential features of which are schematically represented in Fig. 3.1, a converging lens images two diaphragms

mounted in planes Σ_2', Σ_1' into two circles in the conjugate planes Σ_2, Σ_1 at the near and far ends of the capillary discharge. If the circles are of equal radius, the diaphragms define a cylinder of radius a in the discharge from outside of which no light may pass through both diaphragms to enter the subsequent detection apparatus. That this is so may be seen by considering light passing through two arbitrary points in the apertures in Σ_2' and Σ_1'. Such a ray must also go through conjugate points situated within the end faces of the discharge cylinder defined above, and, since a straight line in the image space is conjugate with a straight line in the object space, no light ray, projected backwards if necessary, which cuts the curved cylindrical walls between the end faces, may pass through both diaphragms. This geometry defines not only those atoms which are in the field of view but also the amount of light accepted from each atom, because light leaving an atom at too large an angle to the optic axis may not, when projected backwards, pass through both of the cylinder end faces. At first this restriction on the solid angle of light detected may seem to be a disadvantage, but, if the system admitted light at such large angles to the optic axis that the rays cut the curved surface of the cylinder, then again, light from atoms outside the cylinder would also be detectable. Thus geometrically this is the most efficient light-gathering arrangement possible from a cylindrical object and as such it was adopted to examine the radial profiles in a He-Cd discharge.

Since the near end of the cylinder is imaged through the diaphragm in Σ_1' and since, in practice, the diaphragms are less than 0.5mm in diameter, the effect of diffraction on an image in the plane Σ_2' must be considered. With the criterion that a point is included in the effective field of view if its Airy disc overlaps the exit diaphragm, Webb [19] has shown that, in order to preserve a cylindrical field of view, the radius of the aperture in Σ_2' must be less than the geometrical image of the cylinder end face by an amount

$$\frac{V_2}{U_2} \frac{0.61\lambda D}{a}$$

where (Fig. 3.1) V_2 and U_2 are the conjugate distances of the plane Σ_2 from the lens and D is the length of the discharge cylinder.

The problem of translating the discharge tube sideways across the field of view was approached by fixing a front-aluminised mirror on a laser mirror mount set at one end of the discharge and inclined at 45° to the optic axis (see Fig. 3.2). The mount was cradled on an aluminium plate supported by a bifilar suspension so that the mirror could be displaced perpendicularly to the tube axis by a micrometer screw. It was verified with a collimating telescope and by observing a He-Ne laser beam reflected from the mirror that there was no tendancy for the plate and the mirror to rotate while they were being displaced sideways. The lens and the two apertures

were positioned on an axis parallel to that of the reflected image of the discharge tube so that scanning was effected by adjusting the micrometer screw to track the image sideways parallel to itself.

In travelling a distance of 5mm (the tube diameter) the mirror not only shifts the image 5mm sideways but also displaces it 5mm in the direction of its axis. To keep the flux-collecting efficiency of the optics constant, the diaphragms were arranged to define a cylinder 5mm longer than the capillary discharge, overlapping the mean position of its image by 2.5mm at either end. The success of this arrangement depends upon the flux collection per unit length of the cylinder being constant along its length.

This may be seen using Fig. 3.3 by considering light entering the detection optics through the element dS in the near end of the discharge. Since only light rays cutting the end-faces of the cylindrical field of view may be detected, light passing through dS is accepted only from elements within a cone of base B and apex at dS in A. A and B are the images of the apertures in Σ_2', Σ_1'. The flux gathered from any element is proportional to the volume of the element and the total solid angle of light accepted from it by the optical system. The solid angle subtended at corresponding elements in the cone by dS will be proportional to $1/U^2$ where U is the distance of an element from A. However, the area of a disc in the cone contributing to the flux varies as U^2 where U is the distance of the disc from A. Hence the total flux detected

through dS from any given distance down the cylinder is constant. Since this is true for any element dS in A, we have established the property that the total flux detected from any given length of the discharge is constant.

Two lengths of 5mm bore capillary discharge tube are used in this work, one 3cm long and the other 10cm long. In these two tubes the optics define a field of view of 0.025cm radius (=0.1R) and 0.030cm radius (=0.12R) respectively. The corresponding resolution limits - where the radius of the Airy disc in the plane of the exit diaphragm becomes larger than the geometric image of the field of view - are at 0.04R and 0.07R. Fig. 3.2 indicates the positions of the optical components for each system. The lens used in conjunction with the 10cm tube was of fused quartz with a focal length of 20.7cm at 5300Å.

A 15cm UV achromat was used with the 3cm tube to detect profiles of various wavelengths. A change in focal length of this lens will result in an axial displacement of the field of view defined by the aperture stops. From the data supplied with the lens the profile distortion resulting from the slight wavelength dependence of the focal length was calculated using a computer program similar to that in Appendix I. Let us define here a "dip ratio" which, throughout this work, will mean the height of the profile at 0.7R from the axis divided by the central value. In all cases the computed distortion was less than 8% for dip ratios of up to 5 over a wavelength range of 2200Å - 5900Å. The distortion is small because

even if the discharge overlaps one end of the diaphragm-defined cylinder, the radius of the field of view in this section of the plasma outside the cylinder increases only slowly with distance from the end of the cylinder. Indeed the above figures represent an "at worst" situation since the radius of the exit diaphragm was calculated for diffraction at the longer wavelengths of those used in this work and so the radius of the field of view will be correspondingly smaller at shorter wavelengths.

As before the resolution was tested by placing an illuminated slit in the discharge space and was found to be within the predicted value for both tubes.

The diaphragms in both cases were Ealing pinholes each 400μm in diameter on mounts adjustable in two dimensions. The complete optical system was again positioned with the aid of a laser and a collimating telescope.

Light from the exit diaphragm was directed through the entrance slit of the monochromator by a 5cm focus quartz lens. The output of the photomultiplier was connected to the Y amplifier of a Bryans Series 26000 XY recorder, the X input being taken from a 5kΩ helical potentiometer driven by the cradle micrometer. The potentiometer brush tapped off a fraction of the constant voltage applied to the potentiometer proportional to the number of turns of the micrometer. Hence radial profiles could be plotted

directly by the recorder.

3.4 Possible Complications in Emission Profile Interpretation

As in Chapter II we wish to assume that the radial profiles are proportional to the pumping rate across the tube. It was verified using the absorption technique to be described later in this chapter that there was no detectable absorption for any profiles taken of lines pumped either by Duffendack reactions (directly or by cascade) or by Penning ionisation, with the exception of the ionic resonance transitions at 2144Å and 2265Å. Allowance is made for absorption on these lines in Chapter IV. The measured gain on the Penning-pumped transitions is greatest at 4416Å being only 6% m^{-1} [20].

The design of the 10cm tube was similar to that used in the selenium experiments and again the contribution to the detected signal from the end-stubs is small. The 3cm tube which was used in certain cases to avoid excessive absorption was similar to that used by Browne and Dunn [11]. The boundaries of the 3cm discharge are well defined by forcing the discharge into the capillary through a 1/2mm gap at the anode end and making it turn sharply out of the capillary at the cathode end. The cadmium enters the tube through a 2mm slit in the capillary wall 2mm from the anode end of the column, the reservoir of cadmium being contained in a heated outer jacket coaxial with the discharge. Thus the end-stubs are eliminated in this design

and the discharge and the metal vapour are arranged to enter and leave the capillary tube on a diameter perpendicular to the scanning direction to minimise possible asymmetries at the ends. Under similar conditions the profiles taken from both tubes were alike.

Details of a computer program to evaluate the instrumental distortion of the profiles appears in Appendix I. The limiting case of geometric optics is used: diffraction effects are neglected. For an aperture of 0.1R the profile distortion is small as may be verified from Fig. A.1.2,3. At a given wavelength the dip ratio for an instrumentally distorted profile is always within 9% of the undistorted value even for ratios as large as 13. Because the finite-apertured optics cannot faithfully reproduce the extremes of peaks or troughs, the true ratios for dipped profiles tend to be higher than indicated by experiment. Ratios for undipped profiles are accurate to within 2% and signals described by a zero-order Bessel function are unaltered as has been demonstrated by Webb [19].

Movement of the ionic states from their point of creation during their finite lifetime is discussed in Chapter IV.

3.5 Absorption Experiments

Because of their role in the pumping of the 4416Å and 3250Å upper levels [24] it is important to investigate the radial profiles of the helium triplet $2s\ ^3S$ metastable population. Since no spontaneous emission can be detected from the metastable levels the measurements must be done using absorption techniques. The number densities of

the neutral and ionic ground states and metastable states of cadmium must be similarly determined.

The following transitions are examined in this work to determine number densities:

3889Å ($3p\ ^3P_{o,1,2} \rightarrow 2s\ ^3S_1$) for the helium triplet metastable state,

3261Å ($5p\ ^3P_1 \rightarrow 5s\ ^1S_o$) for the cadmium neutral ground state,

2144Å ($5p\ ^2P_{3/2} \rightarrow 5s\ ^2S_{1/2}$) for the cadmium ion ground state and

3404Å ($5d\ ^3D_1 \rightarrow 5p\ ^3P_o$) for the cadmium metastable state $5p\ ^3P_o$.

For a given length of discharge the concentration of a species may be determined from the degree to which it absorbs light from a radiative transition of which it is the lower level. (Strictly, it is the reduced number density, η, which is observed, where this is given by [54]

$$\eta = N_l \left(1 - \frac{g_l}{g_u} \frac{N_u}{N_l}\right)$$

where $N_{u,l}$ are the upper and lower states of the transition and $\frac{g_l}{g_u}$ is the ratio of their statistical weights. The reduced number density, η, is generally close to the value of N_l but upper level effects may become noticeable in helium [11]. The broad features of the behaviour of the metastables should still be well represented by η.)

Ladenberg and Reiche [54] employed a technique in which the light to be absorbed came from a source separate from the test-cell. To use this method the line profile of the source light must be known as well as that of the test discharge. The absorption is found by shining

source light through the test-cell and comparing the signal from the source when the absorption cell is switched off to that when it is running. The same optics is used to define a field of view in the absorption cell as in the emission experiments.

In all measurements involving the 3261Å cadmium neutral resonance line, care had to be taken that the absorption cell was cold before taking measurements when switched off, otherwise cadmium vapour from the hot walls would have produced misleading results.

Under the present discharge conditions spectral lines are broadened principally by Doppler and Stark effects, collisions with other atoms and by the finite natural radiative lifetime of the states [54]. Of these the Doppler effect is the most significant broadening mechanism [11] producing a linewidth of 5.2GHz for 3889Å at 600°K. The source discharge is run at a low current producing a temperature of 500°K as determined by Doppler and wall temperature measurements described in Chapter VI, and so the linewidth is generally less than that of the absorbing discharge. Fig A2.2 shows the results of a computer program written to evaluate the absorption on the 3889Å line assuming a Doppler-broadened source with no self-absorption. Details of the calculation of these absorption curves, including the structure of the triplet 3889Å line, appear in Appendix II.

The Doppler effect is also the most significant source of line-broadening for the other wavelengths examined in this work. Cadmium

of naturally-occurring isotopic composition was used and so it is necessary to take into account the hyperfine structure of the cadmium lines due to the isotopic shift and also the hyperfine splitting on the two odd-numbered isotopes. These shifts are well documented for 3261Å [55] but the structure of 2144Å has not been completely analysed. However, sufficient information is available in the literature to allow a reasonable estimation of the structure, details of which appear in Appendix III. Using this structure, absorption curves have been computed and are described in Appendix IV.

3.6 Apparatus

To ensure that the light entering the absorption cell is not detectably self-absorbed, sidelight from a 3mm diameter He-Cd capillary discharge is used as the source. This was set at the far end of the test cell perpendicular to its axis (Fig. 3.4). To verify that no self-absorption occurs in this optically thin source, this capillary discharge was placed across the entrance diaphragm of the detection optics with the test cell then acting as source. No absorption was detected in this configuration. For the measurement of the cadmium ion ground state densities a 5mm bore He-Cd discharge was run as a source cell and under the same conditions of current and pressure as the absorption cell, but this time the two discharges were coaxial and not perpendicular as before. The axial electric field was in the same direction in both tubes so that the

Doppler shift of each line profile due to the axial ion drift was the same. The transverse Doppler effect introduced by radial ion drift for the present range of velocities ($\sim 10^{-5}$ x velocity of light) is orders of magnitude smaller than in the longitudinal case, and may be neglected. Again, the concentration of cadmium in the source tube was kept low enough to avoid self-absorption.

Because the source light signal was usually an order of magnitude weaker than that of the absorption cell, detection was facilitated by modulating the source light at 1600 Hz with a toothed chopper wheel driven by a synchronous motor. In this way the source light was distinguished from the emission from the absorption cell by connecting the output of the photomultiplier to a Brookdeal 401 lock-in amplifier. (The chopper wheel also interrupted light from a photodiode which provided the reference signal for the phase-sensitive detector.) The output from this was fed into the Y amplifier of the XY recorder and so radial profiles of the absorption could be found directly by taking the ratio of the absorbed source-signal to the unabsorbed. In the case of 2144Å absorption a U.V. converging lens was placed between the two discharge tubes to ensure the diameter of the test cell was completely illuminated. The 3cm long tube was used as the test cell in all the absorption experiments.

3.7 The Axial Dependence of Cadmium Vapour Density

To test the assumption in equation (2.2) of the axial independence of the ground state cadmium neutral concentration, the sidelight of the

Cd I level at 4799Å ($6s\ ^3S_1 \rightarrow 5p\ ^3P_1$) was measured along the length of the discharge. (The 10cm discharge tube, which does not have an outer jacket, was used.) Following Sosnowski [2] this signal was normalised to the intensity of the helium line at 4921Å also taken along the tube length. In order to maintain the same light-collecting efficiency at all points along the tube and to save moving the monochromator, the discharge was imaged into the focal plane of a lens by a mirror inclined at 45° to the tube axis and the two components were moved together to scan down the tube (Fig. 3.5). This way, the angle subtended by the lens as seen by the discharge was constant and the emergent parallel light was focused at the entrance slit of the monochrometor. The axial distance was traced directly on the XY recorder by arranging that a helical potentiometer was turned by a toothed track running in a groove in the optical bench carrying the mirror and lens. The track was fixed to the lens and mirror mounts. Absorption on the 4799Å line as viewed in the sidelight is small at the oven temperature used in this experiment (245°C). For given discharge conditions the normalised cadmium sidelight signal is taken to be proportional to the neutral ground state density. Results are shown in Fig. 3.6 for extreme conditions of 2.5 torr 100 mA and 10 torr 400 mA. In no case does the fractional change of cadmium density exceed 3% cm^{-1} which justifies neglecting the axial dependence compared with the radial dependence in equation (2.2).

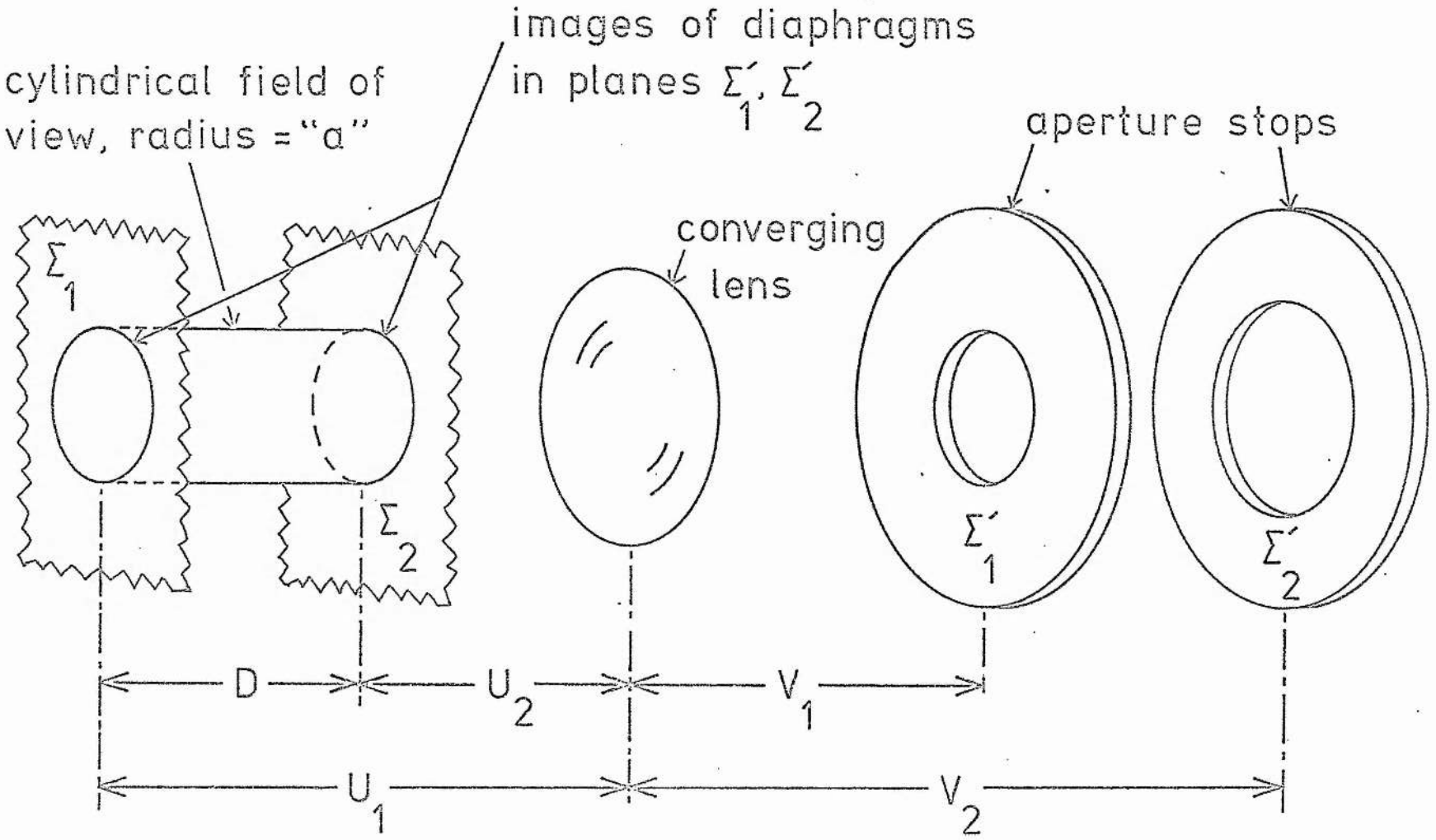

Fig. 3.1 Schematic diagram of the optical system

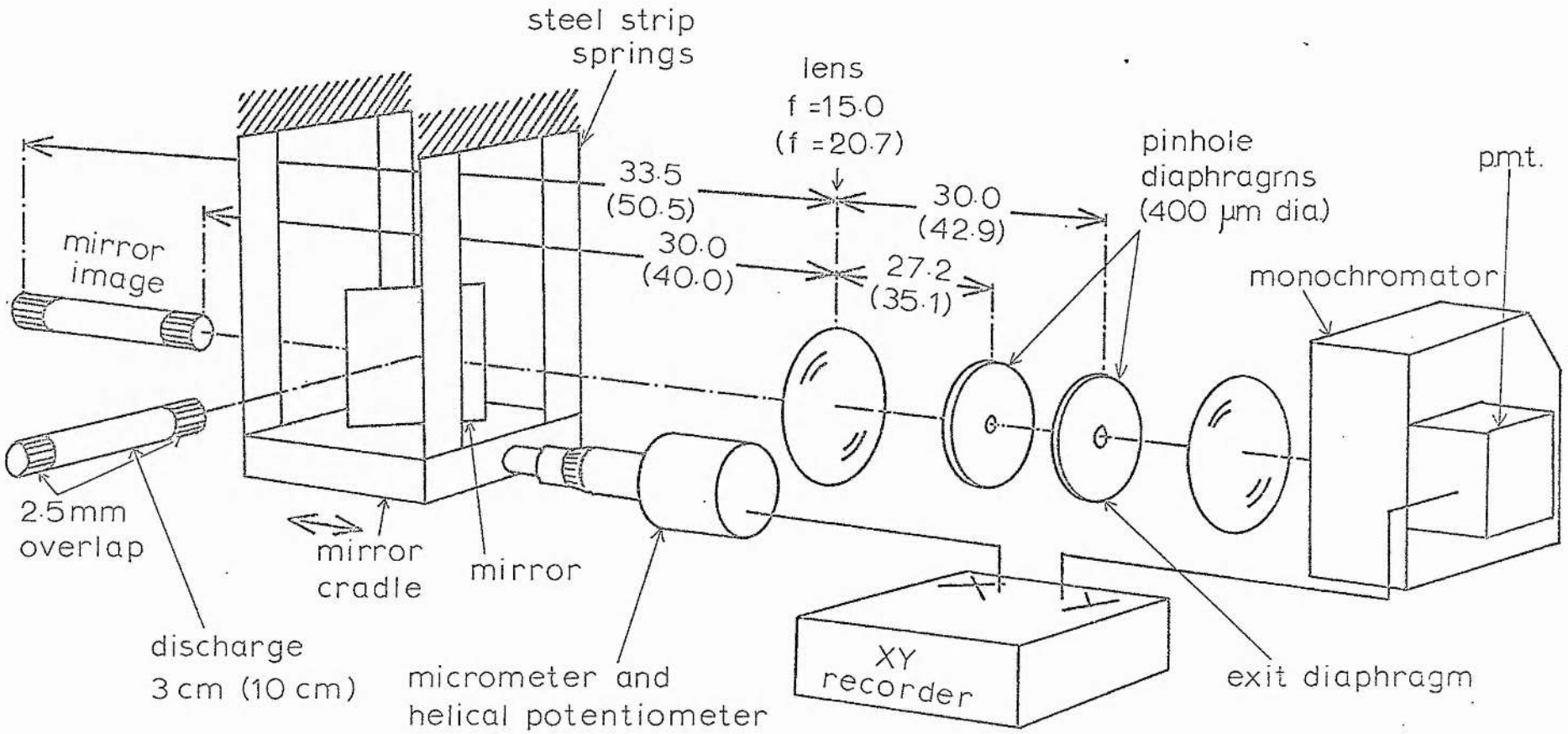

Fig. 3.2 Schematic diagram of the apparatus for obtaining radial emission profiles. Distances in cm unless otherwise specified. Numbers in brackets refer to 10cm tube.

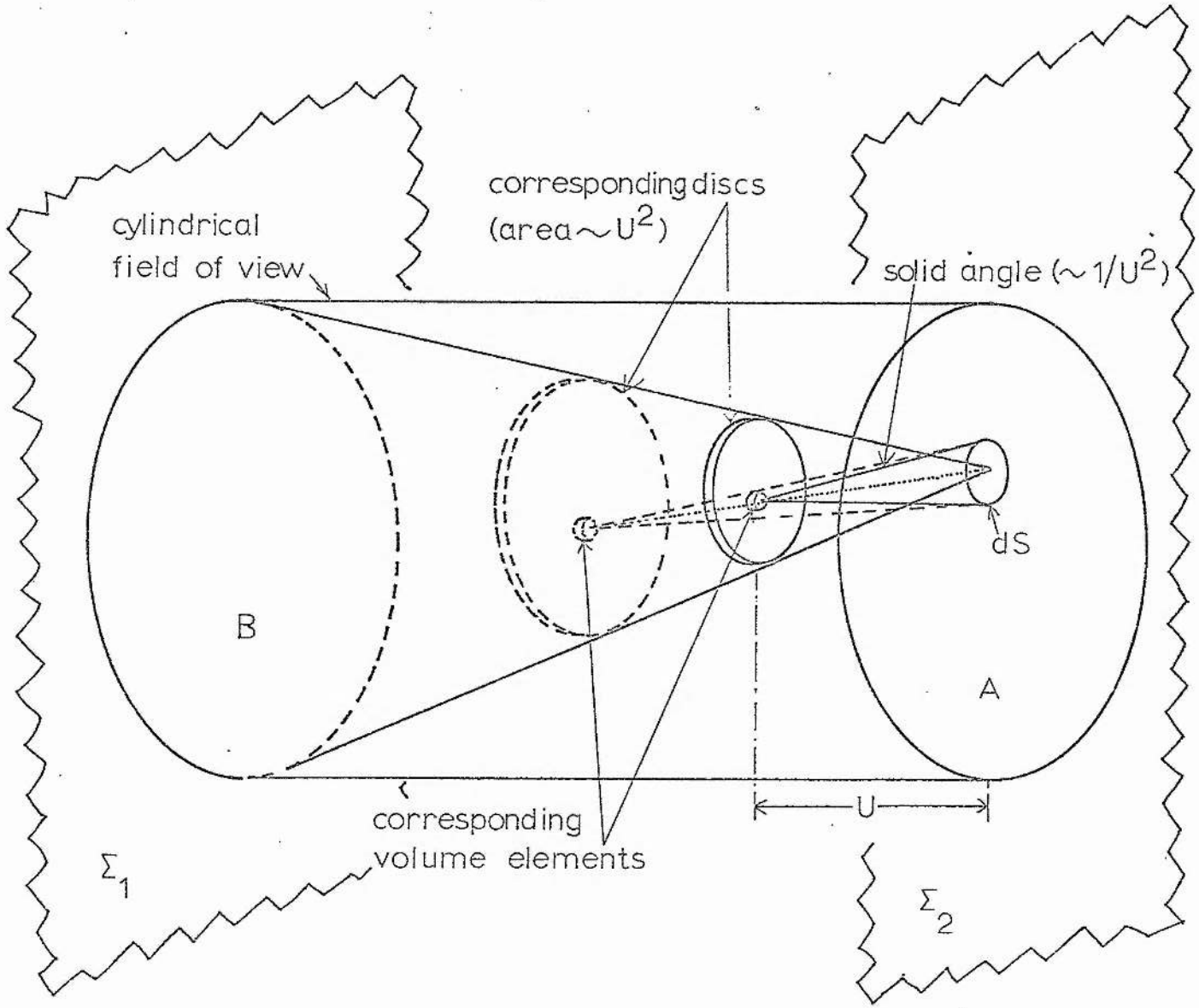

Fig. 3.3 Diagram to show the linearity of flux collection along the field of view.

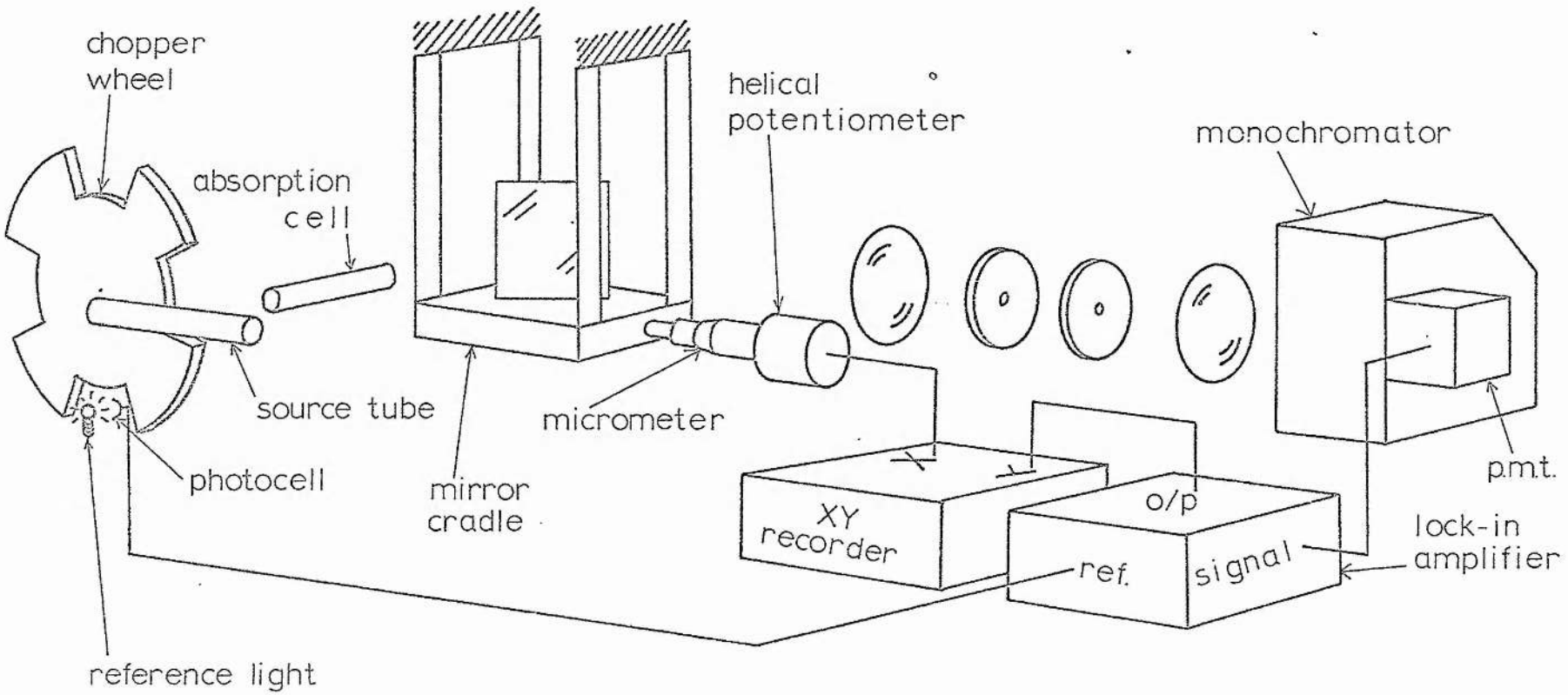

Fig. 3.4 Schematic diagram of the apparatus for obtaining radial absorption profiles.

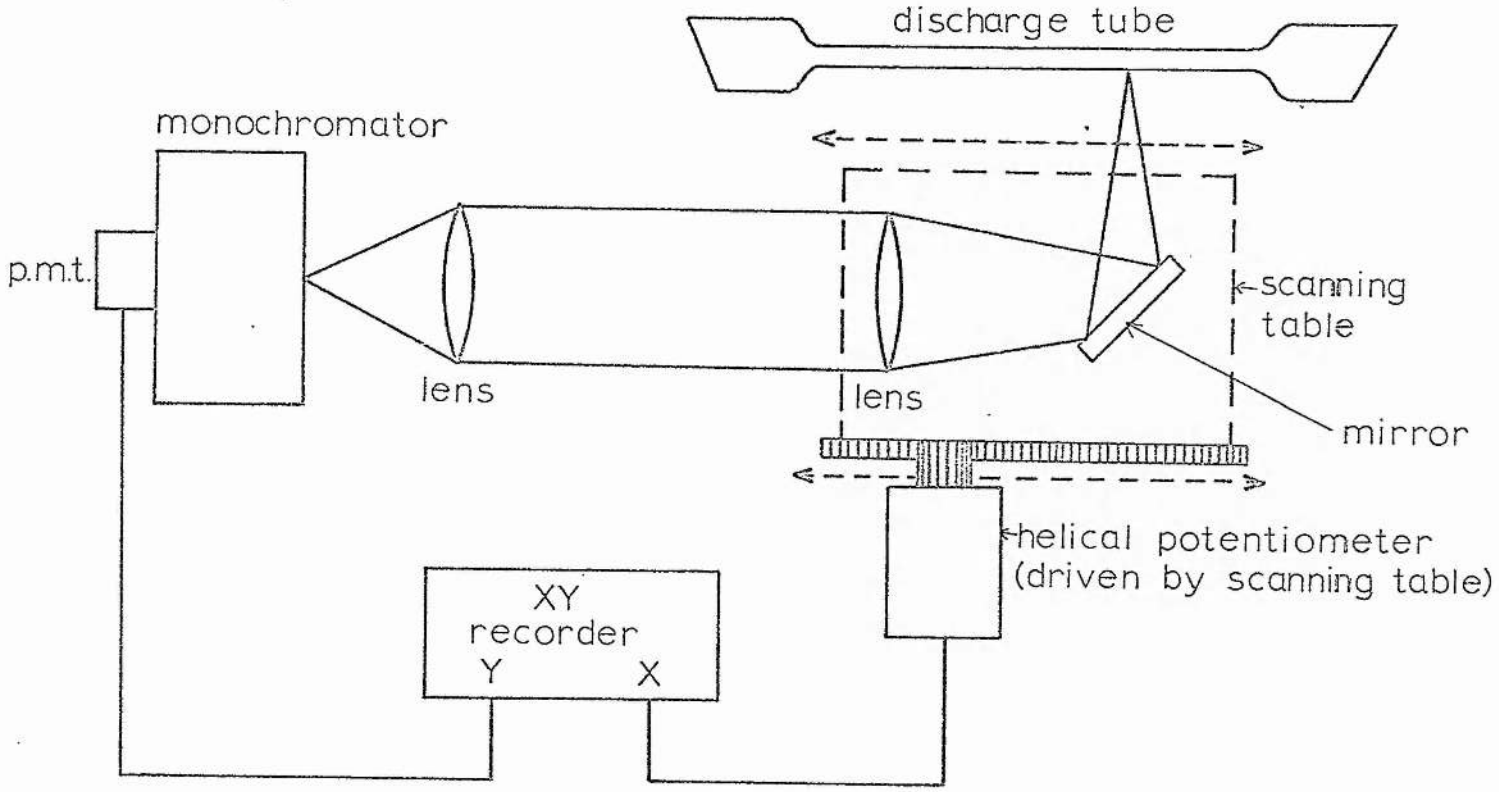

Fig. 3.5 Schematic diagram of the system used to measure the axial distribution of cadmium.

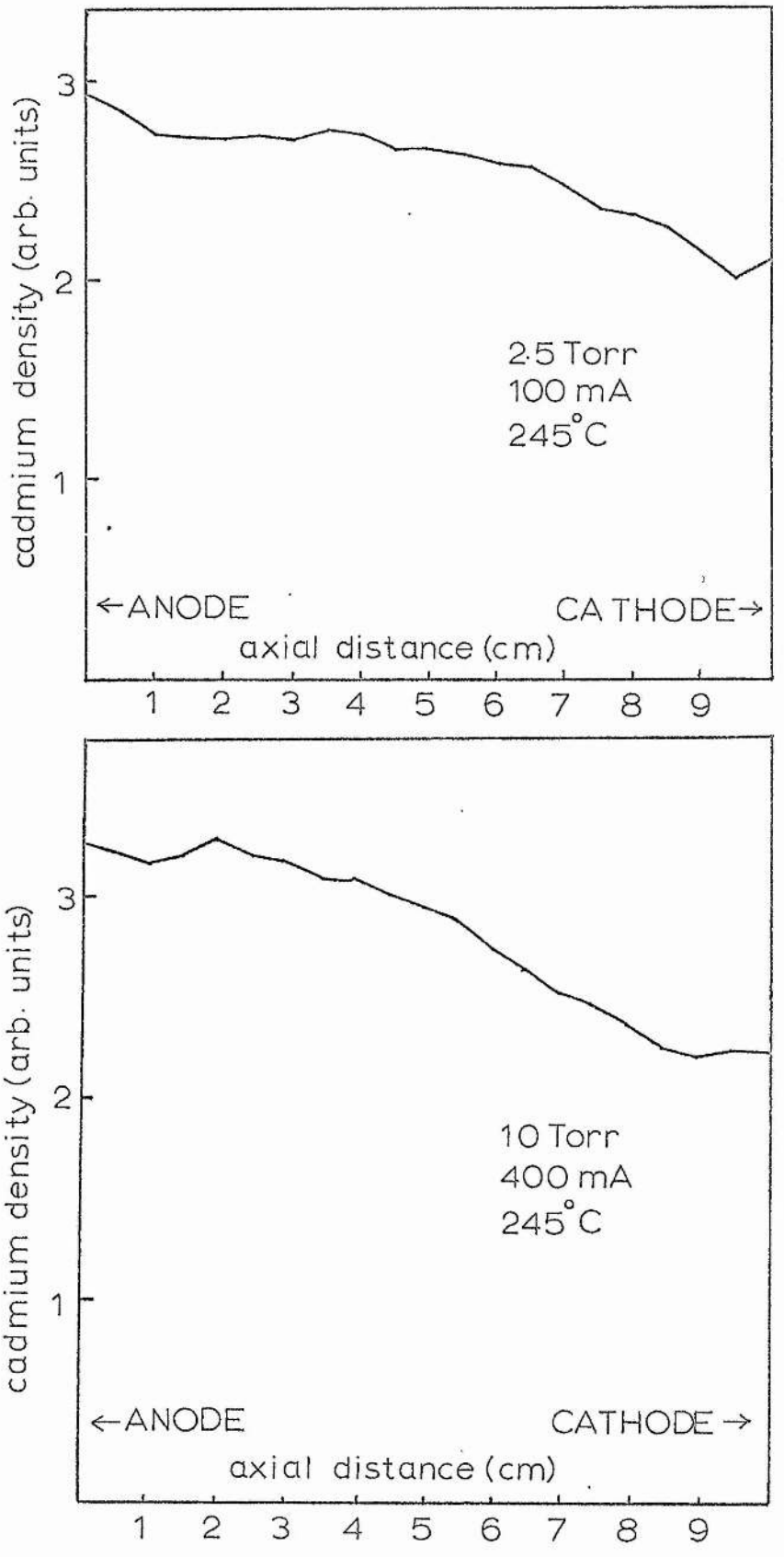

Fig. 3.6 Variation of cadmium vapour density along the tube.

CHAPTER IV

RESULTS OF RADIAL PROFILE EXPERIMENTS IN A HELIUM-CADMIUM DISCHARGE

Abstract

Results are given of absorption measurements to determine cadmium ground state ion and neutral density profiles and cadmium and helium metastable profiles. Emission profiles of excited cadmium ions are described. There seems to be a significant amount of electron pumping of some of the latter states from the cadmium ion ground state.

4.1 Introduction

The first part of this chapter describes the results of the absorption measurements of cadmium ion and neutral ground state profiles and cadmium and helium metastable profiles. The second part describes emission profiles of cadmium and helium transitions.

4.2. Results of Absorption Experiments

4.2.1 Profiles of Helium Triplet Metastable Species

The reduced triplet metastable density was obtained for various discharge conditions and in all cases the profiles were flatter in shape than the zero-order Bessel function which is expected for the electron and helium ion density profiles (section 4.3.7).
An example for the pure helium case is given in Fig. 4.1. Such behaviour was expected since the lifetime of the metastable atoms near the tube axis is determined by electron collisional destruction rather than diffusion to the walls with the currents and pressures used in these experiments. Using the diffusion coefficient found by Phelps [56] for helium metastable atoms, the diffusion rate per atom

from the axis to the wall is $\sim 10^4 s^{-1}$ at 5 Torr, 850°K. This is much smaller than the destruction rate of helium metastables by electrons which Browne and Dunn [11] have estimated to be $\sim 6 \times 10^{-8} N_e s^{-1}$. For the present discharge this gives an axial destruction rate of $3 \times 10^5 s^{-1}$ and so the local metastable population is saturated with respect to electron density. However, the diffusion loss rate increases towards the walls and the electron destruction rate decreases radially with electron density which means the metastable population becomes dependent upon the electron concentration near the walls. This axial saturation explains the flattened appearance of the radial profiles.

In the same Figure, two further profiles are shown for the same discharge parameters except that cadmium has been introduced at oven temperatures of 245°C and 265°C. Besides decreasing the overall metastable density the addition of cadmium also suppresses the profile near the walls.

Two explanations of this suppression may be proposed. Either the saturation condition has been relaxed to some extent or the peripheral build-up of cadmium lowers the electron temperature which in turn lowers the metastable production rate near the walls.

As we have just seen, saturation occurs when the metastable atoms cannot diffuse appreciably from their point of creation before they are destroyed by electron collisions. As the cadmium partial pressure is increased, and the electron temperature lowered

as a result, the loss of metastables by electron ionisation (the principal electron destruction mechanism [11]) will fall with the electron temperature. Thus diffusion becomes an increasingly competitive loss process and the saturation region withdraws towards the centre of the discharge leaving a progressively more peaked metastable distribution as the cadmium oven temperature is raised.

The other viewpoint is that the production rate of metastables (involving electrons of $\geq$ 19 e V) will be more sensitive to electron temperature changes than the ionisation rate of metastables (requiring about 5 e V). Thus, even before the saturation condition may be noticeably relaxed, the production rate of the metastable species may be reduced, especially near the walls where the electron temperature is lowered by the high metal concentration. This would also result in the lower peripheral metastable densities observed.

To see whether it is reasonable to speak of an electron temperature which varies across the tube, we must consider whether a newly produced electron diffuses appreciably towards the tube walls before it reaches its equilibrium temperature. This may be determined roughly as follows.

Assume that each electron loses a constant fraction κ of its energy each time it collides with a neutral helium atom. It may be shown [30] that an electron which starts from rest under an applied electric field reaches about 94% of its final random speed,

c, after a time τ where

$$\tau = \frac{\lambda_e}{\kappa c} \qquad (4.1)$$

and λ_e is the electron mean free path (assumed, like κ, to be independent of the electron energy for the purposes of the approximation). The fraction κ may be estimated from the relation [30]

$$\frac{v}{c} = (\tfrac{1}{2}\kappa)^{\frac{1}{2}}$$

where v is the steady-state electron drift velocity (see Table 6.1).

Since both the numerator and the denominator of equation (4.1) decrease with increasing number density, the time required for the electron to reach its ultimate speed is fairly constant and is about 10^{-7}s. The radial distance which the electron has diffused by this time is given by $\sqrt{D_a \tau}$ where D_a is the ambipolar diffusion coefficient. Calculating this from the expression [30]

$$D_a = \frac{kTe}{e}\,\mu+$$

the maximum distance which an electron diffuses in the present experiments is 700μm at 3.5 Torr filling pressure and 500mA discharge current. This distance becomes less at greater number densities.

This analysis has neglected the variation of κ and λ_e with electron energy and cadmium concentration. However, the result that the electron achieves its ultimate temperature within a distance of less than the tube radius suggests there is a case for assuming that the electron temperature may vary radially.

The suppression of the metastable densities near the wall with increasing cadmium partial pressure is also apparent in the profiles of 4416Å emission (Fig. 4.2), the upper level of which is pumped predominantly by Penning collisions with helium metastable atoms [1]. However, any reduction in the dips of the neutral cadmium ground-state profiles through reduction of the cadmium ionisation rate with lower electron temperatures will also contribute to the suppression of the 4416Å profile wings. (It is shown in Chapters V and VI that cadmium ionisation proceeds mainly by electron collision rather than by Penning or charge-transfer processes.)

4.2.2 Profiles of Cadmium Neutral Ground-State Density

It was not possible to measure unambiguously the profiles of the neutral ground-state cadmium atoms because of the metal vapour present in the "dead space" between the observation windows and the discharge column.

The ground state neutral dip ratio determined by absorption measurements at 3261Å never exceeded the excited state ratio, and, at higher pressures and currents, was only about half the value. This result was unexpected since all profiles of excited states should be less dipped than the ground state (the densities of electrons, helium ions and metastables which pump the excited cadmium levels being greatest at the axis). It was noticed however that the neutral

ground-state density increased monotonically towards the walls under all conditions, as expected for the ground-state profiles.

A significant deposit of cadmium was noticed on the condensing bulb at the cathode end of the discharge. This means that there must be cadmium vapour absorbing the source light between the end of the capillary discharge and the bulb. The rate of deposit seems to be less here than on the bulb surrounding the cathode itself (out of the line-of-signt of the detection optics.) However, the transport velocity of cadmium down the positive column will be very much greater (owing to cataphoresis) than the diffusion velocity in the buffer volume at the end of the positive column. Therefore the amount of cadmium in the absorption path outside the discharge may well be comparable to that in the discharge. This extra contribution to the absorption will be nearly constant across the tube diameter and will therefore have the effect of reducing the observed dip ratio. In order to investigate properly the shape of the gound-state profiles it would be necessary to design a discharge tube where there was no "dead space" between the windows and the positive column, perhaps using the heat of the discharge to prevent cadmium condensation on the windows.

4.2.3 Profiles of the Metastable Cadmium State $5p^3Po$

If the only loss process of the long-lived metastable cadmium atoms is by diffusion to the walls, the radial profiles should not be dipped. However, we see in Fig. 4.3 that absorption of 3404Å radiation (terminating on the $5p^3P_o$ metastable state) is lowest on

the axis and increases monotonically with radius. This indicates that volume destruction processes are competitive with diffusion losses. One possible process is electron ionisation of the metastable states and this is discussed further in section 6.4.

4.2.4 Profiles of the Ion Ground-State Density

The oven temperature in the absorption cell was adjusted so that the fractional absorption of the 2144Å emission was about 0.5 (at 235°C). The dips in the ion density profiles were generally smaller than those in the charge-exchange-pumped emission lines for the same discharge conditions. Examples of profiles appear in Figs. 4.4 and 4.5.

It may at first be surprising that the ground state ion profiles should be dipped at all because volume recombination is unimportant. (With a typical metal ion recombination coefficient of less than 10^{-11} cm^3 s^{-1} [57, 28] the lifetime against volume destruction is $\sim 10^{-2}$s which is much longer than the ion lifetime of $\sim$ 1μs). The cause of the dip is the radial electric field. At any point the aggregate number of ions crossing unit area in unit time in travelling radially to the walls is equal to the rate at which cadmium atoms diffuse across unit area back from the walls. Since the bulk of the ion population is in the ground state (by lifetime considerations) we have

$$-D_+ \frac{dN_+}{dr} + \mu_+ E N_+ - D_o \frac{dN_o}{dr} = 0$$

The first term represents diffusion of ground state ions, the second is the ion ground state current density due to the radial electric field and the third term is the neutral diffusion. Therefore,

differentiating,

$$-D_+ \frac{d^2N_+}{dr^2} - D_o \frac{d^2N_o}{dr^2} + \mu_+ E \frac{dN_+}{dr} + \mu_+ \frac{dE}{dr} N_+ = 0$$

Thus, near $r = o$

$$\left(\frac{d^2N_+}{dr^2}\right)_{r\to o} = -\frac{D_o}{D_+}\left(\frac{d^2N_o}{dr^2}\right)_{r\to o} + \frac{\mu_+}{D_+}\left(\frac{dE}{dr}\right)_{r\to o} N_+ \quad (r\to o)$$

The two terms on the right are of the same order and it will be seen that if the radial field rises steeply enough or if the ionisation is great enough the curvature of N_+ will be positive, which indicates a profile dip. Such conditions presumably prevail when a dip is detected in the ion ground state population.

4.3 Results of Emission Experiments

Profiles were taken for various discharge parameters of lines with wavelengths between 2000Å and 6500Å.

As was to be expected from the He-Se experiments it was observed that the dip deepens with increasing pressure and current. Because of gas heating effects, the dip is deeper if the pressure quoted is the tube filling pressure than if the discharge has been run open to the vacuum system. Similarly if the tube is lagged with aluminium foil (to avoid cadmium condensation on the capillary walls at currents less than 150mA) the dip is shallower than is observed without lagging. (The depth of the profile may be increased dramatically if the aluminium foil is stripped away while the discharge is running.

A calculation in Chapter VI shows that the gas temperature is not very much higher than that of the tube wall.) Where necessary, the state of the discharge, isolated or open to the vacuum system, lagged or uncovered, is emphasised.

Fig. 4.6 shows a typical set of axially-normalised profiles for various wavelengths at 5 Torr filling pressure of helium (with the tube then isolated from the vacuum system) at a discharge current of 300mA. The 3cm tube was used for this experiment. The cadmium oven temperature was 235°C but, as we shall see in Chapter V, the profile depth was fairly insensitive to cadmium partial pressure over a wide range of oven temperatures. It was necessary to centralise these curves by up to 5% to correct for the slight horizontal displacement found at different wavelengths because of the Brewster-angle mounting of the quartz observation window.

To explain the appearance of the profiles we consider where appropriate five processes which might affect the profile shapes, viz. Duffendack pumping, Penning pumping, electron excitation from the cadmium ion ground state, electron collisional destruction of states and the movement of ions from their point of creation during their lifetime.

Because of the uncertainties in the cadmium neutral ground-state profiles (section 4.2.2) it is not possible simply to calculate the excited-state profiles from a knowledge of the ground-state profiles together with those of the helium ion or metastable densities and to compare the predictions with experiment. The relative appearance of

profiles of different states must be explained in terms of the relative pumping processes which we now discuss.

The profiles of the helium ion population will take the form of a zero-order Bessel function which is the Schottky solution [4] for the electron density in the positive column (see section 4.3.7). The Penning levels arise from collisions with helium metastable atoms. These, we have seen, have a flatter profile than that assumed for the helium ions. Thus the Penning pump-rate profiles will be higher near the walls than those due to Duffendack reactions (see Fig. 4.7).

The ground-state cadmium ion populations have generally shallower dips than either the Duffendack or the Penning pump-rate profiles (see, for example, Figs. 4.4 and 4.5). Hence the profile of electron excitation rate from these levels will be markedly less dipped than for the other two processes.

Electron collisional destruction of a state would deepen a profile dip since the high axial electron population would raise the destruction rate at the centre of the tube.

With the exception of the $5s^2\ ^2D$ and ^2P levels, lifetimes of the ionic states investigated in this work are generally 20 ns or less. It is likely that such short-lived levels are not significantly depopulated by electron collisions [75] and so this process is considered negligible for such states.

It was shown in section 2.4 that levels with lifetimes of around 10^{-8} s move a negligible distance from their point of creation before radiating. Again the only states with significantly long lifetimes

studied in this investigation are the $5s^2\ ^2D_{3/2,5/2,}$ states which are the upper levels of the 3250Å and 4416Å transitions, with lifetimes of 0.3μs [20, 21, 22, 68] and 0.8μs [20, 21, 22, 23] respectively. The consequence of these extended lifetimes is discussed in section 4.3.2.

The profiles for each wavelength will be described in turn, with reference to Fig. 4.6 as a typical set of results. An energy level diagram appears in Fig. 4.8 which shows some of the transitions examined in this work.

4.3.1 6360Å ($6g\ ^2G_{9/2} \rightarrow 4f\ ^2F_{7/2}$), 6355Å ($6g\ ^2G_{7/2} \rightarrow 4f\ ^2F_{5/2}$)

The signal from these transitions was weak and a background signal about 20% of that of the 6360Å transition was detectable. This signal, which seemed to be molecular in origin, was subtracted from the total to obtain the 6360Å and 6355Å profiles.

The profiles for these wavelengths are identical to each other for all discharge conditions. This is to be expected since the upper 6g levels of these transitions are both pumped directly by Duffendack reactions with helium ions [17]. A dip ratio of greater than unity appears for nearly all conditions for these levels.

We are going to treat the profiles of these transitions as being representative of the Duffendack pumping-rate profiles to which profiles of states pumped by other processes will be compared. The 6g states are not significantly depopulated by electrons in an environment of an electron density of $10^{13}cm^{-3}$ [75] having a lifetime of only 23ns, and so this should not distort the profiles. There is a possibility that

the 6g levels are pumped by electron excitation from the cadmium ion ground state, which would produce a less dipped contribution than that of the Duffendack pumping. However, there is insufficient data to estimate the size of the contribution, and, since a threshold of over 15eV is involved, electron excitation of such levels is considered small for the purposes of this work with the reservation that any interpretation based on this assumption be treated with caution.

4.3.2 $\underline{3250\text{Å}\ (5s^2\ {}^2D_{3/2} \rightarrow 5p\ {}^2P_{1/2}),\ 3536\text{Å}\ (5s^2\ {}^2D_{3/2} \rightarrow 5p\ {}^2P_{3/2}),}$

$\underline{4416\text{Å}\ (5s^2\ {}^2D_{5/2} \rightarrow 5p\ {}^2P_{3/2})}$

The profiles of the $^2D_{3/2}$ and $^2D_{5/2}$ states are fairly similar to each other. These levels are excited by Penning collisions with helium metastable atoms [1] and it was expected that the Penning-excited profiles would exhibit higher wings than those pumped by Duffendack reactions (see Fig. 4.7). However, in general the Penning levels are less dipped than the 6g levels as may be seen, for example, in Fig. 4.6.

One explanation for this discrepancy concerns the long lifetimes of these states mentioned earlier. Both levels live long enough to be affected by the sweep-out action of the radial electric field and by the tempering effect of ordinary diffusion. The qualitative effect of the finite lifetime may be judged by considering the situation to be intermediate between the extremes of a zero lifetime which would result in a profile identical to that of the Penning pump rate, and a long lifetime such as that of the ion ground state. An example of such a profile is shown dotted in Fig. 4.7. The combined effect of diffusion

and the radial electric field on the ions is to smooth out the profile dips. In fact there is a tendancy for the 4416Å profile to be less dipped than the 3250Å and 3536Å profiles which may be a consequence of the longer lifetime of the $5s^2\ ^2D_{5/2}$ states compared with that of the $5s^2\ ^2D_{3/2}$ states.

Attendant with the long lifetime is the possibility that the $5s^2\ ^2D$ states have a significant chance of being destroyed by electron collisions. As we have remarked earlier, electron depopulation of such states will tend to deepen the profile dips. The effects of the two processes, electron destruction and diffusion, will tend to cancel each other. As we see from Fig. 4.6, the experimentally observed profile is not very much shallower than that of the 6g levels, which, in turn, will not be much less dipped than the Penning pumping-rate profile. Therefore it is possible that the effect of smoothing by diffusion is greater than the observed profiles would suggest, but that these are deepened by electron destruction. The fact that the $5s^2\ ^2D$ states <u>are</u> less dipped than their pump rates suggests diffusion is the stronger of the two loss mechanisms.

At the pressure of 10 Torr, in an average radial field of 50 Vcm^{-1} (section 6.3) the cadmium ion velocity is about $7 \times 10^4 cm\ s^{-1}$ (using a mobility of $20cm^2V^{-1}s^{-1}$ at 760 Torr [74]). In the lifetime of the 4416Å upper level this represents a distance of about ½mm. From this we see that the diffusion effect may be significant although it is difficult to estimate quantitatively the resulting profile smoothing. This would require a detailed

consideration of the radial behaviour of the electric field. Consequently it is difficult to determine the electron collisional depopulation rate although a rough upper limit may be given. The non-radiative destruction rate cannot be very much greater than the radiative loss rate otherwise the profiles would not have time to flatten out by diffusion and so the observed profiles would be more dipped than the Penning pump-rate because of the electron destruction.

A further explanation for a dip shallower than the Penning pumping rate profile may be that electron excitation from the ion ground state contributes to the pumping of these levels. Such an additional electron-cadmium ion excitation has also been proposed by Janossy, Itagi and Csillag [69].

4.3.3 $\underline{2144\text{Å}\ (5p\ ^2P_{3/2} \rightarrow 5s\ ^2S_{1/2})\quad 2265\text{Å}\ (5p\ ^2P_{1/2} \rightarrow 5s\ ^2S_{1/2})}$

To correct for self-absorption effects on the 2144Å resonance line, a graph is computed (see Appendix V) of I_t/I_m vs Nd. I_t is the intensity which would have been observed had there been no self-absorption and I_m is the measured intensity (cf. ref.[58]). For a given discharge, Nd, the product of the number density of the absorbing species and the discharge length, d, is found from absorption measurements and Fig. A4.1.

Correction for self-absorption does not change the character of the ion resonance lines - they still exhibit shallower dips than any other cadmium transitions observed, under given discharge conditions.

To investigate this effect, radial profiles were taken for both 2144Å and 2265Å and also for all the transitions terminating on the upper levels of these lines which were intense enough to give an acceptably low noise-signal ratio. These were, (Fig. 4.8) for the $5p\ ^2P_{3/2}$ state (upper level of 2144Å), 2749Å, 2313Å, 2321Å, 4416Å, and 3536Å and, for the $5p\ ^2P_{1/2}$ state, 2573Å, 2195Å and 3250Å. The relative photon flux from each transition was estimated by calibrating the entire optical detection system including the quartz window of the discharge tube with a quartz deuterium lamp which had been calibrated at the National Physical Laboratory. Measurements were taken at 25 different discharge conditions in the 3cm tube at an oven temperature of 235°C.

The ratio of the axial photon rate from the observed transitions contributing to the $5p\ ^2P_{3/2}$ state divided by the photon rate from the 2144Å transition is graphed in Figs. 4.9 and 4.10. The dip ratios of 2144Å and 2313Å are compared in Figs. 4.11 and 4.12. At both higher helium pressures and discharge currents the axial radiative decay from the observed upper levels accounts for a diminishing fraction of the pumping of the 2144Å level. The contribution from transitions in the vacuum U.V. is discussed presently. The difference between the dip ratios of the contributing transitions and of 2144Å is also greater at higher pressures and currents with the result that at 10 Torr 400mA all five detectable transitions cascading into the $5p^2P_{3/2}$ state have more than twice the dip of 2144Å. The radial profiles

of the lines concerned are presented for these discharge parameters in Fig. 4.13. The 2265Å system is similar in behaviour to that of the 2144Å system and the results of the latter may be generalised for the former.

Suppose for the moment that we treat the 2144Å upper level as being pumped only by radiative cascade from Penning and Duffendack levels together with any non-radiative contribution arising from electron collisional destruction of higher levels. Any other mechanism such as electron excitation from the cadmium ion ground state is excluded.

We have seen in section 4.3.1 that we may represent the Duffendack pumping-rate profile by that of the 6g levels. (These profiles are very much more dipped than the profiles of the ion resonance transitions.) Thus, assuming that all levels pumped by charge transfer cascade either radiatively or non-radiatively into the 5p states, the total Duffendack contribution to these levels should be dipped as much as the 6g levels.

This assumes that, in cascading into the 5p level, the profiles are not smeared out by diffusion in the time taken to reach the resonance states. For lifetimes of most of the states concerned there will be no significant diffusion effect. For example, in the 6360Å - 5378Å - 2313Å chain the total time is about 35ns (Fig. 4.8) which represents only 30μm of travel in the discharge. The only exceptions to this are the long-lived upper P states, but any profile smoothing on these will be masked by pumping from the S, D, F and G states.

(The only way in which the shallow dip in the ion resonance lines could arise from the charge-transfer levels is for one of the long-lived ^2P states to radiate predominantly into the ground state and at the same time to pump the 5p levels by electron destruction, resulting in a shallow-dipped contribution. Such a process appears unlikely.) In any case the profiles of the contribution from electron collisional destruction will, in this particular case, follow the radial Duffendack pumping rate, since the lifetime against electron destruction is only 5% of the radiative lifetime of the $9p\,^2P$ states at $N_e = 10^{13}cm^{-3}$ [75]. This is not long enough to admit significant smoothing.

A similar argument could show that the total radiative and non-radiative contribution from the Penning levels should follow the Penning pumping-rate profile which should be even more dipped than the Duffendack profiles (Fig. 4.7). However, the picture is more complicated because the long lifetime of the $5s^2\,^2D$ states allows them to diffuse appreciably in the radial electric field before radiating. Hence we cannot apply the argument that the contributions from the Penning levels should be deeply dipped and we consider instead the effect of electron collisional destruction acting upon the observed profiles of the Penning levels. If such a process is important then the shallow dip of the resonance levels could indeed by explained by such a mechanism. The 4416Å transition is the largest contributer to the $5p\,^2P_{3/2}$ state (Figs. 4.9 and 4.10) and electron depopulation, being strongest at the axis, would substantially fill in

the profile dip of the resonance state.

However, if such a process is operative it cannot be the only one as may be seen from Figs. 4.9 and 4.10. The axial helium metastable density saturates or even decreases [11] at the higher pressures and currents shown in these two graphs, while the axial helium ion density must increase with pressure and current, through charge quasi-neutrality. Therefore the total axial radiative plus non-radiative contribution from the Penning levels to the 2144Å upper level must diminish compared with the Duffendack contribution with increasing current and pressure. Since the 2313Å transition itself (resulting from cascade from Duffendack levels) contributes a diminishing fraction to the pumping of the $5p\ ^2P_{3/2}$ state at higher pressures and currents, we conclude that there must be another process which increases in importance compared to Duffendack and Penning reactions at higher pressures and currents.

This conclusion will not be invalidated by the 2313Å transition being partially pumped by electron excitation from the cadmium ion ground state, provided its fractional contribution to the total pumping of 2313Å does not decrease with current. As we shall see with 5378Å (section 4.3.4), electron excitation from the cadmium ion ground state represents a fairly constant fraction of the total pumping of the transition and does not decrease with current and pressure. Any electron pumping of the 2313Å transition will follow a similar pattern. This means that the pure Duffendack pumping rate must still decrease compared to the 2144Å pumping and so the above conclusion still holds.

The axial contribution from the Penning levels may come from ions which diffuse inwards from regions nearer the walls. However, this does not alter the argument. This is because the back-diffusion of $5s^2\ ^2D$ states to the axis will not increase with pressure and so still we have not accounted for the relative axial increase of the 2144Å signal with pressure.

The other process which could contribute to the pumping of the $5p\ ^2P_{3/2}$ level is electron excitation from the cadmium ion ground state. As we have seen the profile of this excitation rate will be much shallower than the other pumping-rate profiles. Moreover, as we shall see in Chapter VI, the fractional ionisation of cadmium increases at higher pressures and currents. The increase in the dip ratio of the observable transitions contributing to the $5p\ ^2P_{3/2}$ levels compared with the dip ratio of 2144Å (Figs. 4.11 and 4.12) may indicate that the electron-cadmium ion pumping of the $5p\ ^2P_{3/2}$ levels is also increasing. The increasing axial signal at 2144Å compared to that of the observable contributing transitions may be due to the same effect.

Referring to Fig. 4.13, when the visible transitions contributing to the $5p\ ^2P_{3/2}$ level are subtracted from the 2144Å profile, the remainder of the profile is still dipped. However, the electron pumping contribution, the product of the cadmium ion ground state profile (Fig. 4.4) and a Bessel profile, will be convex at 10 Torr 400mA. The discrepancy is probably due to vacuum U.V. contributions which have not been included in the subtraction.

It would be expected that vacuum U.V. transitions cascading into the $5p\ ^2P_{3/2}$ level would be dipped at least as much as the observable lines, since such U.V. transitions, arising from levels high above the ion ground state, would be less accessible to electron pumping than the lower states. Thus, although we have not specifically accounted for these lines in the interpretation of Figs. 4.11 and 4.12 the essence of the argument is unaltered, that electron pumping from the cadmium ion ground state is increasing at higher pressures and currents.

Similarly, the discrepancy between the axial signals of the observable cascading transitions and the 2144Å transition (Figs. 4.9 and 4.10) cannot be accounted for by the vacuum U.V. lines contributing more than their share at higher pressures and currents. This is because such a situation would result in a far deeper dip than is observed at 2144Å at higher pressures and currents.

Hence the observations in Figs. 4.9 - 4.12 may be explained in terms of electron pumping of the ion resonance levels from the cadmium ion ground state.

The cross section for this process may be calculated using the equation [67]

$$Q = \frac{2\pi}{E\Delta E\sqrt{3}}\ fg_{eff} \qquad \text{(in units } \pi\ a_o^2\text{)}$$

Here ΔE and E are the excitation energy and the energy of the incident electron in atomic units and f is the oscillator strength of the transition. The effective Gaunt factor, g_{eff}, has not been tabulated for this transition but is generally of the order of unity [67]. The results of this calculation averaged over the electron energy

distributions in a helium discharge [47, 48, 49] at E/p = 5 V cm^{-1} $Torr^{-1}$ give a cross section of 7 x 10^{-16} cm^2. (The cross section in the present circumstances will be somewhat lower because of the influence of cadmium on the electron energy distribution.) This gives an excitation rate of 7 x 10^{-8} N_e N_{cd+} s^{-1} for the 5p $^2P_{3/2}$ state. The corresponding rate by Duffendack or Penning processes is about 10^{-9} N_{He+} N_{Cd} s^{-1} or 10^{-9} N_{He*} N_{Cd} s^{-1} [24, 35]. With a typical figure of 5% ionisation of cadmium, the rate of the electron excitation process is evidently comparable with that of Duffendack or Penning reactions which is necessary if electron excitation is to compete with Duffendack and Penning pumping of the 5p $^2P_{3/2}$ state.

4.3.4 5337Å (4f $^2F_{5/2}$ → 5d $^2D_{3/2}$), 5378Å (4f $^2F_{7/2}$ → 5d $^2D_{5/2}$)

The radial profiles are identical to each other for all discharge conditions. Although these levels are pumped in part by radiative cascade from the 6355Å and 6360Å transitions, the dips on these lines are consistently shallower than those of the 6g levels. Observations show that for any given dip ratio of the 6g levels there corresponds a unique ratio at 5337Å and 5378Å, regardless of the discharge conditions. The relationship between the dip ratios is plotted in Fig. 4.14 for 20 widely differing conditions - the experimental points are fairly collinear.

Again the reason for the shallower dip is probably electron excitation from the ion ground state. It is also possible, of course, that there is pumping of these levels by electron collisional destruction processes populating them at the expense of some higher, longer-lived states.

One such notably long-lived state is the 9p $^2P_{3/2}$ level with a computed lifetime of about 400ns [18]. However, a transition from this level to the 4f levels is radiatively forbidden and so high non-radiative cascade seems unlikely.

Because the departure from the directly pumped Duffendack profiles is greater, as we shall see presently, at lower energy levels (where more electrons have energies above the excitation threshold) we accept electron-ion collisional excitation as the more likely explanation in the absence of evidence to the contrary.

It is possible to estimate roughly the extent of the electron pumping of the 4f levels. It is assumed that all the radiative transitions cascading into these levels are not themselves excited by electrons (which is the assumption already made for the 6360Å and 6355Å transitions). The profiles of the electron pumping will result from the product of the cadmium ion ground state profiles (see, for example, Figs. 4.4 and 4.5) and a Bessel distribution of electrons. Having found this, we ask the question: what weight must be given to the electron pumping profiles when added to the 6360Å and 6355Å profiles in order to produce the dips of the 5378Å and 5337Å profiles? Analysing the latter transitions into their components (see Fig. 4.15 and Appendix VI), it turns out that, at the axis, very roughly a third of the pumping of the 4f levels is from electrons at discharge conditions ranging from 5 Torr 100mA to 10 Torr 400mA. This fraction must be regarded as a lower limit since the actual electron pumping

of levels above the 4f states is unknown. The similarity of the 5337Å profile to that of 5378Å reflects the fact that the 4f levels are separated by less than 0.002eV which results in a similar electron contribution to both these states.

The situation in the case of the ion resonance lines is more complicated since some of the cascading contributions to the states are themselves electron-pumped to different degrees. However, the fractional excitation by electrons is evidently significantly greater than for the 4f level case.

4.3.5 2313Å ($5d\ ^2D_{5/2} \rightarrow 5p\ ^2P_{3/2}$), 2195Å ($5d\ ^2D_{3/2} \rightarrow 5p\ ^2P_{1/2}$), 2321Å ($5d\ ^2D_{3/2} \rightarrow 5p\ ^2P_{3/2}$)

The profile dips of these transitions which are pumped by cascade from charge-exchange levels [18] are less again than those of the 4f levels. The cause is once more attributed to additional electron excitation from the ion ground state. The 5d upper levels of the transitions are separated by only 0.02 eV which explains the similarity of the profiles to each other.

The smoothing of the profile dips on these transitions is unlikely to be due to pumping from a smoothed-profile P state, because the contribution from the P states will not be particularly great, and, as we have seen, the lifetime of the P state is shortened by electron destruction which reduces the effects of diffusion.

4.3.6 2749A ($6s\ ^2S_{1/2} \rightarrow 5p\ ^2P_{3/2}$), 2573A ($6s\ ^2S_{1/2} \rightarrow 5p\ ^2P_{1/2}$)

The common upper level of these two transitions is more dipped than the 5d states even though it is almost 1eV lower in energy. Presumably this is because it is pumped not only by cascade

from Duffendack-excited levels but also directly by Penning reactions [18] which would have a deeper pumping profile. Again, contributions from P states should not result in a serious departure from a pure Duffendack profile.

4.3.7 4713Å Helium Transition ($4s\ ^3S_1 \rightarrow 2p\ ^3P_{0,1,2}$)

This neutral helium line has been included in Fig. 4.6 for comparison with the cadmium lines. The profile shape follows reasonably well that of a zero-order Bessel function with the first zero at the tube walls. This is Schottky's solution for the electron density profile [4] using the ambipolar diffusion model of the positive column of the glow discharge. For such a model to be applicable to the present situation it must be shown that λ_e and λ_+, the mean-free-paths of the electrons and ions, are much less than the tube radius, R, so that diffusion to the wall is the important process rather than free fall. Also volume recombination should be negligible compared to wall recombination so that all ions and electrons produced in the discharge may be considered to diffuse to the walls.

The number densities of helium neutral ground-state atoms in the present discharge range from $5 \times 10^{16} cm^{-3}$ to $3 \times 10^{17} cm^{-3}$ (Table 6.1). The cross section for charge-transfer in pure helium, σ_T, is about $20 \times 10^{-16} cm^2$ [26]. From the relation (ref [26] page 376)

$$\sigma_D = 2\sigma_T$$

where σ_D is the momentum-transfer cross section for an ion in its parent gas, σ_D is $40 \times 10^{-16} cm^2$. Therefore the ionic mean-free-path

varies from 8×10^{-4}cm to 5×10^{-3}cm which is evidently much less than the tube radius. Similarly, with an electron collision cross section of 5×10^{-16}cm^2 [27], the mean-free-path varies from 6×10^{-3}cm to 4×10^{-2}cm. The condition that $\lambda_+, \lambda_e \ll R$ is satisfied.

The rate of volume recombination of helium ions with electrons is negligible compared to the loss rate by ambipolar diffusion of ions to the walls. The recombination coefficient, α (ref [26] Chapter 7), decreases sharply with increasing electron temperature ($\alpha \sim T_e^{-9/2}$) and is less than 10^{-11} for $N_e = 10^{13}$ at $T_e = 0.3$eV [28, 29]. This implies a recombination rate of 10^2 s^{-1} for a helium ion at the above electron concentration. With a characteristic diffusion length of $\Lambda = 0.1$cm this is to be contrasted with the ambipolar diffusion loss rate, D_a/Λ^2, of 10^6 s^{-1}. This assumes for the ambipolar diffusion coefficient,

$$D_a = \frac{kT_e}{e}\mu_+ \quad \text{(from ref [30])}$$

$$= 10^4 \text{cm}^2\ \text{s}^{-1}$$

Therefore the loss rate by volume recombination is insignificant compared with the wall recombination rate. It is also of interest to note that the volume destruction of helium ions by Duffendack reactions is a competitive process only at relatively high values of cadmium concentration. With an average relative velocity of 2×10^5cm s^{-1} and a cross section for the charge-exchange process of 4×10^{-15}cm^2 [24], the destruction rate is only comparable with the wall loss rate at metal vapour concentrations of 10^{15}cm^{-3} which is an order of magnitude

greater than typical vapour densities in such systems.

It is also possible that there may be stepwise ionisation of helium via the metastable levels. Near the axis where there is a tendancy for the metastable population to be saturated with respect to electron density the ionisation rate would still be essentially linear in N_e, but nearer the walls the quadratic dependence on N_e would become more important. However such a mechanism has little effect on the Schottky solution for the electron density as may be seen by considering the case of complete stepwise ionisation throughout the whole tube. This problem was treated by Spenke [31] who showed there was only a slight departure here from a Bessel solution for electron density.

The above conditions being satisfied, it is reasonable to assume Schottky's solution for the electron concentration and it is assumed that the cadmium ion densities are not large enough at low oven temperatures ($\sim 2 \times 10^{11} cm^{-3}$ - Figs. 4.4 and 4.5) to upset seriously the profiles of the helium ion or electron concentrations ($\geq 2 \times 10^{12}$ - Chapter VI). The Bessel-shaped radial dependence of the electron population should also be found for excited levels of helium assuming a direct electron excitation process and a radially-independent electron temperature.

The profile of 4713Å in Fig. 4.6 is a reasonable approximation to a Bessel function. Departure from this shape may result from absorption on the 4713Å line, a non-uniform electron temperature

distribution across the tube and the possible involvement of long-lived excited and metastable helium states in a two-step excitation process.

4.4 Conclusion

In this chapter we have studied radial profiles by emission and absorption techniques in a helium-cadmium discharge. As was expected from the helium-selenium experiments, a significant dip is present in the profiles of cadmium states. Not only do charge-exchange transitions suffer this axial depletion as was the case with the selenium system, but the Penning-pumped levels, too, are dipped. Because the Penning levels are excited by collisions between cadmium atoms and helium metastables which are saturated with current [11], the laser lines originating from these levels will be especially sensitive to the behaviour of the cadmium neutral ground-state density at the axis.

Profiles of the cadmium ion ground state are noticeably less dipped than those of the excited ion and, hence, the neutral ground state profiles. Because of this, contributions to excited states arising from electron excitation from the ion ground state are much less dipped than the cascade contributions from Duffendack and Penning levels. This is taken to be the explanation for the decrease in dip depth of levels progressively nearer to the ion ground state.

We have also considered as an explanation for this, the pumping of excited ion states by electron collisional destruction from the long lived P states. While such a process might account for the profile

of any one state, it is not likely that the effect would remain so marked when distributed amongst all the states which exhibit shallow profiles. In any case, we have seen that the lifetime of the P states is greatly reduced by electron collisional destruction, which will prevent significant smoothing of the profile dips. Therefore we conclude that pumping of excited ion states from the cadmium ion ground state is an important process in He-Cd laser discharges.

Profiles of the helium metastable densities are shown to be flat-topped as expected from electron saturation processes. However, although this should lead to the $5s^2\ ^2D$ Penning-pumped levels being more deeply dipped than the Duffendack-pumped states, this is not found to be the case. The shallow dip of these Penning levels is attributed to diffusion of these long-lived states.

It has proved impossible to obtain unambiguous profiles of neutral ground state cadmium densities with the present apparatus.

The cadmium metastable profiles exhibit dips which indicate that volume destruction processes are active (including electron ionisation).

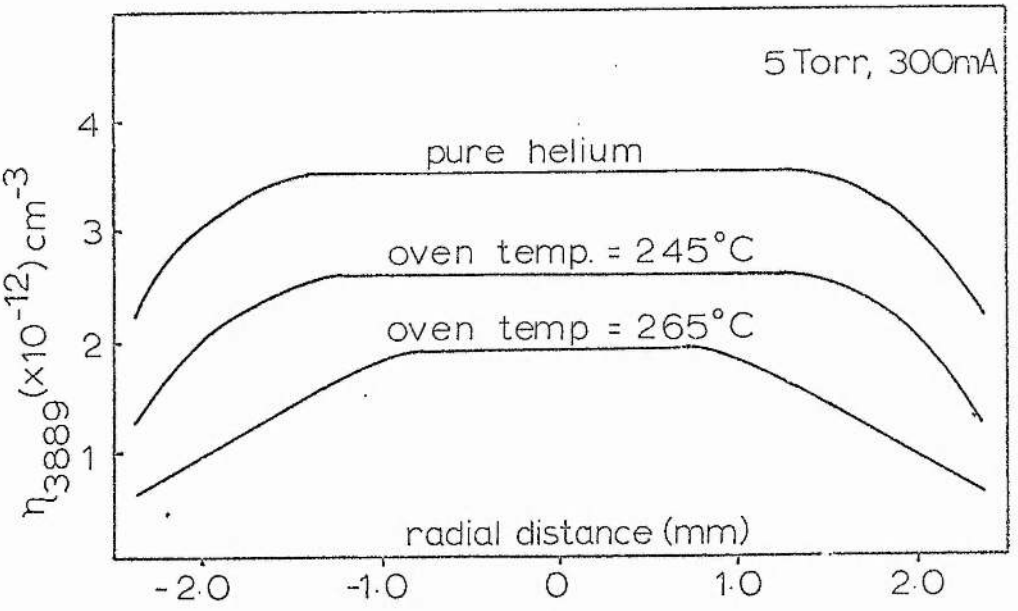

Fig. 4.1 Radial profiles of the reduced helium triplet metastable density, η_{3889}, showing suppression near the walls at higher oven temperatures.

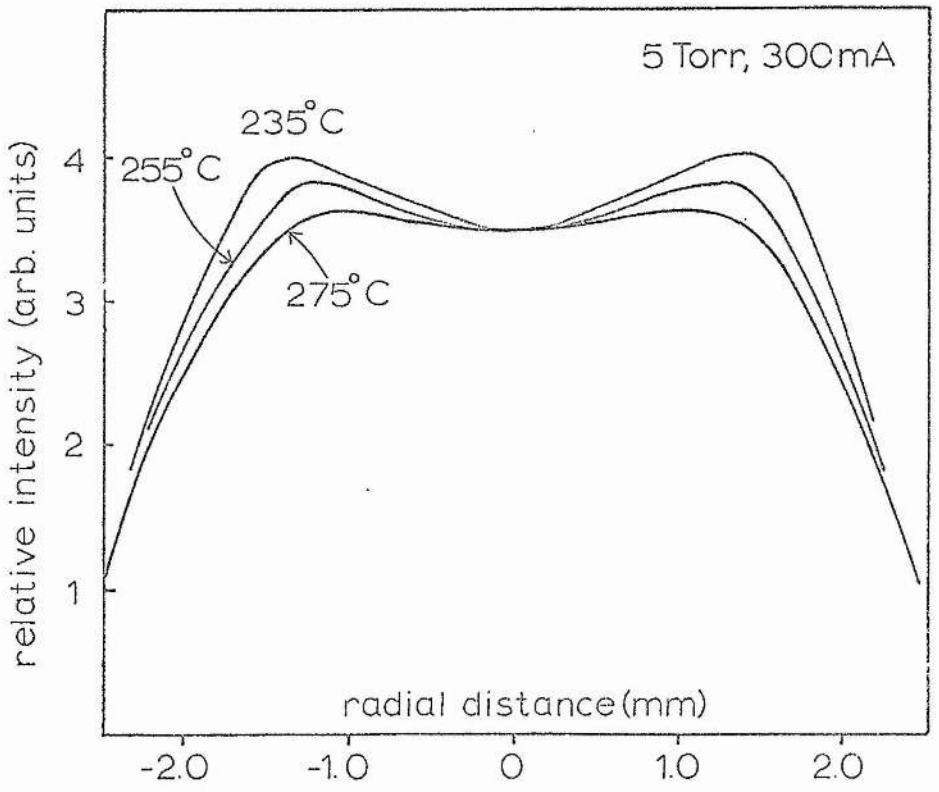

Fig. 4.2 Radial profiles of 4416Å emission at various oven temperatures.

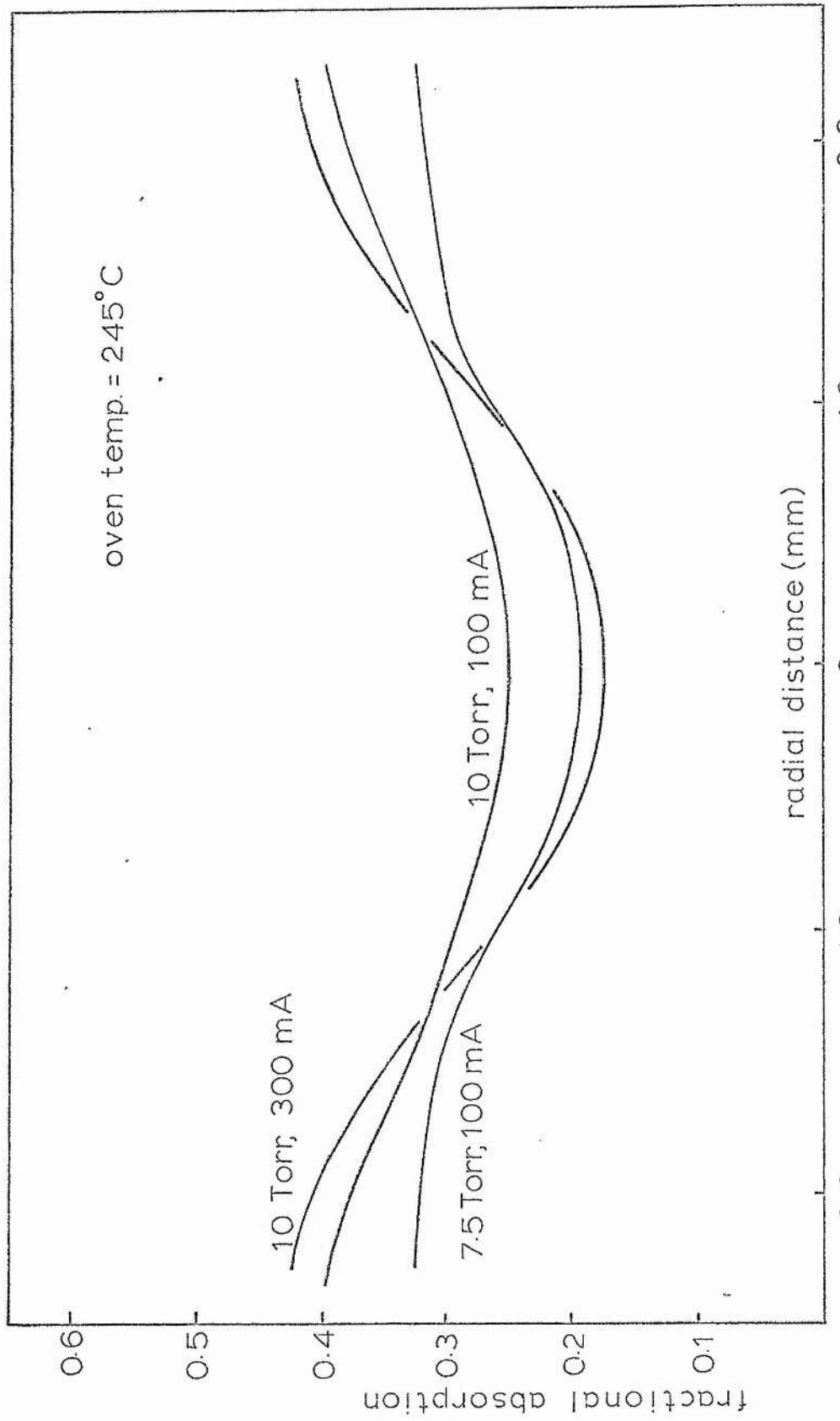

Fig. 4.3 Radial profiles of the fractional absorption of 3404Å, indicating the behaviour of the reduced cadmium metastable $5p\,^3P_o$ density.

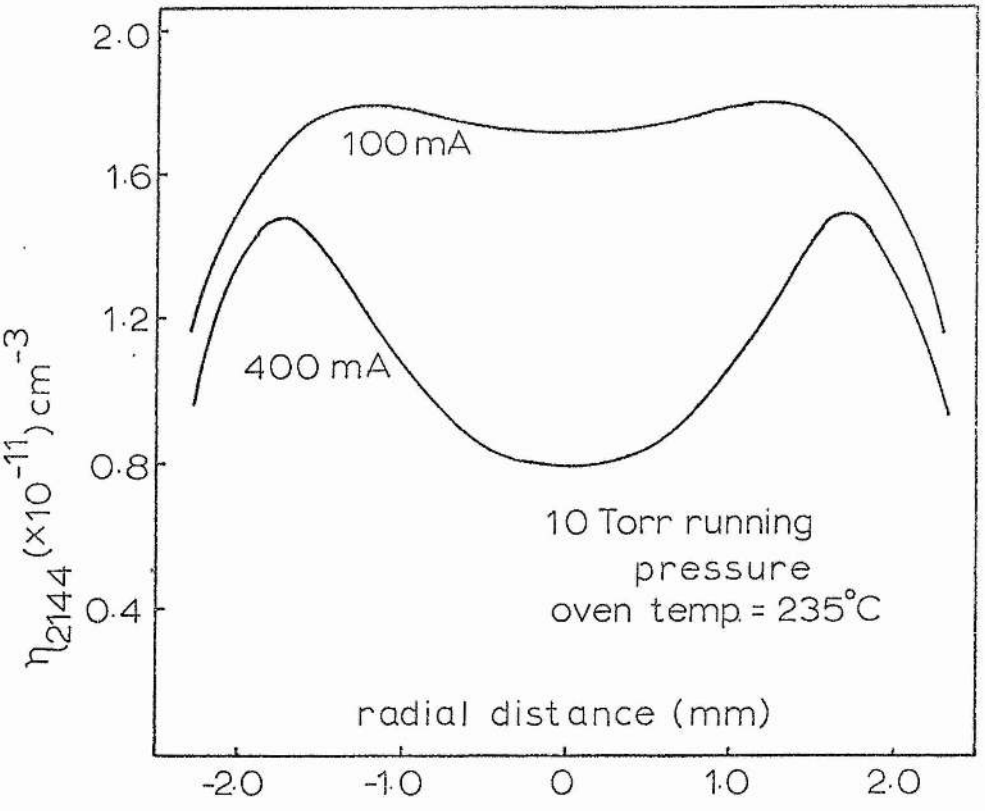

Fig. 4.4 Radial profiles of the reduced cadmium ion ground-state density, n_{2144}.

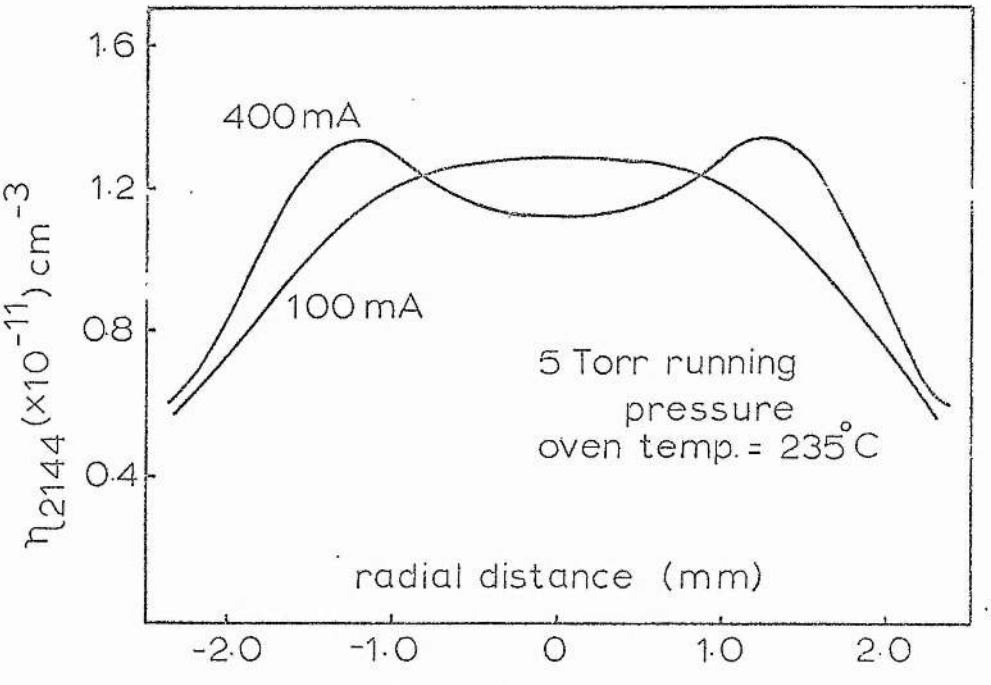

Fig. 4.5 Radial profiles of the reduced cadmium ion ground-state density, n_{2144}.

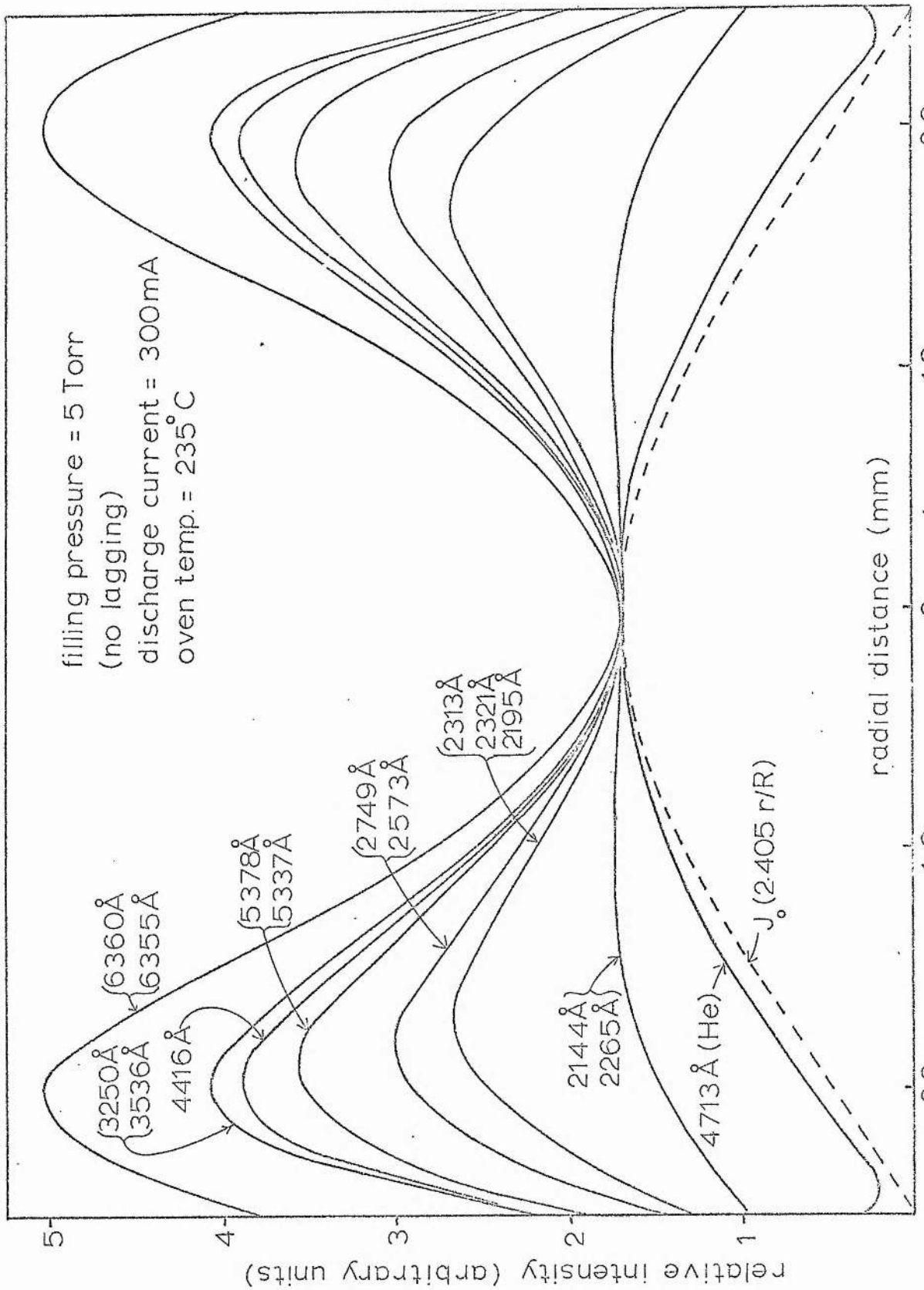

Fig. 4.6 Set of radial emission profiles taken under the same discharge conditions.

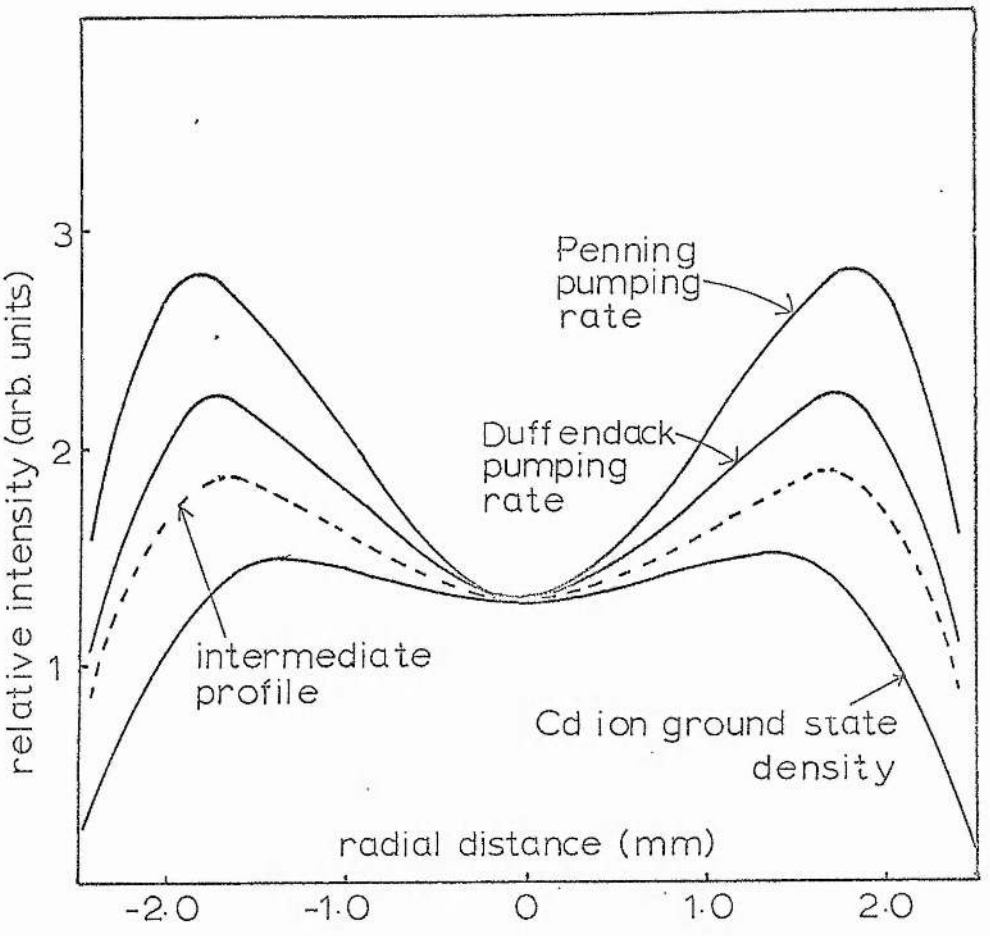

Fig. 4.7 General relative appearance of different pumping processes. The dotted profile intermediate between the Penning profile and the cadmium ion ground state profile is taken as an example of how the profile of a long-lived Penning-excited state may be smoothed by diffusion.

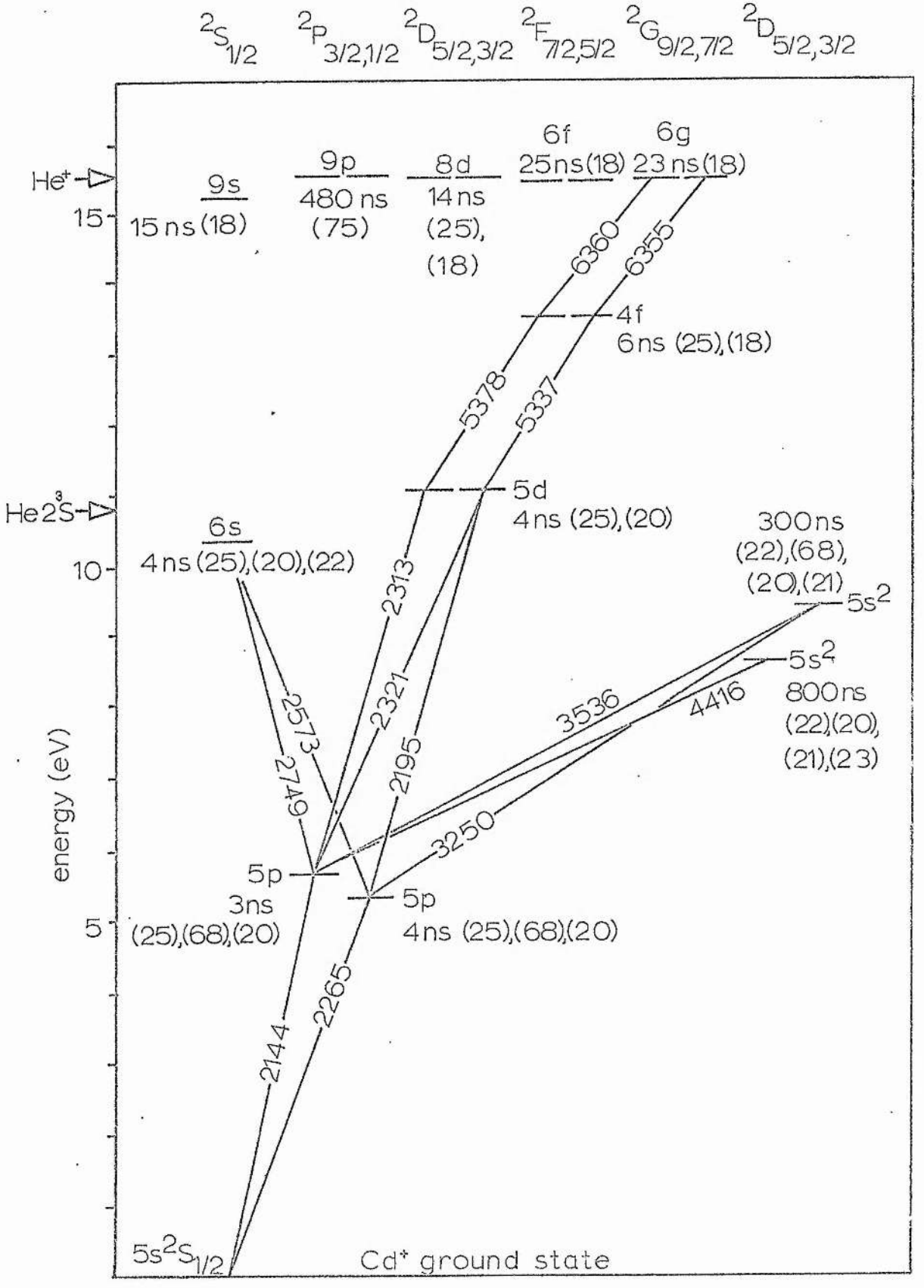

Fig. 4.8 Energy levels of the cadmium ion. References to the state lifetimes are given in brackets.

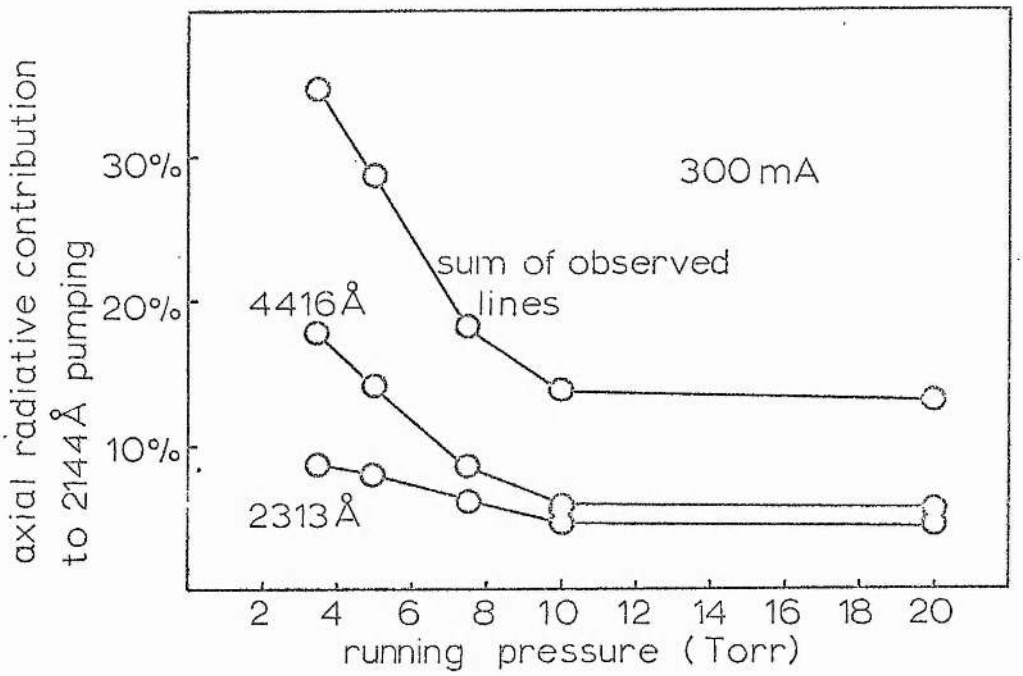

Fig. 4.9

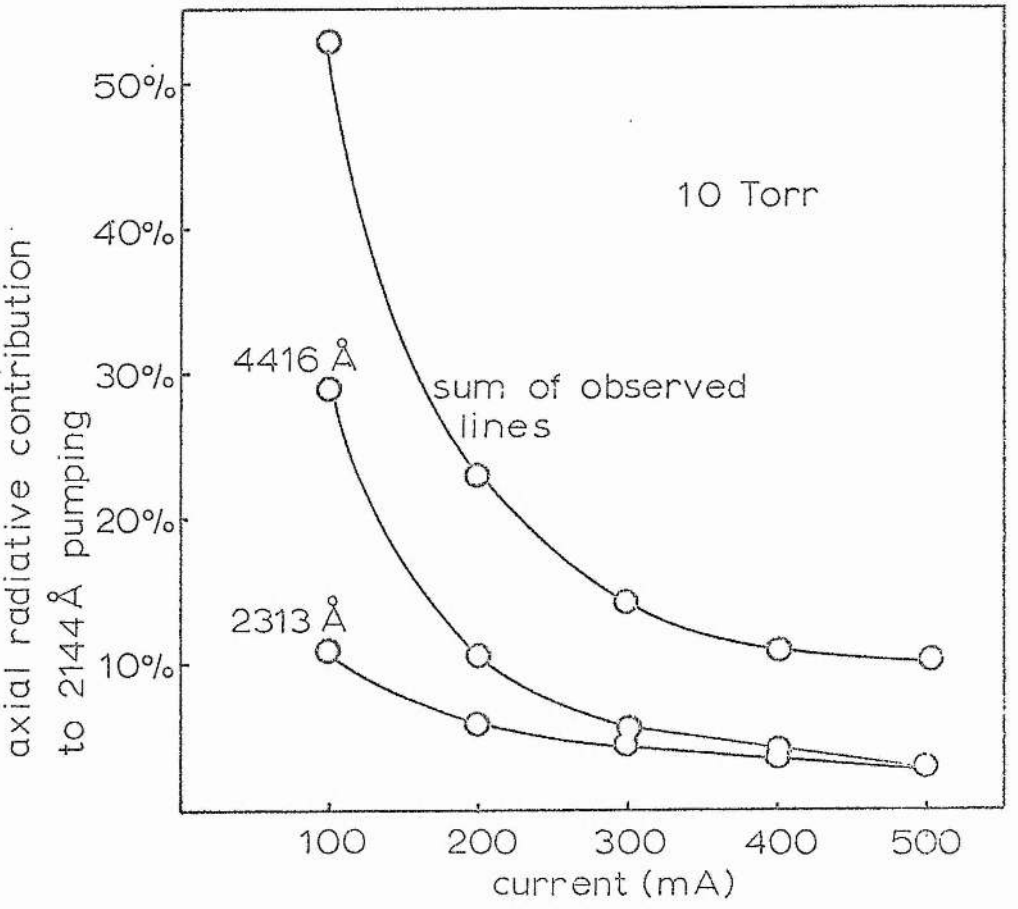

Fig. 4.10

Fig. 4.9, 4.10 Axial radiative contribution to the 2144Å transition.

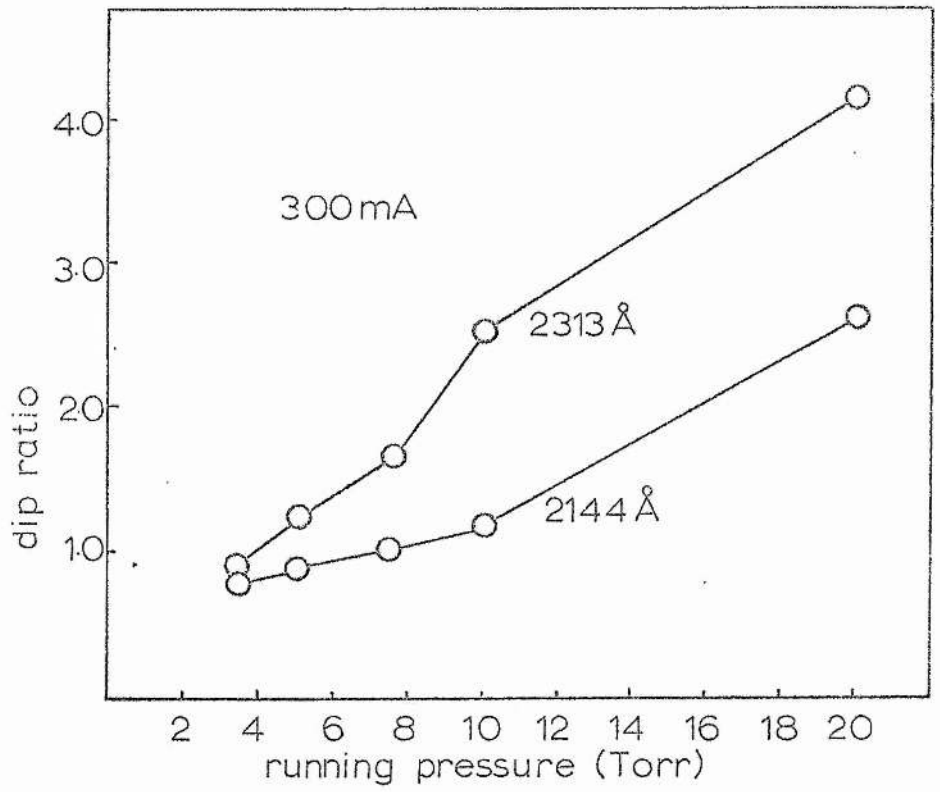

Fig. 4.11

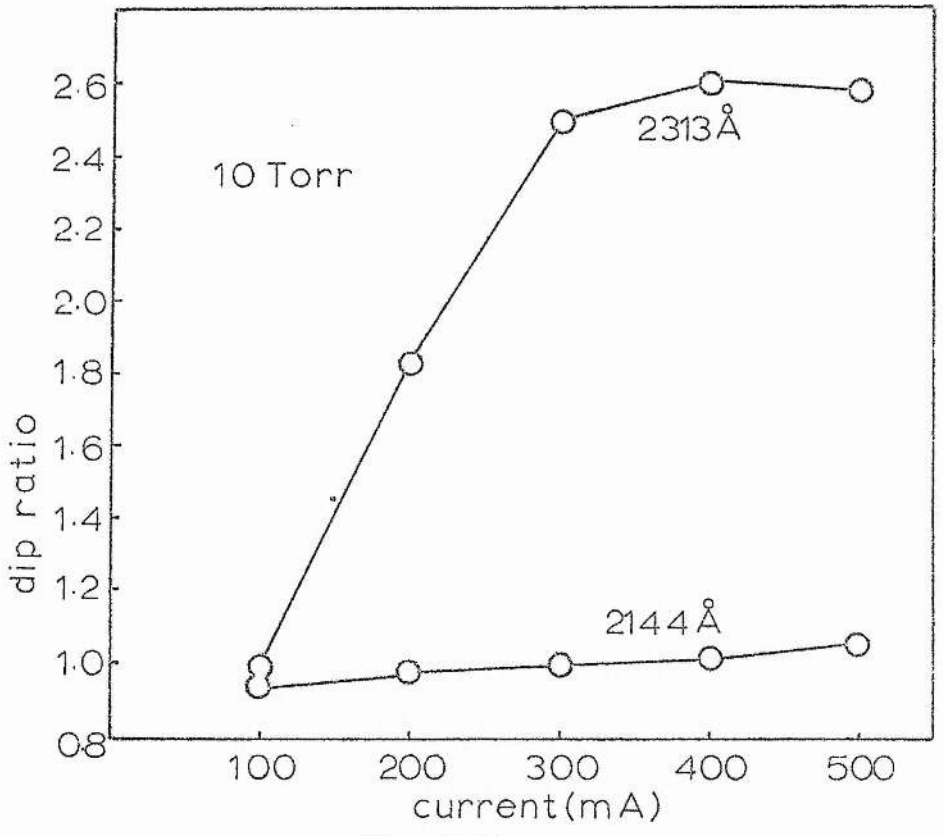

Fig. 4.12

Fig. 4.11, 4.12 Comparison of dip ratios at 2313Å and 2144Å

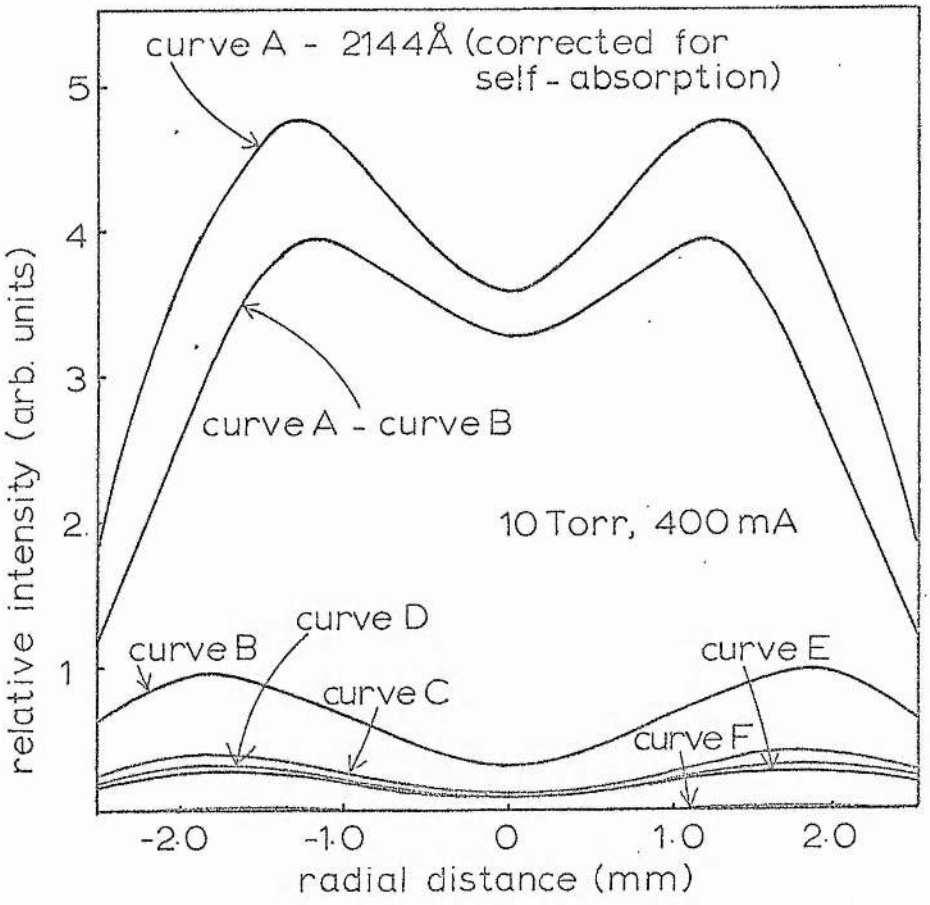

curve A - 2144Å (corrected for self-absorption)
curve B - sum of 4416Å, 3536Å, 2749Å, 2321Å and 2313Å

curveC - 4416Å
curve D - 2313Å
curveE - 2749Å
curve F - 2321Å and 3536Å

Fig. 4.13 Relative radiative contribution of 5 transitions cascading into the 2144Å upper level.

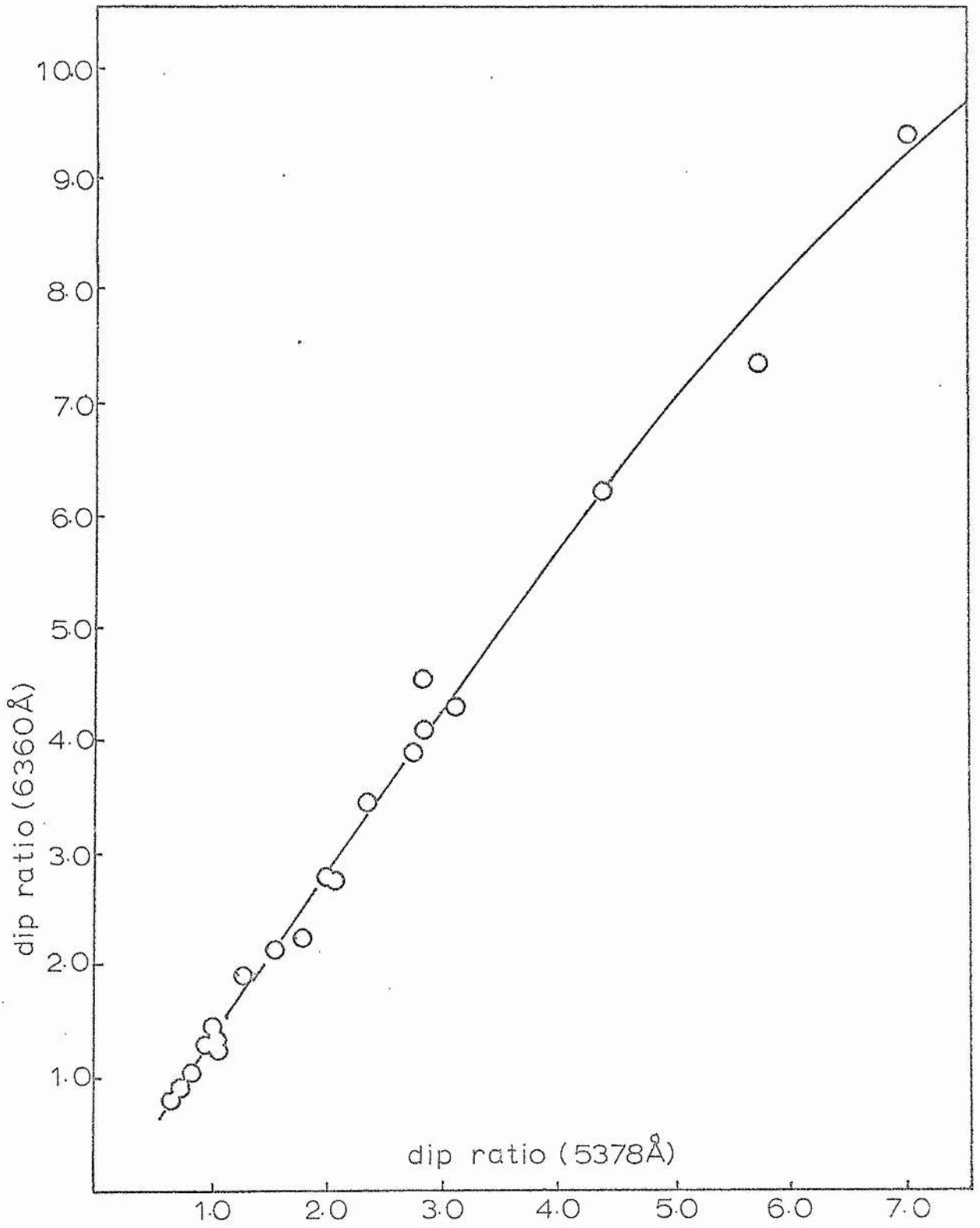

Fig. 4.14 Dip ratio of 6360Å vs. dip ratio of 5378Å for 20 discharge conditions.

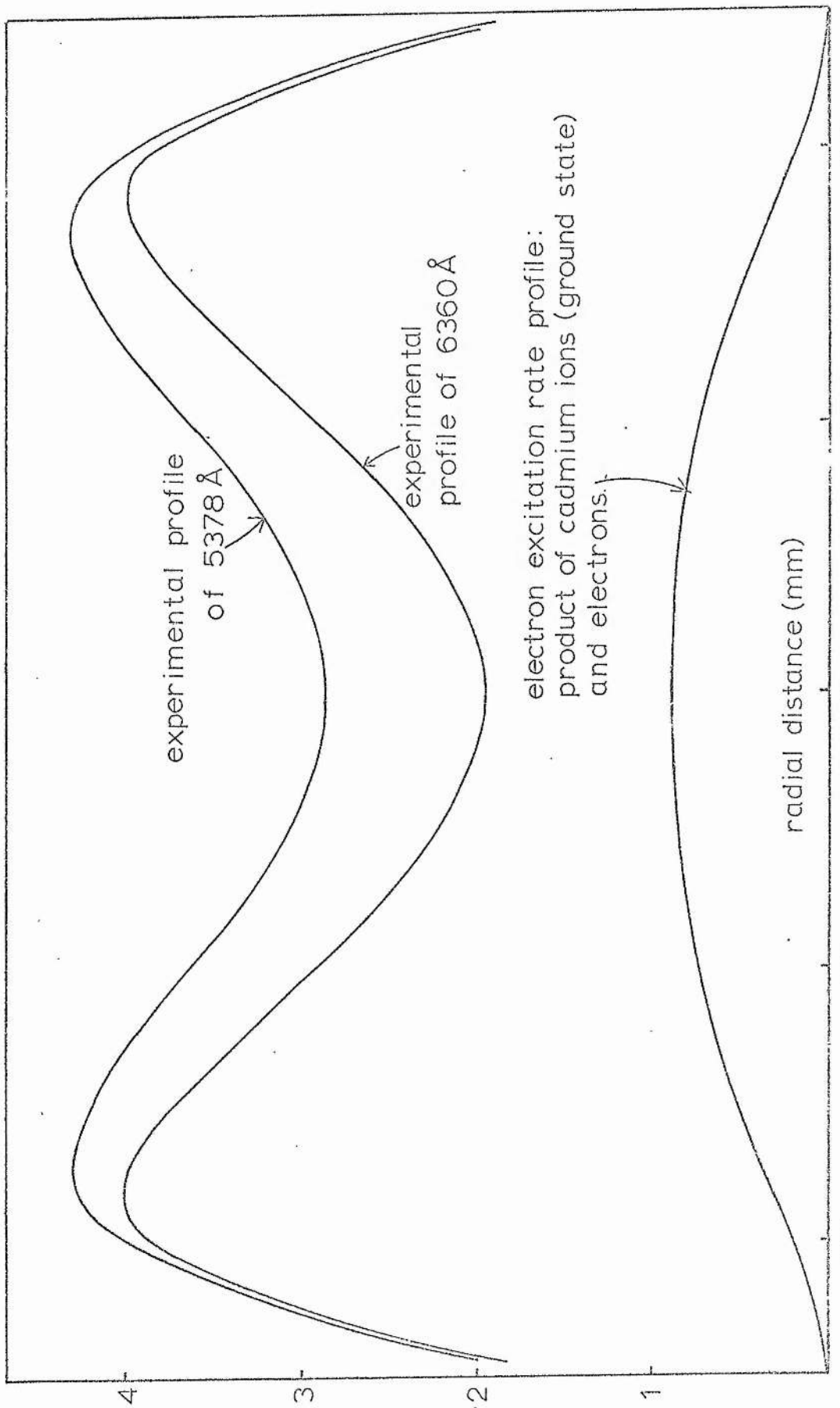

Fig. 4.15 Addition of Duffendack pumping and electron excitation from the Cd ion ground state to produce the profile of 5378Å.

CHAPTER V

OVEN TEMPERATURE DEPENDENCE OF RADIAL PROFILES

Abstract

The dip in the radial profile of 6360Å remains reasonably unaffected by increasing the cadmium partial pressure in the dishcarge. This suggests that the principal ionisation species of cadmium cannot be helium ions or metastable atoms, the overall density of which must decrease with increasing oven temperature.

5.1 Introduction

In this chapter we examine the dependence of the radial profiles on cadmium partial pressure. These experiments will enable us to decide which of the three processes, electron ionisation, Penning or Duffendack reactions is the most important in ionising the cadmium.

In Chapter II we showed that the dip in the neutral metal atom ground state profile was similar whether the ionisation profile was flat or Bessel-shaped. The size of the dip depended on α which was defined to be proportional to the ionisation rate constant, f, and the electron (or helium ion) density. (In the case where Penning reactions are considered to be a significant ionisation process, a term varying as the helium metastable density would be added to the electron density term in the definition of α.)

Although the density of cadmium may be increased in the discharge, the radial distribution of the neutral ground state species should remain unaffected, apart from the change of scale, provided that the ionisation rate and, hence, α, stay constant. Should either the helium ion density or the triplet metastable concentration be observed to decrease before the neutral dip ratio decreases, then that

particular process is ruled out as an important ionisation mechanism.

5.2 Results and Discussion

Fig. 5.1 shows measurements of the dip ratio in the 10cm tube at 6360Å, the ratio of the sidelight intensities of 6360Å and 3261Å and the axial electric field derived from probe voltages by the method described in Chapter VI. For a given cadmium atom density the sidelight of the 6360Å and 3261Å transitions are taken to vary as the radially-averaged helium ion and electron densities respectively. The effects of any electron pumping of the 6360Å upper level from the ion ground state will be minimised by observing the sidelight rather than, for example, the axial intensity. This is because the sidelight covers emission from right across the diameter of the plasma, including the wings where the cadmium neutral density (and, hence, the Duffendack pumping) is high, but the cadmium ion ground state population (and, hence, the electron pumping) is low. The effect of self-absorption on the 3261Å line is discussed presently but it does not upset the argument.

Measurements are made at 10 Torr, 300mA for various values of oven temperature. The upper limit to the temperatures used is fixed by the onset of discharge instabilities.

As the oven temperature rises, the increased cadmium density lowers the electron temperature which will reduce the pumping rate of helium ions. The electron excitation of cadmium neutral atoms will be much less affected since all neutral cadmium excited levels are less than 9eV above the ground state. (States of lower energy are much less

sensitive to a change in the electron temperature than levels such as those of helium which lie more than 19eV above ground.)

The radial electric field will depend much less sensitively on electron temperature [16] than the ionisation rate of helium and so the lifetime of helium ions in the discharge will not change fast enough to prevent a drop in the helium ion population.

From the decreasing sidelight emission ratio of 6360Å and 3261Å with increasing oven temperature, the helium ion population has dropped by a factor of 2.5 relative to the electron density when an oven temperature of 275°C is reached. Any increase in the absorption on the 3261Å neutral resonance line means that the true 6360Å - 3261Å emission ratio is decreasing still faster with increasing oven temperature. Similarly, at higher cadmium densities, a smaller fraction of the electron population has sufficient energy to excite the 3261Å transition and so the reduction in the helium ion - electron ratio will be even greater than implied by the ratio of intensities.

In order to check that this fall in the helium ion - electron ratio is a consequence of a drop in the helium ion density and is not attributable to an increase in the average electron density, we consider the drift velocity, v_d, of electrons in the discharge. Vokaty and Masek [46] have computed the electron drift velocities in a He-Cd discharge. At 10 Torr, 300mA, the discharge parameters in our experiment are (Table 6.1) $E/N = 10^{-16} Vcm^2$ and $N = 14 \times 10^{16} cm^{-3}$ where E and N are the axial electric field and the helium atom density.

The average electron density, normalised to the helium atom density, is about 3×10^{-5} ($x_e = 3 \times 10^{-5}$ in the notation of ref. [46]). The cadmium density probably does not exceed $4 \times 10^{14} cm^{-3}$ (0.01 Torr) in this series of measurements which corresponds to $n_{cd} < 3 \times 10^{-3}$ in the scheme of Vokaty and Masek. The authors do not calculate the drift velocity for these particular parameters but it is evident that v_d varies little with cadmium partial pressure at a given E/N value. For example, at $E/N = 10^{-16} Vcm^2$ and $x_e = 10^{-7}$, v_d increases by only 20% when the cadmium density is increased from $n_{cd} = 10^{-5}$ (virtually pure helium) to $n_{cd} = 10^{-2}$. Again, at $E/N = 5 \times 10^{-17}$ and $x_e = 10^{-5}$, v_d rises by a similar fraction in going from $n_{cd} = 10^{-5}$ to $n_{cd} = 10^{-2}$. Hence we may conclude that the electron mobility is virtually independent of the cadmium density for the oven temperatures used in this experiment.

The axial electric field does not change significantly before the oven temperature of 275°C is reached, and so, along with the mobility and the drift velocity, the electron density may be assumed to stay virtually constant. Such a conclusion, that the electron density remains reasonably unaffected at high (≥ 7.5 Torr) helium pressures over a wide range of oven temperatures, is supported by Dunn [33] from microwave measurements in a He-Cd discharge.

Although we have measured neither the helium ion nor the electron density directly, our conclusion that the helium ion density is decreasing is reasonable when the metastable density is considered.

Absorption measurements ([14] and Chapter III) show that the helium metastable population is also reduced at higher cadmium partial pressures. If the helium ions are populated by two-step excitation with the metastable levels as an intermediate stage then the production rate will fall with that of the metastables and the electron temperature. If the ions are produced directly from the ground state, the pumping rate will be even more sensitive to the electron temperature.

So there is strong evidence that the helium ion density drops while the graphs show that the dip ratio of 6360Å remains relatively high.

Although the helium ion density has decreased, the departure from a zero-order Bessel-shaped radial profile will not be serious. It might be suspected that the wings of the cadmium ion ground state profile would, through the requirements of charge quasi-neutrality, result in a severe depletion of helium ions near the walls. However the probability that an electron makes an ionising collision will be greater near the walls where there is a high concentration of cadmium vapour than near the axis. So a radial profile of electron density will tend to be higher at the wings than for the pure helium case, which will help to accommodate the higher peripheral cadmium ion concentration. In any case, absorption results (Chapter IV) show that the cadmium ion ground state profile is much less pronounced at the wings than the excited species.

In the light of the constant dip ratio of 6360Å, any suppression near the walls which the helium ion density <u>does</u> suffer simply emphasises that the ground state <u>neutral</u> cadmium dip does not decrease

with increased oven temperature.

From the apparent lack of dependence of the ground-state neutral dip on the helium ion and metastable populations we may conclude that the ionisation rate of cadmium depends not on the density of helium ions or metastable atoms but largely on the electron population. It may be imagined that the reduction in electron temperature at higher oven temperatures would result in a smaller ionisation rate of cadmium, but, just as with the excitation of neutral cadmium states, the ionisation of the metal atoms will not be so greatly affected as the helium ion production. It is important to notice that the radial variation of the ionisation probability per cadmium atom may change slightly as the metal vapour pressure is increased, owing to the possible electron temperature non-uniformity. However we can see from Chapter II that the dip is dependent on the average ionisation in the discharge rather than the particular radial dependence.

The theoretical ionisation rate per cadmium atom may be estimated using an approximate value of $4 \times 10^{-15} cm^2$ [34, 35, 24] for both the Penning and the Duffendack cross sections and $2 \times 10^5 cm\ s^{-1}$ for the relative velocity of cadmium atoms and helium ions or metastable atoms. With a rough figure of $5 \times 10^{12} cm^{-3}$ for both the helium ion and metastable densities, the ionisation probability per cadmium atom for each process is $4 \times 10^3\ s^{-1}$. The corresponding result for electrons, using an energy-averaged cross section of $10^{-16} cm^2$ and an electron velocity of $10^8 cm\ s^{-1}$, is $5 \times 10^4\ s^{-1}$. Thus order-of-

magnitude calculations bear out the experimental suggestion that electron collision is the most important process in the ionisation of cadmium.

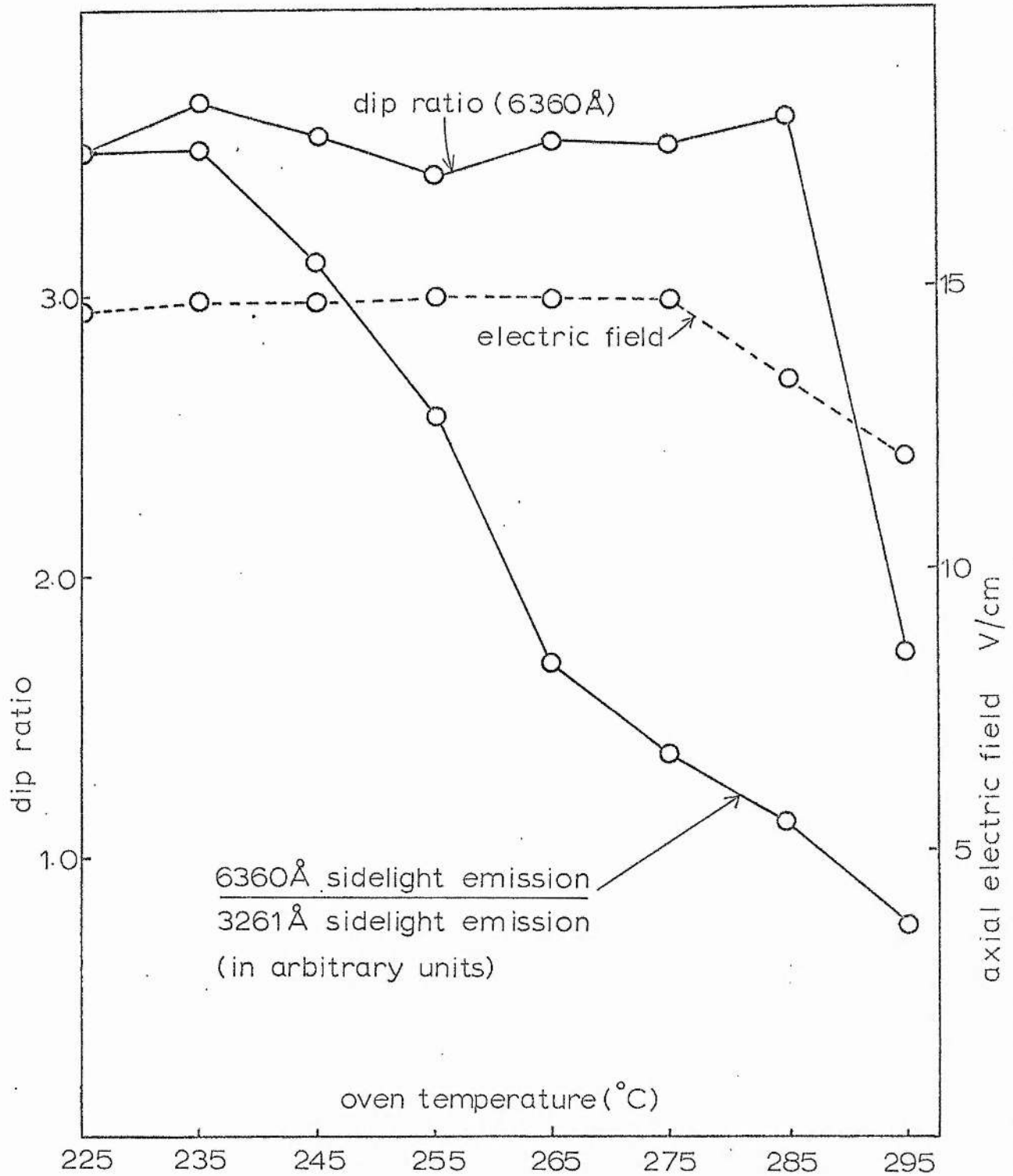

Fig. 5.1 Cadmium oven temperature dependence of 6360Å dip ratio, axial electric field and ratio of 6360Å sidelight to 3261Å sidelight.

CHAPTER VI

THE IONISATION RATE CONSTANT OF CADMIUM IN A HELIUM-CADMIUM DISCHARGE

Abstract

The model for the dip effect is tested by using it to predict values for the ionisation probability of cadmium. These values are collinear when graphed against E/N for widely differing discharge conditions and show a behaviour consistent with that expected for an electron ionisation process. A typical ionisation rate constant (at $E/N = 1.5 \times 10^{-16} Vcm^2$) is $3 \times 10^{-8} cm^3 s^{-1}$. Estimations of the electron ionisation of cadmium from the ground and metastable states agree with this figure. The fractional ionisation of cadmium is shown to increase with current and pressure.

6.1 Introduction

This chapter examines quantitatively the behaviour of the profile dips with changing discharge conditions.

The parameters on which the dip depends, electron density (N_e), and the binary diffusion coefficient (D) of cadmium in helium, cannot be varied independently of each other for a given discharge tube. D depends strongly on gas temperature which in turn is determined by the current (and the convection losses to the atmosphere which depend on the diameter of the tube and whether it is lagged or not). N_e also changes with helium pressure for a given current and so too, of course, does D. One way to circumvent this would be to treat α as a discharge parameter and to graph values of the dip against α instead of pressure and current explicitly,

under various discharge conditions. If the expression for the profiles is valid then not only should the graph be of the correct scale and shape but also the experimental points would be collinear, justifying the use of α as a parameter.

Unfortunately this is not feasible because the form and magnitude of f, the ionisation rate constant, is not known. If the principal mechanism is electron ionisation, f may change appreciably with different discharge conditions. Nevertheless the status of α as a parameter may be investigated by rearranging equation (2.4) to give

$$f = \frac{\alpha D}{N_{eo} \lambda R^2} \qquad (6.1)$$

and then examining the dependence of f on the specific electric field, E/N, where N is the helium atom density. E/N is a measure of the electron temperature (ref. [30] Chapter 8) provided the fractional energy loss per electron collision is not affected by the varying cadmium concentration. This indicates that we should work at low oven temperatures for this experiment. If α is to be meaningful as a discharge parameter, there should be a functional relationship between f and E/N, since f will be an explicit function of the electron temperature.

6.2 Experiment

Observations are made with the 10cm tube at an oven temperature of 225°C for 25 conditions of filling pressure and current (Table 6.1). Values of the neutral ground-state dip are derived from measurements of the dip at 6360Å by dividing this by the dip ratio, 0.4, for a zero-

order Bessel function with the first zero at the tube walls (Table 6.1). (This assumes that this transition is excited mainly by helium ions in Duffendack reactions as discussed in Chapter IV. The ionisation probabilities derived from this experiment would need to be increased slightly if electron pumping of the 6g $^2G_{9/2}$ level from the ion ground state were significant.) The assumption of the Schottky solution for the helium ion profiles has been justified following the discussion in section 4.3.7. The value of α corresponding to a particular dip (Table 6.1) is assigned from a computed graph of the neutral ground-state dip vs. α (Fig. 6.1) using equation 2.2 (see Appendix I).

6.3 Determination of Dishcarge Parameters

The axial electric field was found from the voltage measured by a valve voltmeter between two probes in the discharge. The probes were sharpened tungsten rods enveloped in fused quartz sheaths except for the exposed tips. Because of the symmetry of the arrangement it is assumed that the readings give a true indication of the plasma potential difference between the two tips. The electric fields found with various probe separations agreed to within 10%.

To find the gas temperature, a calibrated iron-constantan thermocouple was placed in contact with the discharge tube and the tube was then well lagged with asbestos tape and aluminium foil. In this way the thermocouple gives a reasonably accurate indication of the outside wall temperature (see Table 6.1). The inside wall temperature was calculated from the thermocouple results, the thermal conductivity of fused quartz and the power input to the

discharge. Neglecting heat transfer by radiation, this gives an expression 0.0353W C^{o} for the temperature drop across the wall where W is the power input in Watts m^{-1}, found from the electric field and the discharge current.

Conditions inside the discharge tube are well removed from thermal equilibrium and the gas temperature at the wall is not necessarily that of the wall itself. Assume that for every helium atom which strikes the wall with energy $\frac{3}{2}kT_g$, where T_g is the peripheral gas temperature, an atom leaves the wall with energy $\frac{3}{2}kT_w$ where T_w is the temperature of the inside quartz surface. Since this occurs with frequency $\frac{1}{4}Nc.2\pi R$ per unit length (N is the atom density and c is the average speed of the atoms) the total power per metre conducted by atoms to the walls is $\frac{3}{2}k(T_g - T_w)\ \frac{1}{4}Nc2\pi R$. Energy transfer by radiation and ion recombination at the walls are separate processes. The above power loss is balanced solely by the energy derived by gas atoms from elastic collisions with electrons and from collisions with helium ions. Inelastic processes lead ultimately to radiation or ionisation - cross sections for second-kind collisions between metastable atoms and unexcited atoms with the release of heat are small enough to be negligible [36]. The above expression must be equated to the elastic power loss of electrons and the power losses of the helium ions which will now be estimated.

The fractional energy lost by an electron of energy E_2, mass m, in colliding with atoms of average energy E_1, mass M, is $\frac{2m}{M}\ (1-\frac{E_1}{E_2})$ per collision [37]. Under the present conditions this may be simplified to $\frac{2m}{M}$. Thus the total power per unit length given by

electrons to gas atoms in elastic collisions is

$$\frac{2m}{M} \langle E_2 \nu \rangle \langle N_e \rangle \pi R^2$$

Brackets < > denote averaged quantities. The electron density N_e is spatially averaged here. ν is the momentum transfer collision frequency of electrons with helium atoms. Using the momentum - transfer cross section for electrons in pure helium [38], the collision frequency for an atom density, N_o, of $3.54 \times 10^{16} cm^{-3}$ rises to a plateau of about $3.2 \times 10^{9} s^{-1}$ above 5eV. Treating ν/N_o as a constant ($3.2 \times 10^{9} \div 3.54 \times 10^{16}$) for all electron energies (which will lead to a slight over-estimate) the power in Wm^{-1} derived from elastic collisions is $0.33 N N_{eo} \langle E_2 \rangle$. N_{eo} is the axial electron density in units of $10^{12} cm^{-3}$ assuming a zero-order Bessel distribution. $\langle E_2 \rangle$ is the electron energy in eV. The quantity N (in units of $10^{16} cm^{-3}$) arises because the collision frequency is proportional to the number density.

Results of the power calculations are given in Table 6.1. Values for $\langle E_2 \rangle$, N and N_{eo} had to be estimated before the power could be calculated. To do this, discharge temperatures slightly higher than those of the tube wall were assumed. This gave values for N and N_{eo} from simple kinetic theory and electron drift velocity measurements, using the calculations described presently. The corresponding electron energies were deduced from the T_e vs pR curve of von Engel and Steenbeck (ref. [30] page 243). This assumes a pure helium discharge which is reasonable at very low cadmium concentrations. The final values calculated for N and N_{eo} are close to the estimated values (see Table 6.1) justifying their use in the first instance. The electron energies

originally assumed are similar to those tabulated by Schmit for the corresponding E/p ratios listed in Table 6.1. Comparison from Table 6.1 of the elastic power with the input power shows that the fractional loss through electron elastic collisions, ϕ, is exceptionally large at 20 Torr, 100mA, 200mA. This is probably due to our over-estimation in ν at low electron energies, but an error of even 50% here results in only a 4% difference in the average discharge temperatures obtained later. This is because we are dealing here only with corrections to the temperature estimated from the wall measurements.

Electrons moving within a Debye length of an ion transfer energy to the ion as a result of the long-range Coulomb interactions. The total power given to an ion by electrons of given density and temperature is derived by Glasstone and Lovberg [72]. The power transferred to the helium ions in the present discharges is less than $3Wm^{-1}$ and is therefore neglected in comparison with the elastic loss to the neutral particles (which is greater by one or two orders of magnitude).

Helium ions move under the influence of the radial and axial electric fields in the discharge. The calculated [16] axis-sheath voltage is fairly constant over the range of discharge parameters used in this experiment. This is because the effects of electron mean free path and electron temperature with changing helium pressure tend to cancel each other out. The radial voltage is around 12V.

Since the discharge is diffusion controlled (section 4.3.7) the velocities of the helium ions may be estimated from their mobility. The temperature dependence of the mobility of helium ions in their parent gas has been examined by Chanin and Biondi [70] and is slowly varying in the gas temperature range of the present discharges. The mobility may be written

$$\mu = \frac{2.7}{N} \, m^2 V^{-1} s^{-1}$$

where, as before, N is in units of $10^{16} cm^{-3}$.

Just before it recombines at the wall a helium ion is unlikely to be travelling any faster than $3 \times 10^5 cm \, s^{-1}$ from consideration of the mobility and the radial voltage. This sets an upper limit of 0.2eV to its kinetic energy. Hence its kinetic energy is generally negligible compared with the energy it has acquired in travelling in the radial field direction from its point of creation. This energy must have been transferred to the plasma either through elastic collisions with helium atoms or by charge-transfer collisions producing fast neutral helium atoms and slow helium ions. Hence the helium ions contribute to the heating of the plasma.

Because the exact expression of the radial variation of the electric field is complicated (for example, see Fowler [71]) we make the assumption that both the field and the helium ion density are constant across the radius. This will lead to a radially-independent power loss from the ions. Although in fact the helium ions are more concentrated near the axis, the radial field goes to zero there, by symmetry,

leaving only the weaker axial field. The decrease in density with increasing radius will tend to be balanced by the increasing radial field and so the assumption of a constant power loss is reasonable in this respect. As in the case of electron heating, the effect of errors here is small in the gas temperatures determined ultimately. The assumed radial field will be therefore $12 \div \frac{1}{4} = 48 Vcm^{-1}$ in the discharges in the investigation. The vector sum of the radial field and the largest axial field found in this experiment ($20 Vcm^{-1}$) is $52 Vcm^{-1}$ and so the axial field is neglected for the purposes of calculating the ion power loss.

As we have seen, the helium ions derive their energy from the electric field (the energy then being lost again as heat). The power given to a helium ion (and, hence, the power given to the discharge as heat by a helium ion) is

$$\text{power} = eEv = e\mu E^2 = e\mu V^2/R^2$$

where v is the ion drift velocity and V is the voltage (12V) from the axis to the edge of the sheath. The total power produced per metre is

$$e\mu \frac{V^2}{R^2} \pi R^2 \langle N_{He^+} \rangle$$

$$= e \pi \mu V^2 \langle N_e \rangle$$

$$= 85 \frac{N_{eo}}{N} \ Wm^{-1}$$

where N_{eo} is in units of $10^{12} cm^{-3}$ as before. The estimated ion power loss is listed in Table 6.1.

From the equivalence of the gas heating and the power loss by gas transport at the walls considered earlier, the temperature of the

gas at the walls, T_g, is calculated. This exceeds the inside wall temperature by a few degrees only.

Since there is heat flow outwards there will be a temperature gradient in the discharge. The fraction of electrons within r of the tube axis is

$$\frac{\int_o^r (1 - \frac{r^2}{R^2})\ 2\pi\ r\ dr}{\int_o^R (1 - \frac{r^2}{R^2})\ 2\pi\ r\ dr} = 2\frac{r^2}{R^2} - \frac{r^4}{R^4}$$

assuming a parabolic radial distrubution. Thus, with a uniform electron temperature across the tube and a constant value of ν for given discharge conditions, the power derived by the gas from elastic collisions with electrons within a unit-length cyclinder of radius r coaxial with the tube is

$$\phi\ W\ (\frac{2r^2}{R^2} - \frac{r^4}{R^4})$$

where ϕ W is the elastic power per metre already calculated. Since we have assumed that the helium ion power generation is uniform across the discharge, the corresponding power gained from the ions in this cylinder is

$$\psi\ W\ (\frac{r^2}{R^2})$$

where ψ is the ratio of the helium ion heating to the total electrical input power, W.

This gas heating is conducted through a thin coaxial cyclindrical shell of radius r and thickness dr. Therefore

$$-2\pi r K(r)\frac{dT}{dr} = \phi W\left(2\frac{r^2}{R^2} - \frac{r^4}{R^4}\right) + \psi W\left(\frac{r^2}{R^2}\right)$$

where K(r) is the gas conductivity at a radius r. Values for K at various temperatures are described well by [39]

$$K' = K_o T^{\frac{1}{2}}$$

where $K_o = 0.011\ Wm^{-1}\ {}^oK^{-1}$. This temperature dependence is predicted by simple kinetic theory [40]. Thus

$$-2\pi r K_o T^{1/2}\frac{dT}{dr} = \phi W\left(2\frac{r^2}{R^2} - \frac{r^4}{R^4}\right) + \psi W\left(\frac{r^2}{R^2}\right)$$

and so

$$\int_{T_o}^{T_r} T^{\frac{1}{2}}\,dT = -\frac{\phi W}{2\pi K_o}\int_o^r\left(2\frac{r}{R^2} - \frac{r^3}{R^4}\right)dr - \frac{\psi W}{2\pi K_o}\int_o^r\frac{r}{R^2}\,dr$$

where the limits of the left-hand integral are temperatures on the axis, T_o, and at r, T_r. Therefore

$$\frac{2}{3}\left(T_r^{3/2} - T_o^{3/2}\right) = -\frac{\phi W}{2\pi K_o}\left(\frac{r^2}{R^2} - \frac{r^4}{4R^4}\right) - \frac{\psi W}{2\pi K_o}\left(\frac{r^2}{2R^2}\right)$$

and

$$T_o^{3/2} - T_g^{3/2} = 16.3\,\phi W + 10.9\,\psi W$$

where T_g is the gas temperature at the wall calculated earlier. This equation is used to derive the axial gas temperatures which may be up to 200 K^o higher than the wall temperature. Results are given in Table 6.1.

If we define an average temperature for any set of discharge parameters as indicating the average atomic number density, N, we have

$$N = \frac{p\,V}{k\,T_{av}} = \frac{p}{k}\int_{o}^{R} \frac{2\pi\, r\, dr}{T(r)} \qquad \text{per unit length}$$

whence

$$\frac{1}{T_{av}} = \frac{2}{R^2}\int_{o}^{R} \frac{r\, dr}{T(r)}$$

where k is the Boltzmann constant, V is the volume of unit length of the discharge and p is the discharge pressure. Using a parabolic distrubution of temperature (which approximates very well to the conductivity-calculated profile) and integrating,

$$T_{av} = \frac{T_o - T_g}{\ln\left(\frac{T_o}{T_g}\right)} \qquad (6.2)$$

This expression is in fact very close to the arithmetic mean of T_o and T_g where these are not very different from each other. For example, at 10 Torr 300mA, the value given by equation (6.2) is 890°K in close agreement with the mean 889°K. The column in Table 6.1 for T_{av} has therefore been taken simply as the arithmetic mean of T_o and T_g.

These temperature measurements were within 20% agreement with those obtained using a scanning Fabry-Perot interferometer with a reflection finesse of 50 to examine the linewidths of the 5016Å helium singlet transition. It was assumed, following Browne and Dunn [11], that the Doppler effect is the most important line-broadening mechanism at these discharge conditions. The measurements were taken of sidelight emission to minimise absorption effects on the line shape. Although this provided a useful check on the gas temperature

calculations, it was decided to use the values derived from wall temperatures in preference to the Doppler values because of the probably smaller errors involved.

The number density N (Table 6.1) is found from the expression

$$N = 2.69 \times 10^{19} \left(\frac{p}{760} \times \frac{273}{T_{av}}\right) \text{ cm}^{-3}$$

derived from simple kinetic theory using Loschmidt's number. The pressure p (in Torr), which must be used is the operating pressure and not the filling pressure.

The electron drift velocity, v_d, was found from the results of Dunn [33] at high E/P values and, at low E/P values, from the results of Nielsen [73] which fit well the accurate measurements of Crompton, Elford and Jory [38] in this region. We use the values of N found above to calculate the appropriate E/P values where p is the pressure at 293°K corresponding to the particular number density in question.

In order that the results of the low electron density experiments of ref [38] may be applied to the present high electron density case, we must check whether the momentum loss process of electrons is affected by the long-range Coulomb interaction between the electrons and ions in the plasma. The relaxation time [72] in which an electron suffers a momentum change comparable to its initial momentum is about the same whether produced by the electrons or the ions in the discharge. This period is no less than about

1.3×10^{-8}s in the present discharges, which is evidently much greater than the collision time for electrons with neutral helium atoms (~ 0.3ns at 1 Torr). Hence we may use the results of ref [38] for the lower E/P values in this experiment.

With a zero-order Bessel function radial distribution of electron density and axial concentration N_{eo}, the current is given by

$$I = e\, N_{eo}\, v_d \int_0^R J_o\left(2.4\,\frac{r}{R}\right)\, 2\,\pi\, r\, dr$$

Integrating gives

$$N_{eo} = 73.5 \times 10^{18}\ \frac{I}{v_d}\ \ cm^{-3}$$

where I is in amps and v_d in cm s^{-1}.

Published values for the binary diffusion coefficient of cadmium in helium, $D_{Cd\ He}$, are not found in the literature. An estimate will be made here first of the magnitude of $D_{Cd\ He}$ at N.T.P. and then of its temperature dependence. For rigid elastic spheres of diameter σ_1, σ_2, Chapman and Cowling [41] give the diffusion coefficient as

$$D_{12} = \frac{3}{8\, N \sigma_{12}^2} \left\{\frac{k\, T\, (m_1+m_2)}{2\pi\ m_1\ m_2}\right\}^{\frac{1}{2}} \qquad (6.3)$$

where N is the total number of atoms per unit volume, $m_{1,2}$ are the masses of the two atomic species and

$$\sigma_{12} = \tfrac{1}{2}\,(\sigma_1 + \sigma_2) \qquad (6.4)$$

The equation (6.3) will be applied only to experimental results to derive a value for σ_{12} in the He-Cd case which will then be

re-substituted into the equation to find D_{12} for cadmium in helium. In this way the error incurred by using this simple model will be minimised.

It is important to establish that $D_{Cd\ He}$ will not vary much with the change in cadmium concentration across the tube. Chapman has derived an expression for the concentration dependence of D_{12} which shows (ref. [41] page 246) that variation with extremes of concentration is less than about 10%. This is in agreement with the results of a series of doctoral dissertations by R. Schmidt, R. Deutsch and A. Lonius reported by Chapman and Cowling (ref. [41] page 248). Also, atomic collisions of cadmium atoms with other cadmium atoms, which are the cause of any variation with concentration, will be so rare at the partial pressures used in these experiments that treatment of the binary diffusion coefficient as a constant for given discharge conditions is a very good approximation.

From the diffusion coefficient of cadmium vapour in nitrogen at N.T.P. [42], equation (6.3) gives a value $\sigma_{Cd\ N_2} = 3.21 \times 10^{-8}$cm. It seems to be characteristic of this equation that the atomic diameters predicted by it are smaller by ~ 10% (ref. [41] page 252) than those derived from viscosity measurements (ref. [41] page 229). However, it is useful to check the results with these figures where possible. If σ_{N_2} for nitrogen obtained from diffusion measurements (as opposed to viscosity results) can be found then σ_{Cd} will be given by equation (6.4). Taking the value of σ_{H_2} for hydrogen to be equal to $\sigma_{H_2\ D_2}$ for a hydrogen-deuterium mixture gives a value for σ_{H_2} of 2.53×10^{-8}cm. from the table in ref. [41] page 252. Thus, from

hydrogen-nitrogen results of the same table, σ_{N_2} is 3.49×10^{-8}cm, which, as expected, is lower than the viscosity-derived figure of 3.8×10^{-8}cm (ref. [41] page 229).

From equation (6.4) σ_{Cd} is now calculated to be 2.93×10^{-8}cm. The results of Walker and Westenberg [43] for diffusion in He-N_2 mixtures imply $\sigma_{He} = 1.85 \times 10^{-8}$cm which again is less than the 2.17×10^{-8}cm predicted by viscosity measurements. The resulting value of 2.39×10^{-8}cm for $\sigma_{Cd\ He}$ is now used in equation (6.3) to give

$$D_{Cd\ He} = 0.74\ cm^2\ s^{-1} \text{ at N.T.P.}$$

Equation (6.3) predicts, for constant number density, N, a square-root dependence of D_{12} on the gas temperature. This model was constructed for rigid atomic spheres of infinite repulsive potential inside their diameters. In general the temperature dependence for a force varying inversely as the ν_{12} th power of the distance is given (ref. [41] page 248) as

$$D_{12} \propto \frac{T^s}{N}$$

where

$$s = \frac{1}{2} + \frac{2}{\nu_{12} - 1}$$

To assign a value to ν_{12} use is frequently made of the repulsive term of the Lennard-Jones potential [44] which varies inversely as the twelfth power of the distance ($\nu_{12} = 13$). (At high temperatures collisions are more penetrating and the attractive term becomes less important.) For lack of more specific experimental data s is calculated for $\nu_{12} = 13$ and so

$$D_{Cd\ He} \propto \frac{T^{2/3}}{N}$$

Since

$$N \propto \frac{p}{T}$$

we have

$$D_{Cd\ He} \propto \frac{T^{5/3}}{p}$$

where p is the operating pressure. The values of $D_{Cd\ He}$ (simply written as D from now on) may now be calculated from the expression

$$D = 0.74 \times \frac{760}{p} \times \left(\frac{T}{273}\right)^{5/3}$$

where p is in Torr and T is in K^{o}.

It is appropriate to consider here whether the effects of thermal diffusion due to the temperature gradient in the gas are large enough to affect the concentration-diffusion explanation of the axial dip in cadmium density. The tendancy in this process is for a concentration gradient to be set up such that [45]

$$\frac{1}{N} \frac{d N_{cd}}{dr} = - k_T \frac{1}{T} \frac{dT}{dr}$$

where N is the total atom density (here, effectively the helium density). If k_T is written

$$k_T = \beta \frac{N_{Cd}}{N}$$

where β is here the thermal diffusion factor, then

$$\frac{1}{N_{Cd}} \frac{dN_{Cd}}{dr} = - \beta \frac{1}{T} \frac{dT}{dr}$$

For the collision diameters of helium and cadmium and for their atomic masses, β is of the order unity (ref. [45], Chapter 2). For the worst case of a $200K^{o}$ difference in the axis-wall temperatures

(at 20 Torr, 500mA), the fractional increase of cadmium in going from the axis to the wall will be only 0.15 which is negligible compared with the factor of 20 for the 0.7R - axis ratio in the concentration diffusion case. At lower values of the dip the temperature gradient is correspondingly less and so we may conclude that thermal diffusion is not a complicating factor.

6.4 Results

From equation (6.1) the calculated values of the ionisation rate constant, f, in the Table are graphed against E/N in Fig. 6.2. Three features emerge from the graph and the tabulated values of f:

(1) In view of the wide variation of discharge conditions and considering the number of experimental values and assumptions required to calculate each value of f, the points are remarkably collinear, which is a necessary requirement for α to be a meaningful and useful parameter.

(2) The ionisation rate constant, f, increases with E/N which is consistent with the proposition (Chapter V) that cadmium is ionised principally by electron collisions. Such an explicit dependence of f on E/N is unlikely in the case of either Penning or Duffendack reactions.

(3) In general the ionisation rate of cadmium is higher than would be expected if the principal process were Penning collisions with helium metastable atoms. The experimentally deduced ionisation rate, $N_e f$ (= 0.43 $N_{eo} f$), ranges from 2.5 x 10^4 s^{-1} at 100mA to 14 x 10^4 s^{-1} at 500mA and is fairly independent of pressure. On the other hand,

the metastable densities in a pure helium discharge lie between $4 \times 10^{12} cm^{-3}$ and $8 \times 10^{12} cm^{-3}$ [11] in conditions similar to those in the present cases. Thus with a Penning ionisation cross section of $4.5 \times 10^{-15} cm^2$ [34], the rates lie between 0.4 and $0.7 \times 10^4 s^{-1}$. Clearly electron ionisation is the dominant process, although at low currents the Penning contribution is becoming important, especially if other excited helium states apart from the metastable levels participate in the Penning reactions.

The rate constant, $\langle \sigma v \rangle$, for Duffendack reactions is around $1.2 \times 10^{-9} cm^3 s^{-1}$ [24] which is generally less than f by more than an order of magnitude. Again electron ionisation seems to be the dominant mechanism.

We now calculate whether such a large electron ionisation rate constant is reasonable. Vokaty and Masek [46] have graphed the ionisation cross section of cadmium ($5s\ ^1S_o \rightarrow Cd^+$) using semi-empirical formulae. Using this, and the electron energy distribution functions for helium discharges operating under the present conditions [47, 48, 49], the energy-averaged cross section is about $0.7 \times 10^{-16} cm^2$. This gives an ionisation probability, $\langle \sigma v \rangle$, at E/P = 5 V cm^{-1} $Torr,^{-1}$ of about $0.7 \times 10^{-8} cm^3\ s^{-1}$ with an average electron velocity, c, of $10^8 cm\ s^{-1}$. There will also be a contribution from the ionisation of the metastable species $5p\ ^3P_{2,o}$ present in the discharge. Savchenko [50] has calculated cross sections for the excitation of these two levels from the ground state, and averaging with an electron distribution as above at E/P = 5 V cm^{-1} $Torr,^{-1}$ gives a total cross section of $1.5 \times 10^{-16} cm^2$. Savchenko points out that

his results are about twice those found by Penkin and Redko [51] but that the latter authors' cross sections are not in the ratio of the statistical weights of the levels. (However this argument may be suspect considering that the L - S coupling is broken in these singlet-triplet transitions.)

If the metastable population is considered to be nearly saturated as a result of the high loss rate by electron ionisation compared with other loss processes, then Savchenko's figures imply a further 1.5×10^{-8} cm^3 s^{-1} to the ionisation probability in addition to that for ionisation directly from the ground state. A classical calculation [52] of the cross section for ionisation of a cadmium metastable state yields an energy-averaged value of 2.5×10^{-16} cm^2 at E/P = 5 V cm^{-1} $Torr^{-1}$. The variation with energy of this classical cross section compares well with the calculations of Penkin and Redko [53] at near-threshold values of electron energy but the comparison may not be extended to high energies since their work assumes an electron temperature of only 1 or 2eV. With this classical cross section the ionisation rate of the cadmium metastables is 1.3×10^5 s^{-1} in an environment of 5×10^{12} electrons cm^{-3}. This is greater than the diffusion rate which is 2×10^4 s^{-1} for D = 200 cm^2 s^{-1}. Since the $5p\ ^3P_1$ state (the upper level of the 3261Å transition) lies only 0.07eV above the $5p\ ^3P_0$ state there may be considerable mixing of the two states as a result of collisions with normal helium atoms. In the limit this introduces

an effective radiative lifetime to the metastable state (via the resonance state) of 3μs [22]. Such a radiative loss rate of 3×10^5 s^{-1} would mean that the metastable states are not completely saturated with respect to electron density. Nevertheless, the electron ionisation rate is competitive even in this limit of complete thermalisation and we regard our earlier estimate of the contribution of the metastable states to the ionisation of the cadmium ground state population as an upper limit. (Another consideration which will reduce our estimate is the fact that electronic collisions with metastables lead not only to ionisation but also to the excitation of neutral levels. Although most of these excited states will radiate back into the metastable levels, some will decay into the upper levels of the 3261Å transition.) If, however, the departure from the saturation condition were serious, while, at the same time, ionisation from the metastable states continued to be an important process, equation (2.2) would need to be modified to accommodate a term in N_e^2 which would introduce an electron density-dependent term into the ionisation rate constant, f. Since the results of Fig. 6.2 show no explicit dependence on electron density we conclude that either the metastable contribution to the ionisation process is not large, or that the metastable populations are in a condition of near-saturation with respect to electron density. Nevertheless, we have shown that both the processes of direct electron ionisation from the cadmium ion ground state and of ionisation of the cadmium metastable atoms have rate constants (0.7×10^{-8} cm^3 s^{-1} and 1.5×10^{-8} cm^3 s^{-1})

at a given E/P value (5 V cm^{-1} $Torr^{-1}$) which are of the same order of magnitude as the corresponding f value (3 x 10^{-8} cm^3 s^{-1}) derived from the dip ratio.

One further check on the order of magnitude of the ionisation probability is provided by calculating the average fractional ionisation of cadmium, γ. At 3.5 Torr, 100mA the cadmium ion lifetime is about 10^{-6}s. With a creation rate, $N_e N_{cd} f$, of $\sim 2 \times 10^4 N_{cd}$ cm^{-3} s^{-1}, the cadmium ion density is

$$N_{cd+} = 2 \times 10^4 N_{cd} \times 10^{-6}$$

which gives

$$\gamma = 2\%$$

for the percentage ionisation. This is of the same order of magnitude as Sosnowski's result [2] of 0.7% at 60mA and 2.7 Torr in a 4mm bore discharge. For a given current the ionisation rate at the centre of the tube is almost independent of pressure. (This is deduced by multiplying N_{eo} by f in Table 6.1.) However for a given current the ion lifetime increases with pressure and so, therefore, must the fractional ionisation at the axis. Similarly, for a given pressure the ionisation rate increases with current. Hence, in general, the fractional ionisation of cadmium on the tube axis increases with current and pressure. This point is relevant to the discussion of the radial profiles of 2144Å emission (section 4.3.3).

6.5 Conclusion

It has been shown in this Chapter that the behaviour of the radial profiles is consistent with electron collisional ionisation of the

metal as the main ionisation process in the He-Cd discharge where the metal vapour concentration is kept low. Since the dip changes little with a wide variation in oven temperatures (Chapter V) and since the Penning and Duffendack reactions can contribute only a few percent to the ionisation rate, it is expected that electron ionisation will continue to be the most important process at oven temperatures upto the region of discharge instability.

filling pressure (Torr)	discharge current (mA)	running pressure (Torr)	dip ratio at 6360 Å	implied Cd neutral ground-state dip ratio	dip parameter, α
3.5	100	3.9	0.80	2.00	7.7
"	200	4.3	1.15	2.88	12.6
"	300	4.5	1.35	3.38	15.2
"	400	4.7	1.45	3.63	16.4
"	500	4.8	1.65	4.13	18.4
5.0	100	5.9	1.20	3.00	13.4
"	200	6.3	1.70	4.25	18.9
"	300	6.5	2.05	5.13	22.2
"	400	6.9	2.30	5.75	24.2
"	500	7.3	2.90	7.25	28.6
7.5	100	8.1	1.35	3.38	15.2
"	200	9.2	1.95	4.88	21.2
"	300	9.6	2.65	6.63	26.9
"	400	10.0	3.25	8.13	30.9
"	500	10.3	3.65	9.13	33.3
10.0	100	11.5	2.00	5.00	21.7
"	200	12.5	3.40	8.50	31.8
"	300	12.8	5.45	13.6	42.2
"	400	13.5	6.50	16.3	46.4
"	500	13.9	7.50	18.8	49.8
20.0	100	22.6	4.00	10.0	35.3
"	200	24.8	7.50	18.8	49.9
"	300	25.8	9.20	23.0	55.0
"	400	27.0	10.15	25.4	57.7
"	500	27.8	10.15	25.4	57.7

Table 6.1 Observed and calculated discharge parameters

outside wall temp. (^{o}K)	inside wall temp., T_w (^{o}K)	axial electric field ($V\ cm^{-1}$)	input power per metre (W)	guessed electron energy, E_2 (eV)	guessed helium number density, N ($\times 10^{-16}$) cm^{-3}
498	502	12.1	121	7.1	7.5
648	655	12.1	242	8.0	6.3
793	807	13.1	393	8.1	5.3
888	906	12.9	516	8.5	4.8
973	995	12.6	630	9.0	4.3
508	512	12.6	126	5.7	11.0
653	662	12.6	252	6.2	9.1
783	796	12.6	378	6.3	7.5
883	901	12.6	504	6.5	7.0
963	985	12.5	625	7.1	6.8
523	528	14.3	143	5.3	14.0
673	683	13.7	274	5.7	12.5
803	817	13.5	405	5.7	10.7
898	916	13.2	528	5.7	9.7
983	1006	12.9	645	5.7	9.2
558	564	16.7	167	4.8	18.8
698	708	14.6	292	4.8	16.0
818	833	14.2	426	5.1	13.9
923	943	14.0	560	5.4	12.8
1003	1027	13.6	680	5.7	12.0
613	621	21.3	213	3.9	33.0
773	786	18.4	368	4.2	28.0
898	917	17.8	534	4.3	25.0
998	1022	16.9	676	4.4	23.0
1073	1101	16.1	805	4.4	22.0

Table 6.1 (continued)

guessed axial electron density, N_{eo} ($\times 10^{-12}$) cm^{-3}	electron elastic power loss per metre (W)	helium ion power loss per metre (W)	total electron and ion gas heating per metre (W)	gas temp. at tube wall, T_g (^oK)	axial gas temp., T_o (^oK)
1.9	34	22	56	507	529
3.2	54	43	97	664	690
4.0	57	64	121	818	855
4.6	63	82	145	920	962
5.4	70	107	177	1013	1060
2.65	55	20	75	516	547
4.3	82	40	122	669	712
5.5	87	62	149	806	855
6.8	103	83	186	914	970
8.2	132	103	235	1001	1062
3.1	76	19	95	535	577
5.6	133	38	171	691	755
7.3	150	58	208	827	891
9.0	168	79	247	928	1000
10.0	191	100	291	1021	1100
3.5	106	16	122	569	620
6.8	176	36	212	715	790
9.0	214	55	269	843	935
11.3	260	75	335	956	1060
12.9	294	91	385	1041	1155
4.9	213	13	226	625	715
9.8	387	30	417	794	945
13.4	482	46	528	927	1100
17.3	585	64	649	1035	1234
21.6	699	83	782	1117	1350

Table 6.1 (continued)

average gas temp., T_{av} (^{o}K)	helium number density, N ($\times 10^{-16}$) cm^{-3}	reduced electric field, E/N ($\times 10^{16}$) V cm^{2}	electron drift velocity, v_d ($\times 10^{-6}$) $cm\ s^{-1}$	axial electron density, N_{eo} ($\times 10^{-12}$) cm^{-3}
518	7.27	1.66	4.0	1.84
677	6.14	1.97	4.8	3.06
837	5.20	2.52	6.2	3.55
942	4.82	2.68	6.55	4.48
1037	4.47	2.82	6.9	5.33
532	10.7	1.18	2.8	2.63
691	8.80	1.43	3.45	4.26
831	7.56	1.67	4.0	5.51
942	7.08	1.78	4.3	6.84
1032	6.83	1.83	4.45	8.26
556	14.1	1.01	2.4	3.06
732	12.3	1.11	2.65	5.54
859	10.8	1.25	3.0	7.35
964	10.0	1.32	3.15	9.33
1061	9.4	1.37	3.3	11.1
595	18.7	0.89	2.1	3.50
753	16.1	0.91	2.1	7.00
889	13.9	1.02	2.4	9.18
1008	12.9	1.09	2.6	11.3
1098	12.2	1.11	2.65	13.9
670	32.6	0.65	1.5	4.90
870	27.5	0.67	1.55	9.48
1014	24.6	0.72	1.6	13.8
1135	22.9	0.74	1.65	17.8
1234	21.8	0.74	1.65	22.3

Table 6.1 (continued)

diffusion coefficient of cadmium in helium, D ($cm^2\ s^{-1}$)	ionisation rate constant, f ($\times 10^8$) $cm^3\ s^{-1}$
419	2.81
594	3.91
808	5.54
943	5.52
1083	5.98
290	2.36
419	2.97
554	3.57
642	3.63
706	3.91
227	1.80
309	1.89
396	2.32
460	2.44
525	2.52
179	1.78
244	1.77
314	2.31
367	2.41
414	2.37
111	1.28
157	1.32
194	1.24
225	1.17
250	1.03

Table 6.1 (continued)

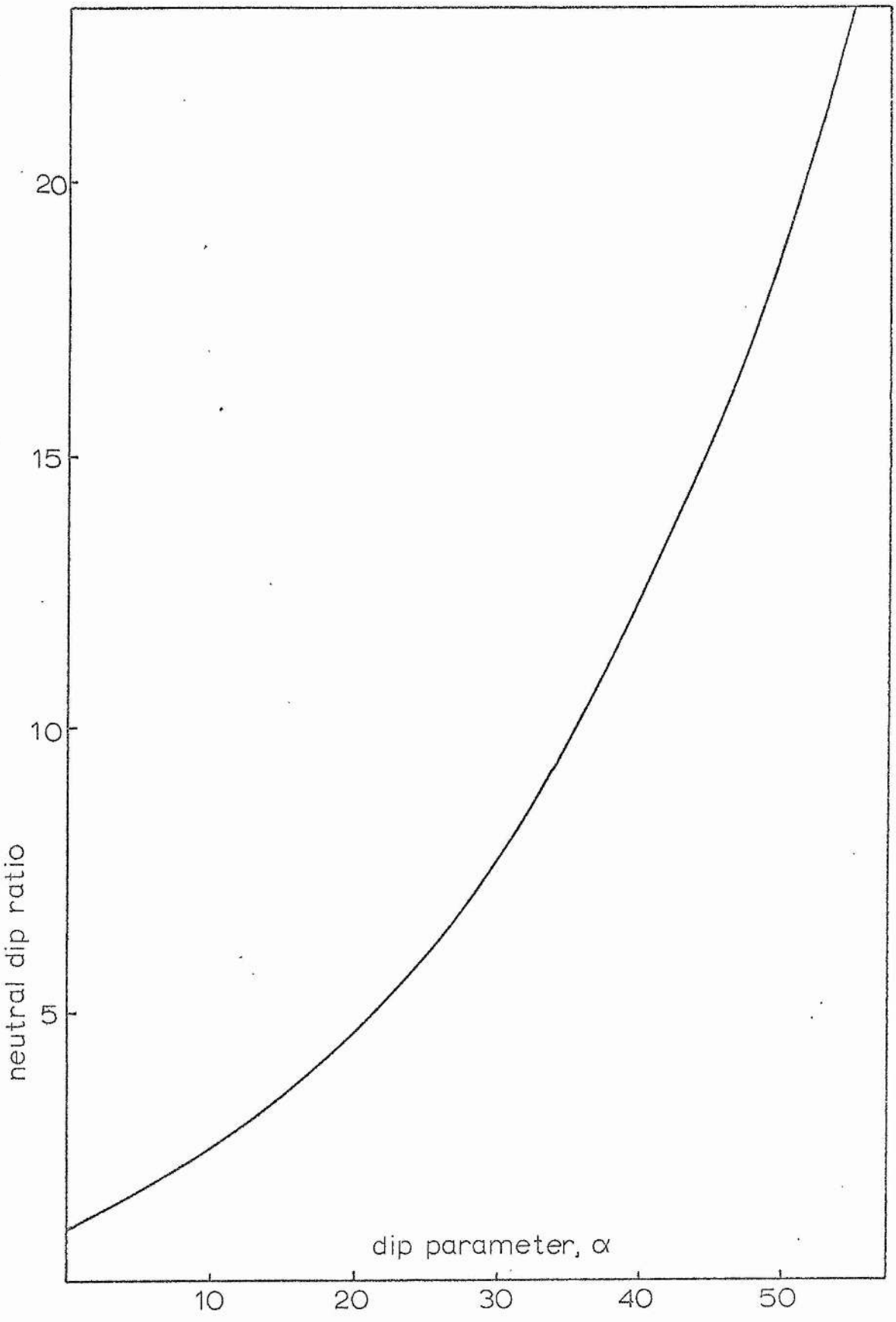

Fig. 6.1 Computed behaviour of neutral ground-state dip vs.α

Fig. 6.2 Ionisation rate constant, f, derived from 6360Å dip ratio and discharge parameters, vs. E/N.

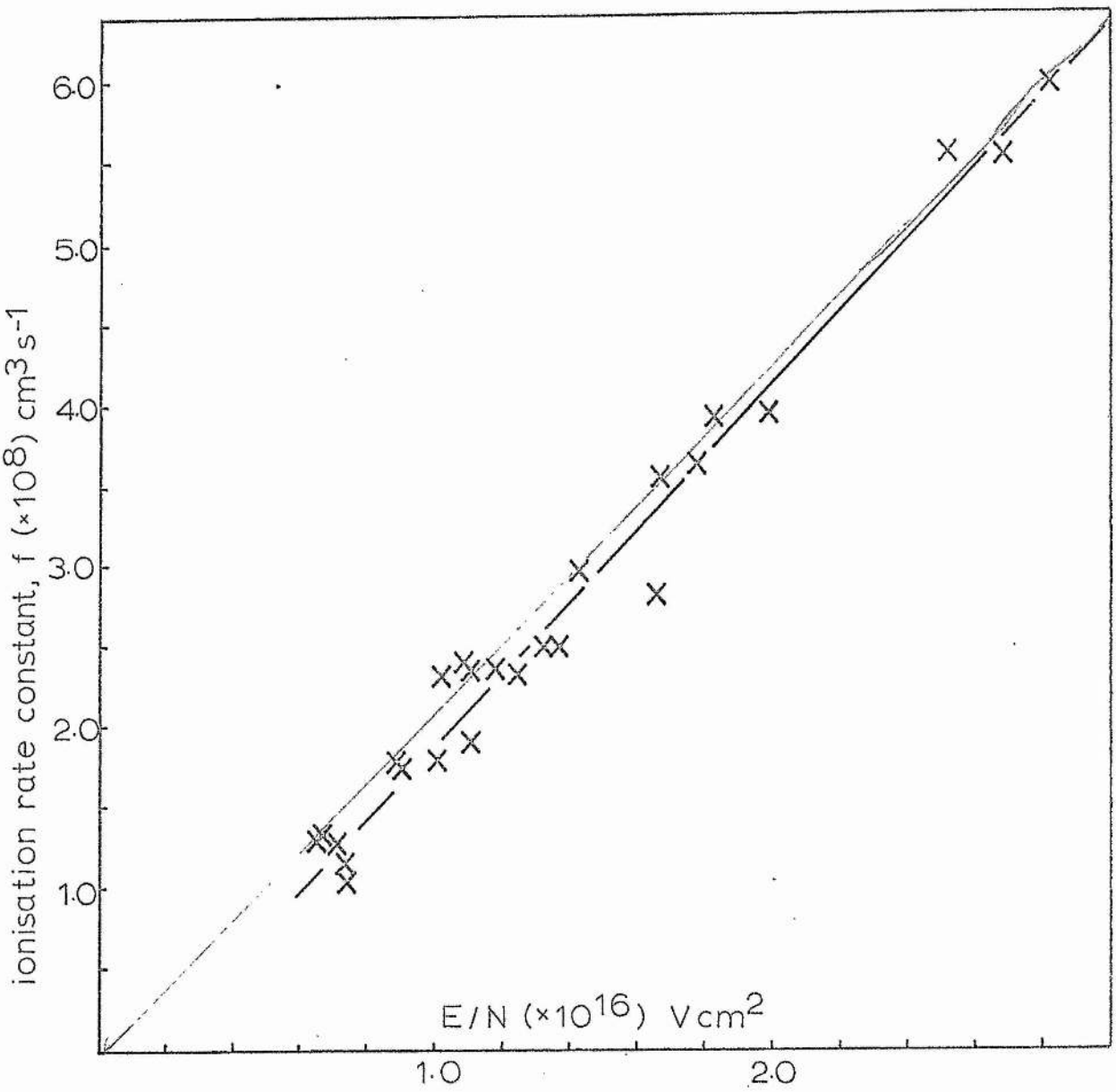

CHAPTER VII

CURRENT MODULATION OF THE HELIUM-CADMIUM DISCHARGE

Abstract

A current-modulation technique is used to estimate the ionisation rate of cadmium in a He-Cd discharge by observing the 5378Å transition. The ionisation rate constant predicted by this experiment agrees with that found in Chapter VI to within a factor of 2. The phase behaviour of the transitions at 4416Å and 2144Å relative to that at 5378Å is explained in terms of the different pumping mechanism of these lines. The wall sticking-time of cadmium atoms is estimated experimentally to be about 3×10^{-4} s.

7.1 Introduction

At high pressures and currents the dip effect is so great that with a current increment the axial emission from the charge-exchange levels actually decreases. This suggests a current-modulation experiment to observe the phase change of the axial signal as the modulation frequency is increased. At low, "quasi-stationary" frequencies the axial cadmium ground-state neutral density is in antiphase with the current. As the frequency is increased the cadmium has less time to diffuse back from the walls between current pulses and so the antiphase behaviour will lag further and further behind the current modulation. This is equivalent to a lead of 180° over the current at low frequencies, decreasing at higher frequencies.

It is simpler to observe the change in the modulation of the 5378Å emission with frequency than the neutral ground-state modulation. This transition is chosen because it is excited by helium ions, the density

of which is assumed to modulate in phase with the current. The final modulation of this transition will then be determined by the product of the modulations of the helium ion density and the cadmium neutral ground-state density. As we have seen, there will also be some electron excitation from the cadmium ion ground state. While the fractional contribution from this source does not vary greatly over a wide range of discharge parameters, there is a tendancy for the fraction of electron pumping to increase with current. This is to be expected from the fact that the cadmium ion population on the axis will increase compared to the neutral ground-state population with increasing current (section 6.4). This additional pumping will weaken the antiphase modulation due to the pure Duffendack pumping and will complicate the interpretation of the results.

It would have been preferable to have used the 6360Å transition which we have seen (section 4.3.4) is less affected by electron pumping. However, the signal from this transition was weak and subject to discharge noise, and, in any case, there is a possibility that it, too, is pumped partially by the same electron process. Therefore the 5378Å line was used in the modulation experiments and is treated for the purposes of the analysis as though it were entirely pumped by Duffendack reactions (or by cascade therefrom).

To investigate the behaviour of the neutral ground state metal vapour density in a current-modulated discharge we must solve the time-dependent form of equation (2.1) viz.

$$\frac{\partial N_{cd}}{\partial t} = D \nabla^2 N_{cd} - N_e N_{cd} f$$

The electron density, N_e, will be an explicit function both of the radial distance from the axis and of time. The radial dependence of N_e is assumed to be a zero - order Bessel function with the first zero at the tube walls. We assume that the time variation of N_e is sinusoidal in phase with the discharge current. No account is taken in this model of the ambipolar diffusion time of helium ions and electrons or of the drift time of cadmium ions to the wall. This will generally be of the order of 10μs or less. The population of a Duffendack - pumped line (5378Å) is obtained simply by multiplying the cadmium neutral ground state by N_e at any given instant.

The variation of f with current is assumed negligible in this experiment. Although, in general, the electron temperature will increase as cadmium is removed from the centre of the discharge (in the high-current phase of the modulation) the cadmium oven temperature is kept low and so this effect is not considered important.

Boundary conditions are determined by the population of cadmium atoms on the tube walls which, in turn, is determined by a wall-sticking-time, τ_w (section 7.4). (It is found that if the finite dwell-time on the wall is not considered, the predicted phase lead may be reduced by up to 15%.)

A computer program is developed to solve the above time-dependent equation, and details are listed in Appendix VII.

A parameter is chosen such that

$$\phi = N_{eo} f \qquad (7.1)$$

where N_{eo} is the mean axial electron (or helium ion) density and f is the ionisation rate constant of cadmium as before (section 2.5). Thus the dip parameter, α, becomes

$$\alpha = \frac{\phi}{D} R^2 \qquad (7.2)$$

Using the program, the computed value of the unmodulated dip ratio for a given α is in agreement with the dip obtained from equation (2.3) graphed in Fig. 6.1 and is independent of the sizes of ϕ and D which determine α. This emphasises that, for a given α, the dip ratio is insensitive to the detailed shape of the ionisation profile since Fig. 6.1 was derived for a parabolic and not a Bessel-shaped profile.

It turns out that, for a given dip, by computing phase-frequency graphs for different ϕ (with D adjusted to keep α constant) there is a whole range of curves only one of which matches the curve obtained in the experiments to be described. This means that to find the value of ϕ for the discharge it is only necessary to select the closest-fitting computed curve and its associated ϕ. This matching procedure can therefore give an estimate of f if N_{eo} is known. Note that no prior knowledge of D is necessary - the diffusion coefficient may be found from the value of ϕ and α from equation (7.2).

7.2 Apparatus and Experiment

It is necessary to avoid the situation where, in the high-current half of a cycle, cadmium in the discharge is swept out of the tube by

increased cataphoresis and is not replaced by diffusion from the source. This is more likely to occur where the neck of the cadmium reservoir is narrow. This will be enhanced if the sweep-out distance travelled by the neutral cadmium down the tube in half a cycle is comparable with the tube length. If the axial cadmium ion velocity is 1.3×10^4 cm s^{-1} (the approximate velocity found by Mash [59]) and up to 7% ionisation is assumed, the aggregate velocity of neutral cadmium is 10^3 cm s^{-1}. Thus, in half a cycle at 250Hz, the distance covered is 2cm.

These two considerations account for the design features of the tube used in this experiment. To avoid the problem of flow constriction from the reservoir the cadmium is contained in an enlarged bulb-section of the tube instead of in a sidearm as before. The bulb is cooled by whisper fans regulated by a temperature controller. Also, the 5mm bore tube is 10cm long and so with these provisions any modulation of the cadmium lines will be due to radial and not longitudinal sweep-out. Optics appropriate to the 10cm tube were used (described in Chapter III) to select the axial signal (a 300μm radius cylinder).

The sinusoidal current modulation was provided by an Advance signal generator connected into the discharge circuit as shown in Fig. 7.1. The resulting phase-frequency graphs were independent of the amplitude of the modulation which in no case exceeded 70mA p-p and was generally below 30mA p-p. The current was monitored by measuring the voltage across a 5Ω resistor connected in series with the discharge tube. This voltage was fed through a filter to provide

a reference signal for the Brookdeal 401 lock-in amplifier. The output from the photomultiplier was fed into the signal channel and the phase of the light modulation was indicated by the phase-shifter reading of the lock-in amplifier at null deflection.

While the phase change with radius might have yielded information about the discharge (the signal was generally in antiphase at the centre while it was in phase with the current near the walls), the shape of this curve varied little when pressure and current were altered - only the overall phase lead changed. Thus this was considered to be too insensitive to yield useful data.

7.3 Results

Results were taken at wavelengths 4416Å, 5378Å and 2144Å at various currents at 10 Torr helium pressure. A selection of these results is shown in Fig. 7.2. From the 5378Å curves we see that, at higher average currents, the phase lead of this transition over current is greater. The 5378Å signal is also ahead in phase of that of 2144Å and behind that of 4416Å for similar discharge conditions.

7.3.1 4416Å

The explanation for the 5378Å modulation lagging behind that of the 4416Å signal probably lies in the pumping mechanisms of the two transitions. The 4416Å line is pumped by Penning collisions with helium metastable atoms, which, as we shall see below, are modulated less strongly than the electrons and helium ions. The 5378Å transition is pumped by helium ions, the modulation of which follows that of the

electrons, and so this line has a larger in-phase component than the 4416Å line.

To see that the metastable population is only slightly modulated, recall that if there were no cadmium present in the discharge, the metastable population would be saturated at the axis with respect to electron density (section 4.2.1). We have seen that the introduction of cadmium into the discharge lowers the helium metastable population: if the oven temperature is increased from 245°C by 20C° (corresponding to an increase of about 400% in the cadmium partial pressure) the metastable population drops by about 30% (Fig. 4.1). However, from the general relationship between cadmium neutral ground state density and electron density (Fig. A7.1) we see that the current modulation required to produce such a large cadmium modulation would itself need to be large: much greater than the 30% modulation of the helium metastable population. Because of this, and the fact that the cadmium concentration is kept low in this experiment, we conclude that the helium metastable modulation is less than that of the current.

7.3.2 2144Å

It is difficult to explain the difference between the 5378Å and the 2144Å curves without considering electron pumping of the latter transition from the cadmium ion ground state. If the $5p\ ^2P_{3/2}$ state were pumped by a combination of cascade from Duffendack and Penning reactions alone, then the current modulation of the state would follow that of the 5378Å upper level, or be ahead of it in phase, since the

modulation of the 4416Å transition is ahead in phase of the 5378Å line for a given current. (Self-absorption of the ion resonance line would probably not account for the large phase difference, since the cadmium ion ground state would be modulated approximately in phase with the 2144Å transition. Also, low oven temperatures are used which will reduce the importance of absorption.)

If we now consider electron excitation from the cadmium ion ground state we see that, broadly speaking, if the cadmium ion ground state density depends on the product $N_{cd}\ N_e$, then the contribution to the $5p\ ^2P_{3/2}$ state will be proportional to $N_{cd}\ N_e^2$. Such a term will tend to pull the phase of the 2144Å modulation towards that of the current itself and this is the trend exhibited by the 2144Å modulation when compared to that of 5378Å (of which a smaller fraction is pumped by electrons). This is consistent with our conclusion of section 4.3.3.

7.3.3 <u>5378Å</u>

The computer analysis is applied to a particular set of discharge parameters for 5378Å. At 10 Torr, 100mA with no modulation, the observed dip ratio of the 6360Å profile is 2.0. The values of ϕ and D which the computer program requires to produce such a dip are in the ratio

$$\frac{\phi}{D} = 364$$

which, with a tube radius of 0.25cm implies that $\alpha = 22.8$ from equation (7.2). This is in close agreement with 21.7, the size of α predicted for a parabolic ionisation profile in Fig. 6.1 for an excited species dip ratio of 2.0 (neutral dip = 5.0). When current modulation is considered

it is noticed that the curve of $\phi = 4.0 \times 10^4\ s^{-1}$ fits well the experimental results of Fig. 7.3. Two other curves are also computed to "bracket" the experimental points and to examine the sensitivity to a change in ϕ.

With $\phi = 4.0 \times 10^4\ s^{-1}$ (which means $D = 110\ cm^2\ s^{-1}$ for this particular discharge) and $N_{eo} = 3.5 \times 10^{12}\ cm^{-3}$ (Table 6.1), the ionisation rate constant, f, is $1.1 \times 10^{-8}\ cm^3\ s^{-1}$ from equation (7.1). Both f and D fall short of the values predicted in Chapter VI ($1.8 \times 10^{-8}\ cm^3\ s^{-1}$ and $179\ cm^2\ s^{-1}$) by estimating discharge parameters, although they agree to within a factor of 2. The reason for the discrepancy is probably that no account has been taken here of the electron pumping of 5378Å mentioned earlier. If there had been no such pumping, the 5378Å modulation would have remained in antiphase with the current until higher frequencies, just as the observed modulation of 5378Å is more in antiphase than the 2144Å line, which is highly pumped by electrons. Modulation of a pure Duffendack-pumped line would therefore be expected to be shifted towards the upper bracket in Fig. 7.3 : $\phi = 8 \times 10^4\ s^{-1}$ and $D = 220 cm^2\ s^{-1}$. This would produce a resulting f and D closer to the values derived in Chapter VI.

The phase lead at high frequencies tends to be smaller than the computed value. This may be because there are processes which we have not accounted for in the computer program, such as the finite diffusion time of helium and cadmium ions to the walls. Such effects may become important enough at higher frequencies to affect the predicted phase behaviour of a Duffendack-pumped transition.

7.4 Wall Sticking-Time

In computing the phase-frequency graphs it is important to consider the finite wall sticking-time, τ_w, of the cadmium atoms. With a steady current the wall population per unit area, N_w, will be in dynamic equilibrium with the neutral and ionic cadmium species in the discharge. The flux of atoms leaving the wall may be equated to the total radial flow of ions per unit area arriving at the wall plus the random flux from the neutral discharge population, $N_d(R)$, at the boundary of the discharge. Thus

$$\frac{N_w}{\tau_w} = \frac{1}{2\pi R}\left(\frac{N_i}{\tau_i}\pi R^2\right) + \frac{N_d(R)C}{4}$$

The term in brackets is the ionisation rate of cadmium per unit length of the discharge, τ_i is the characteristic cadmium ion lifetime and C is the average speed of the cadmium atoms. Putting

$$N_d(R) = \beta N_d$$

$$N_i = \gamma N_d$$

where N_d is the average cadmium neutral density per unit volume in the discharge,

$$\frac{N_w}{\tau_w} = \frac{\gamma N_d R}{2\tau_i} + \frac{\beta N_d C}{4} \qquad (7.3)$$

The sticking-time, τ_w, is a time constant for the walls which will act as a "sink" for cadmium atoms during the high-current half of a cycle before equilibrium can be re-established. This leads to a modulation of the total and axial discharge population in addition to that due directly to the dip ratio modulation. The effect of

τ_w may be seen in more detail in Appendix VII.

To estimate τ_w, suppose that cadmium is suddenly introducted into a "clean" discharge tube and is carried along it by cataphoresis. The transport rate will be much slower than the 10^3 cm s^{-1} mentioned earlier because the cadmium must first coat the clean walls before it can proceed down the tube. This assumes that equilibrium is quickly established between the walls and the discharge as the column of metal vapour advances towards the cathode. This does seem to be the case, because experiments (described below) show that the density of cadmium is constant right up to the leading edge of the column.

The amount of cadmium which travels down the tube in a time dt is $\pi R^2 \gamma N_d v_i dt$ where v_i is the ion drift velocity. The amount of cadmium required to fill a length dx of the walls and discharge is $\pi R^2 N_d dx + 2 \pi R N_w dx$. Therefore the velocity of the head of the column is

$$v_{head} = \frac{dx}{dt} = \frac{\pi R^2 \gamma N_d v_i}{\pi R^2 N_d + 2 \pi R N_w}$$

Using equation (7.3) this becomes

$$v_{head} = \frac{\gamma v_i}{1 + \gamma \frac{\tau_w}{\tau_i} + \frac{\beta C \tau_w}{2R}}$$

whence

$$\tau_w = \frac{\frac{\gamma v_i}{v_{head}} - 1}{\frac{\gamma}{\tau_i} + \frac{\beta C}{2R}} \qquad (7.4)$$

The velocity of the column, v_{head}, was measured experimentally.

7.5 Measurement of v_{head}

A 190cm long 4mm diameter discharge tube was first run with pure helium and then the cadmium oven was switched on and the progress of the metal vapour was monitored down the tube. This was achieved by observing the discharge through an Ilford Spectrum Filter No. 625 which suppressed all lines except the 5337Å and 5378Å transitions of cadmium and the 5875Å line of helium. In this way the position of the leading edge of the cadmium column was clearly visible. The cadmium intensity was also monitored by collecting the discharge light with a fibre-optic tube one end of which was fixed at the entrance slit of the monochromator tuned to the cadmium 4799Å transition. Measurements showed that the column head velocity quickly settled to a steady value after leaving the oven and that the intensity of the column was constant along its length upto its head.

The head velocity at 5 Torr, 100mA for several oven temperatures was found to be 2.5cm s^{-1}. The wall temperature in this case is the same as that for the tube used in the modulation experiment and so difficulties over the temperature dependence of τ_w should not arise.

Using equation (7.4) and approximate values of

$$\gamma = 10^{-2}$$

$$\tau_i = 10^{-6} \text{ s}$$

$$\beta = 2$$

$$C = 3.7 \times 10^{4} \text{ cm s}^{-1}$$

$$v_i = 1.3 \times 10^{4} \text{ cm s}^{-1}$$

$$v_{head} = 2.5 \text{ cm s}^{-1}$$

we obtain for the wall sticking-time

$$\tau_w \doteqdot 3 \times 10^{-4} \text{ s}$$

This is the dwell-time derived for cadmium as it encounters a "clean" quartz surface. It may be that a monatomic layer of cadmium quickly develops which provides a surface for which the sticking-time in subsequent adhesions differs from the above value. At a wall temperature of 570°K the vapour pressure of cadmium from tables is 5×10^{-2} Torr, or 8×10^{14} atoms cm^{-3}. Assume that the vapour is in equilibrium with a cadmium surface with an atomic spacing of 3Å or a surface density of $N_s = 10^{15}$ cm^{-2}. In this case the sticking-time τ_s on the cadmium surface is

$$\frac{N_s}{\tau_s} = 8 \times 10^{14} \times \frac{C}{4}$$

and so

$$\tau_s \doteqdot 1.4 \times 10^{-4} \text{ s}$$

Thus cadmium atoms in the discharge hitting a cadmium-coated wall at 570°K have about the same sticking time as that worked out for the clean-wall case. Great accuracy is not necessary here because the computed behaviour of the phase-frequency graphs shows little sensitivity to variations in τ_w of up to two orders of magnitude.

7.6 Conclusion

A current-modulation technique has been used to estimate the ionisation rate of cadmium in a He-Cd discharge. Use is made of the property that cadmium vapour builds up around the tube walls.

By varying the current, we observe, in effect, how quickly the cadmium takes to adjust by diffusion to the current modulation. This is done in practice by observing, at the centre of the tube, the phase difference between current and a transition pumped by Duffendack reactions (5378Å).

In general the modulation of the cadmium emission lines is ahead of the current modulation in phase. The phase lead at 5378Å is less than at 4416Å, presumably because the latter transition is pumped by Penning reactions with current-saturated helium metastable atoms, whereas the former is pumped by helium ions which modulate in phase with the current. The 2144Å phase lead is even less than that of 5378Å. This is probably due to the large contribution which the 2144Å transition receives from electron excitation from the cadmium ion ground state (which, in turn, will have a component in phase with the current, being pumped largely by electron ionisation from the cadmium ground state).

Using the parameters $f = 1.1 \times 10^{-8}$ cm^3 s^{-1}; $D = 110$ cm^2 s^{-1}, the computed behaviour of the phase lead of 5378Å modulation over current modulation agrees well with experiment. These values of f and D are lower than predicted in Chapter VI but this may be because we have neglected here the contribution to the 5378Å transition of electron excitation from the cadmium ion ground state. (There was too much background noise on the weak 6360Å transition, pumped mainly by Duffendack reactions, to use it in this experiment.)

In computing the phase lead of the cadmium modulation, we have taken account of the sticking time of cadmium on the tube walls. This was estimated to be 3×10^{-4} s by observing the time taken for cadmium to flow down a "clean" tube, which was much longer than would have been the case had the sticking-time been zero. If this refinement is not included in the computer program, the calculated phase lead is less by as much as 15%.

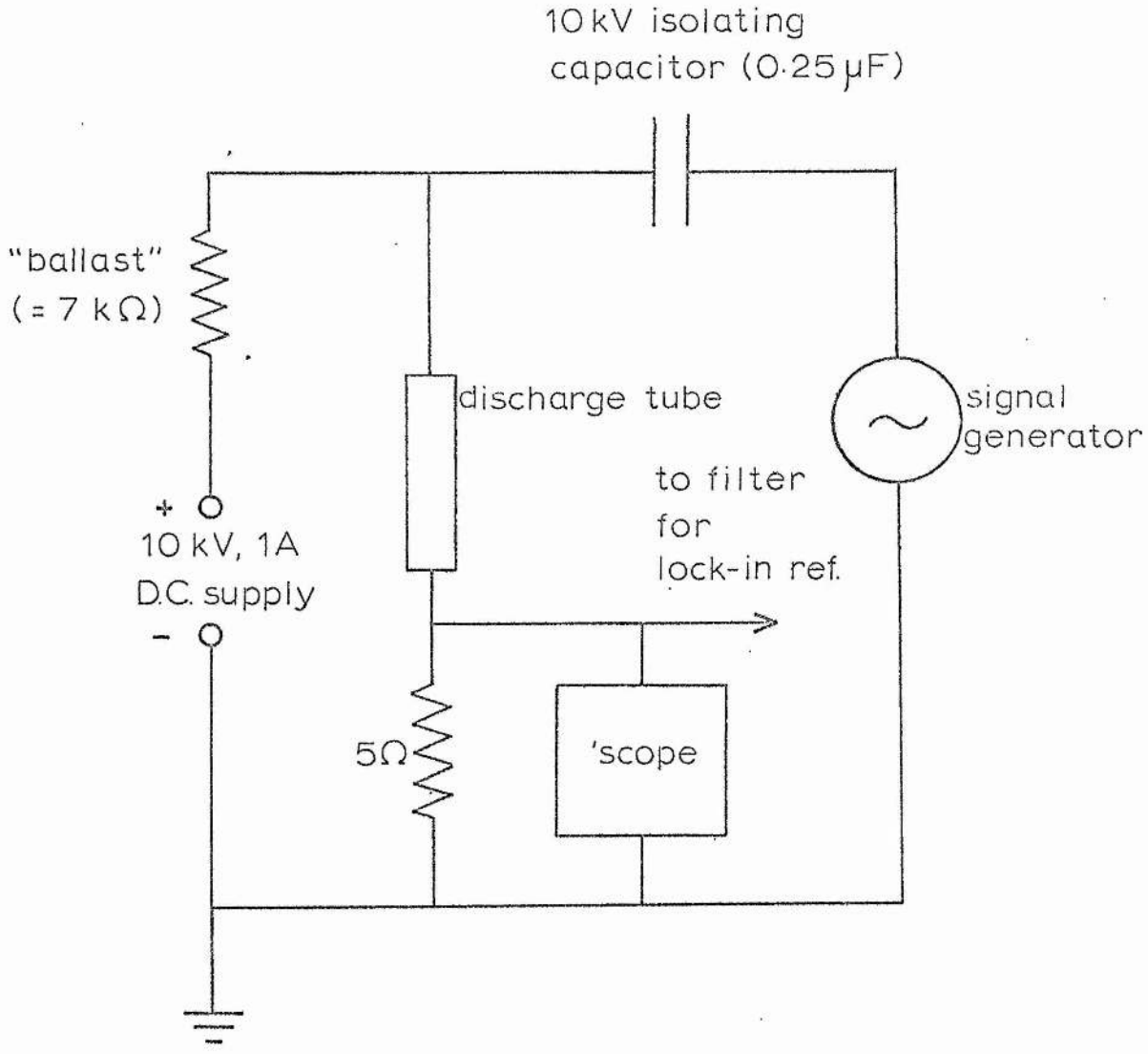

Fig. 7.1 Circuit diagram for current-modulation experiment.

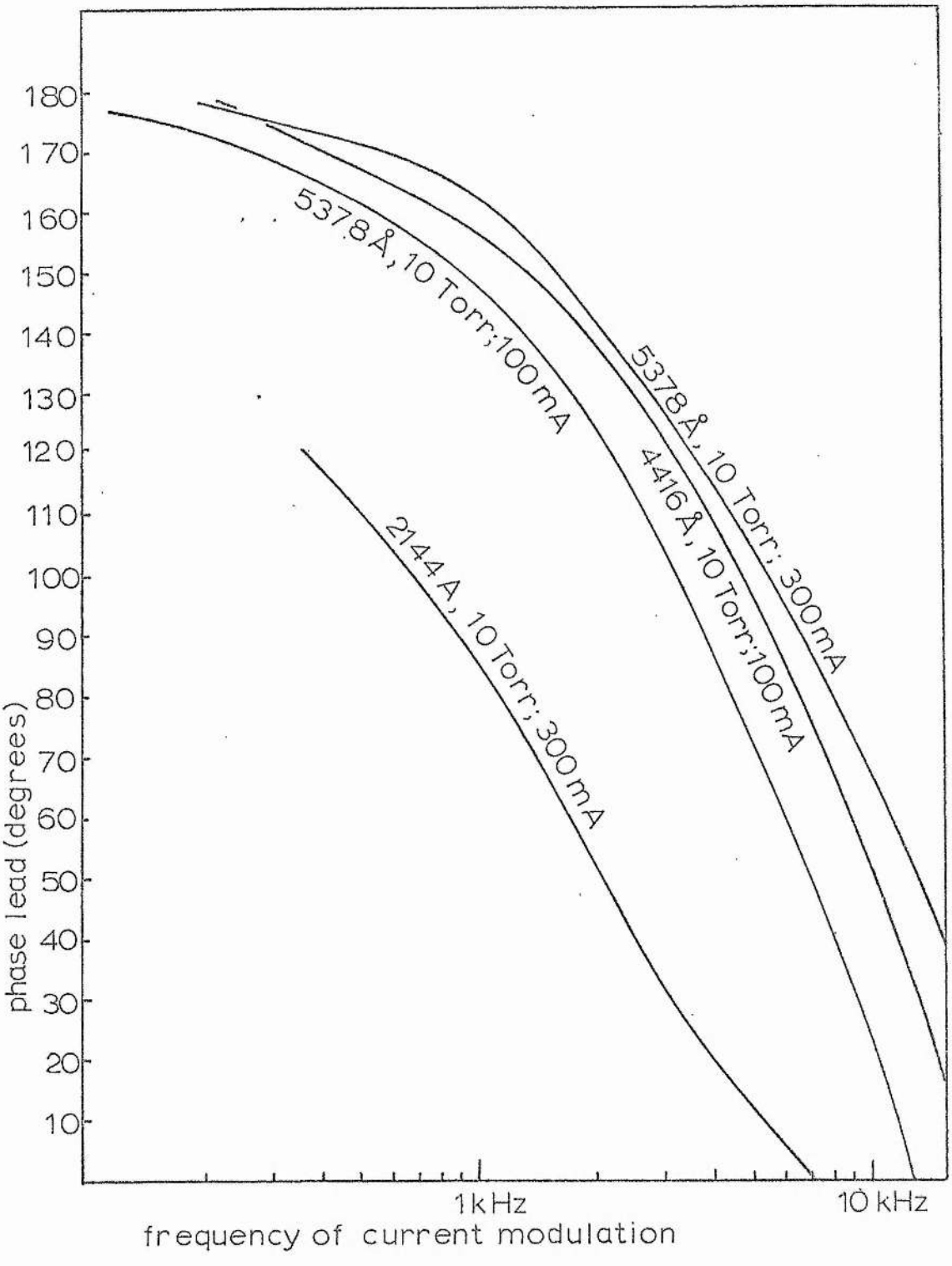

Fig. 7.2 Frequency dependence of phase lead over current for transitions 5378Å, 4416Å and 2144Å. The spread of individual experimental results may be gauged from Fig. 7.3.

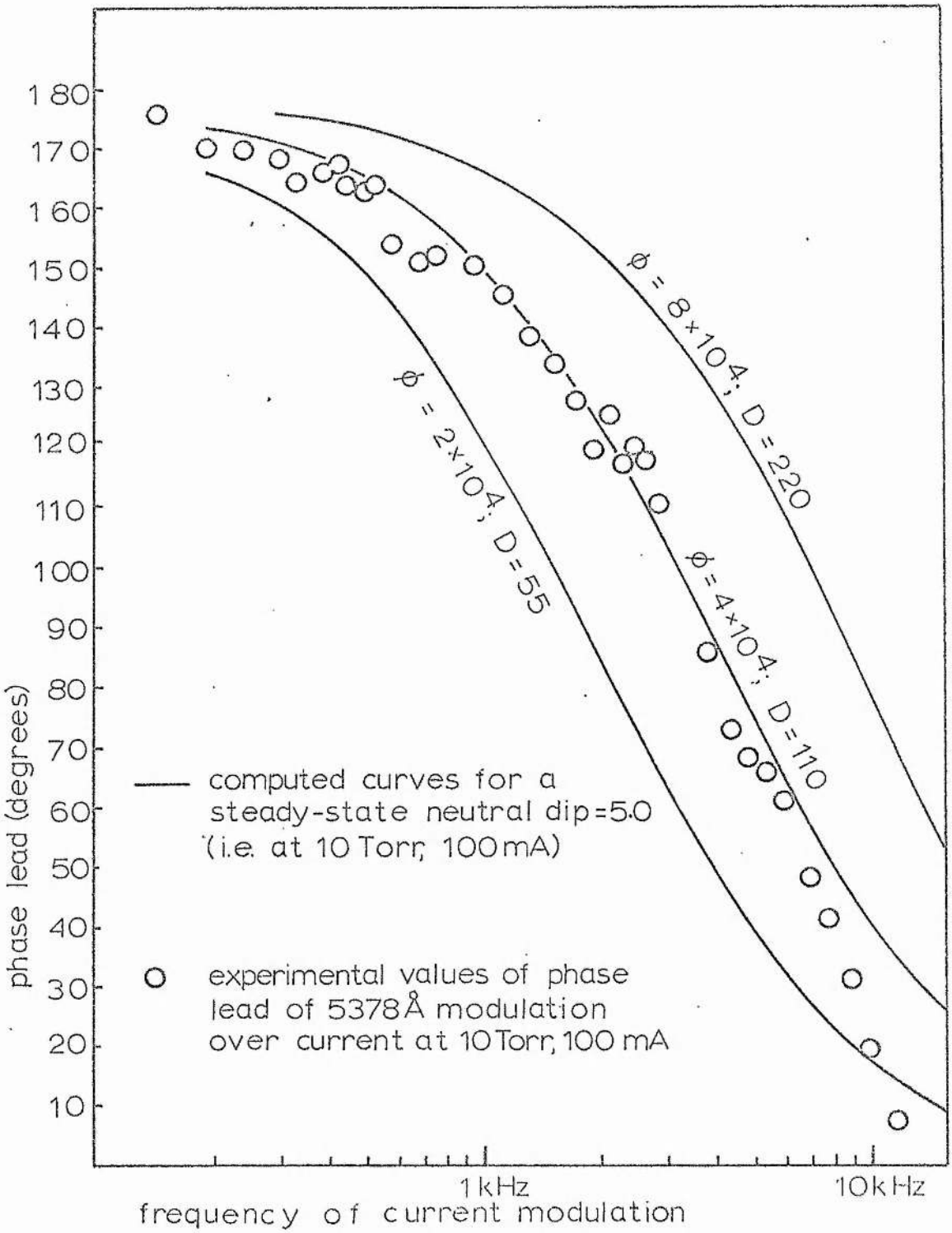

Fig. 7.3 Fitting of computed behaviour of phase lead of 5378Å modulation over current modulation to experimental results.

CHAPTER VIII

REVIEW

8.1 Introduction

The experiments performed in this work fall into two classes : those which establish the existence of a power-limiting phenomenon in the positive column of metal vapour laser discharges and those which subsequently use the effect diagnostically to examine excitation mechanisms in the He-Cd system in particular. This involves the analysis of both radial profiles of excited states in a He-Cd discharge and the behaviour of cadmium states in a current-modulated discharge. The techniques involved in the use of the dip phenomenon as an exploratory tool may be applied in general to all metal vapour systems.

8.2 Power-Limiting Phenomenon

The explanations proposed by Klein and Silfvast [12] and Ferrario [9] to account for the power saturation with current in the He-Se and He-Hg laser systems are shown in Chapter I to be insufficient. Chapter II describes the observation of an axial depletion of the upper laser levels in a He-Se positive column discharge. This depletion is aggravated at higher currents and helium pressures which would indeed account for the observed laser power behaviour.

The parametric dependence of the radial dip is deduced from the diffusion and ionisation equations of the metal atoms in the discharge. The magnitude of the dip is shown to be fairly independent of the metal ionisation rate profile. It is recognised that the equations are generally applicable to any metal vapour - rare-gas mixture, and, in order to test them, the He-Cd system is selected for further study.

8.3 Radial Profile Studies

The remainder of this work describes the results of experiments using the optics of Webb [19] to obtain radial profiles in the He-Cd system. Profiles are taken both of radiating levels and of non-radiating levels, the latter states being examined by absorption techniques. For absorption, a separate source is arranged to shine through the test discharge and the absorption is determined at points across the tube diameter.

Absorption experiments were used to examine helium and cadmium metastable profiles and cadmium neutral and ion ground state profiles using transitions terminating on these states.

The cadmium ion ground state profiles are observed to be less dipped than the profiles of excited cadmium ions. This is probably because the ground state ions have time to diffuse from their point of creation and smooth out the profile dips, and, indeed, if diffusion were the only loss process involved, the ground state ion profiles would be convex for all discharge conditions. However, the radial electric field helps to sweep ions to the wall creating a dipped profile and a back-diffusion gradient of the states (section 4.2.4).

Similarly, the cadmium metastable 5p ^3P_o profiles are observed to be dipped and again an alternative process to diffusion is suspected. This is probably a combination of electron ionisation of the metastables, plus thermal mixing with the 5p $^3P_1$ state which has a radiative lifetime of 3μs (sections 4.2.3 and 6.4).

The helium metastable 2s ^{3}S profiles are flatter than the zero-order Bessel function expected for the helium ion and electron radial distribution [4]. This is because the metastable population is saturated with respect to electron density and so the profiles are not as peaked as the electron profiles at the tube axis (section 4.2.1).

The results using the cadmium neutral resonance lines are ambiguous - the neutral ground state profiles are less dipped than expected from a consideration of the profiles of excited states. This is probably due to cadmium vapour in the "dead space" between the end window and the discharge column absorbing the illuminating light (section 4.2.2).

Emission profiles are examined of transitions pumped directly or by cascade from Duffendack or Penning reactions. The 6360Å transition (section 4.3.1) is taken to be representative of the Duffendack pumping rate - that is, the states are assumed to be pumped only by charge transfer with helium ions and, in their short lifetime (23ns), it is assumed that they are neither displaced significantly in the radial electric field nor collisionally destroyed by electrons.

The Penning-pumped profiles (section 4.3.2) are less dipped than the charge-exchange profiles. This is surprising, since the Penning pump rate should be more deeply dipped than the charge-exchange pump rate (because the profiles of the helium metastable atoms which excite the Penning levels are higher at the wings than the helium ions which produce the Duffendack levels.) The shallow dip

may be explained either by the smoothing process of the diffusion of the long-lived Penning states, or by electron excitation of the Penning states from the cadmium ion ground state. Both processes are probably active. There may also be electron destruction of these states but this will act in the opposite direction - deepening the profiles - and the extent of such a process cannot be assessed.

The shallowest dip of all the emission lines is exhibited by the ion resonance line at 2144Å and 2265Å (section 4.3.3). Such a shallow profile might, at first sight, be accounted for by the total radiative and non-radiative contribution from Penning levels smoothed by diffusion. However, as current and pressure is increased, the 2144Å signal increases faster than the Duffendack or Penning pumping rates, and so we deduce from this and the parametric dip dependence that the additional pumping would arise from electron excitation from the cadmium ion ground state. As we see in section 4.3.3, this explains both the current and pressure behaviour of the 2144Å transition and its shallow dip. A calculation of the cross section for this mechanism shows that such a process should proceed with a rate comparable to that of cascade from Duffendack and Penning reactions and so it should therefore provide an important contribution to the pumping of the 2144Å transition.

Emission profiles of the other cadmium ion states (sections 4.3.4 - 4.3.6) exhibit deeper dips the further removed the states are from the ion ground state. This is consistent with a pumping contribution from electron excitation from the cadmium ion ground state. Assuming

that the 6g levels are pumped purely by Duffendack reactions, it is estimated that about one third of the pumping of the 5378Å profiles is by electron excitation (section 4.3.4). Lower-lying states which exhibit shallower dips will receive a correspondingly greater contribution from electron pumping. (It is unlikely that profile smoothing observed in the excited states is due to radiative and non-radiative contributions from the P states. Although these have a long lifetime, the electron collisional destruction rate of these states is high (75) which should prevent significant smoothing of the profiles due to diffusion. In any case, if contributions from the P states were distributed between all the states exhibiting shallow dips, the effect on any one state would be small.)

The oven temperature dependence of the dips of a Duffendack-pumped line (6360Å) is examined in Chapter V. The dip ratio of this transition is constant over a wide range of cadmium partial pressures. This suggests that the ionisation rate constant of cadmium atoms in the discharge is unchanging over this range. At the same time, however, as the cadmium partial pressure is increased, the helium ion concentration decreases. (This is deduced from the decrease of the 6360Å sidelight relative to that of 3261Å, the cadmium neutral resonance line). With increasing cadmium partial pressure, the helium metastable population must also decrease, and so the principal source of ionisation is probably from electron ionisation of cadmium.

This conclusion is supported by the results of Chapter VI. The behaviour of the dip of the 6360Å profile is investigated with changing

discharge conditions and the tendency for the dip to increase with increasing E/N values regardless of the other discharge parameters points to electron ionisation. The rates calculated for this process (typically 3×10^{-8} cm^3 s^{-1}) are an order of magnitude greater than for Penning and Duffendack reactions. It is likely that ionisation from both the cadmium ground and metastable states is involved.

8.4 Modulation Experiments

Finally, in Chapter VII, observations are described of axial emission from excited cadmium levels when the discharge current is modulated. At high frequencies, cadmium which is swept to the walls in one cycle has insufficient time to diffuse back before the next, which introduces a frequency - dependent phase shift in the light emission. By comparing the experimental behaviour of the 5378Å signal with that computed with the program listed in Appendix VII, an estimate of the ionisation probability of cadmium is again obtained, but this time without the need to estimate the diffusion coefficient of cadmium in helium which was required in the static case in Chapter VI.

The phase of the 5378Å signal is found to be ahead of that at 2144Å and behind that at 4416Å. This is explained (section 7.3.1 and 7.3.2) in terms of the different pumping mechanisms of the three transitions.

APPENDIX I

INSTRUMENTAL DISTORTION

The computation of the instrumental distortion of the radial profiles is divided into two parts. The first section of the program (Fig. A 1.4) computes the distribution of the ground-state neutral metal species from the solution of equation (2.2). The solution, for simplicity, is derived for a parabolic dependence of N_e on the radius. This is close to a Bessel-shaped profile and, in any case, the neutral ground state dip is little affected by the particular shape of the ionisation profile assumed (see section 2.5). This leads to a series solution for N_m where N_m is the metal vapour concentration and N_{mo} is the axial density:

$$\frac{N_m}{N_{mo}} = 1 + \frac{\alpha}{4}\frac{r^2}{R^2} + \frac{\alpha(\alpha - 4)}{64}\frac{r^4}{R^4} + \ldots$$

with a three-term recursion relationship between the coefficients of $\frac{r^n}{R^n}$, A_n, given by

$$A_n = \frac{\alpha}{n^2}(A_{n-2} - A_{n-4})$$

Terms up to the twentieth power of the radius are taken which always ensures sufficient convergence for the data used. For each value of α, the cadmium concentration is calculated for one thousand points across the tube radius. The excited population at each point is then determined by multiplying the ground-state profile by a zero-order Bessel function and is referenced Y(NUMBER) where NUMBER ranges from 1 to 1000.

The second part of the program evaluates the signal detected by the instrument as it scans with an aperture of given radius

(0.1R in the program listed here).

It is assumed that the response function of the optical detection system is constant everywhere within the aperture and zero outside it. (This is actually a pessimistic standpoint since the response function will be greatest at the centre of the aperture, hence approaching more closely the ideal delta function.) No account is taken here of diffraction effects.

The coordinate system is shown in Fig. A 1.1. The contribution to the signal of the excited population profile must be summed over the aperture. The tube radius is assumed to be divided into 1000 units which in the present case means the aperture radius is 100 units. The aperture is scanned by the computer program in the horizontal direction by assigning to a parameter J the values 1 to 200. For each value of J an element in the aperture is located in the vertical direction by M which scans from 1 to 100. (The lower half of the aperture is later accounted for by doubling the integration.) From the coordinates J, M and I (where I is the number of units between the tube and aperture centres) the distance of the element from the tube axis is found by computing NUMBER. The value for the cadmium excited density may now be assigned to this element using NUMBER and the stored values of Y(NUMBER). The densities at all the elements falling within both the aperture and the tube cross section are summed - no element either outside the circular aperture or outside the tube boundaries is included in the integration.

The instrumental profiles are normalised for ease of comparison with the undistorted profiles by dividing by $10^4\pi$ (the area of the aperture in this example in square units). The program then prints out distorted and undistorted values of the profile at selected points across the tube radius, determined by I. Examples appear for two values of α in Figs. a 1.2 and A 1.3.

The curve (Fig. 6.1) of neutral dip vs. α was computed using a program similar to the first part of the one listed here except that only the neutral profile is calculated and only at a radius of 0.7R (the dip ratio being defined as the ratio of the densities at 0.7R and at the axis.)

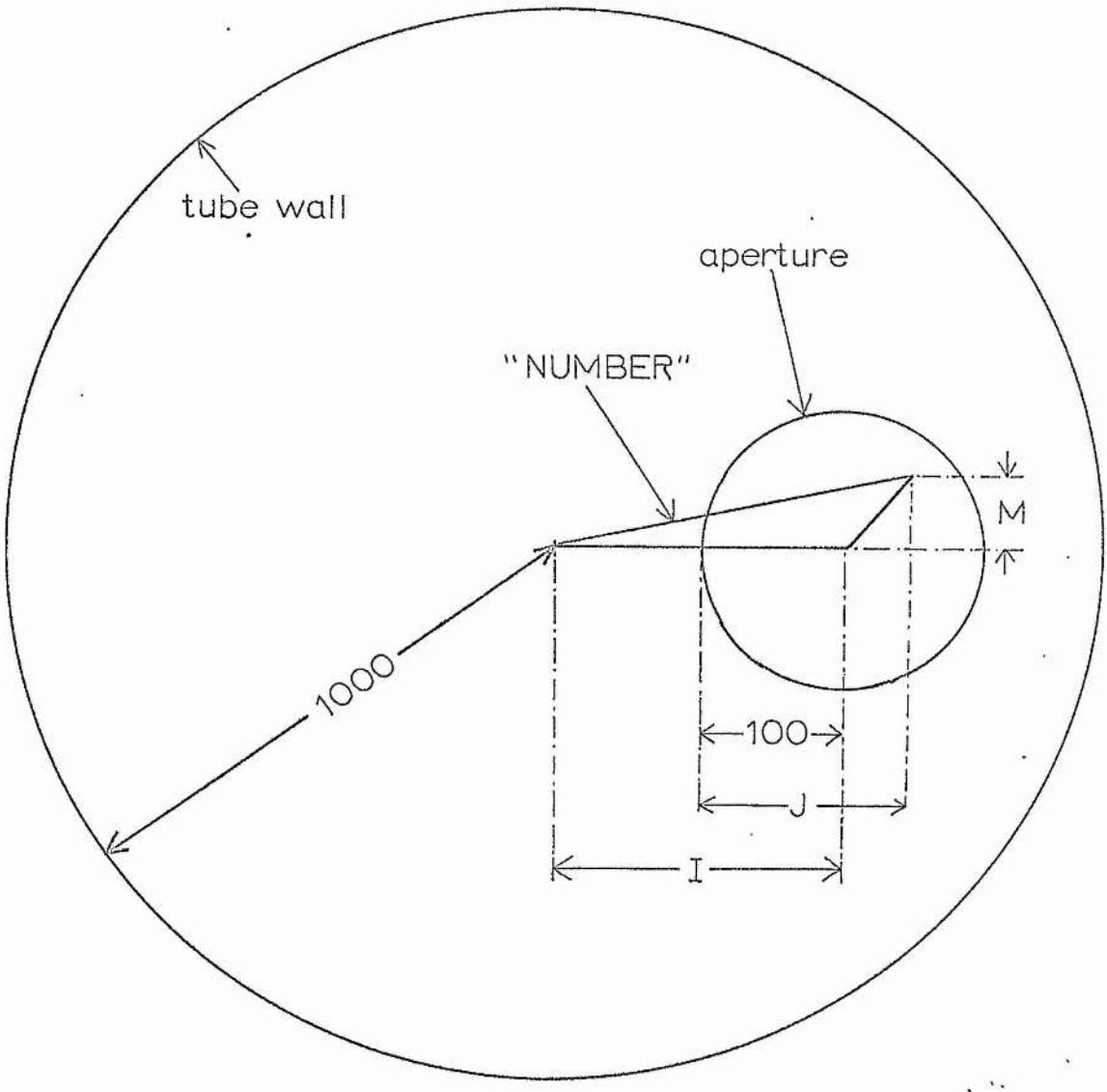

Fig. A 1.1 Co-ordinate system used to compute instrumental distortion of profiles.

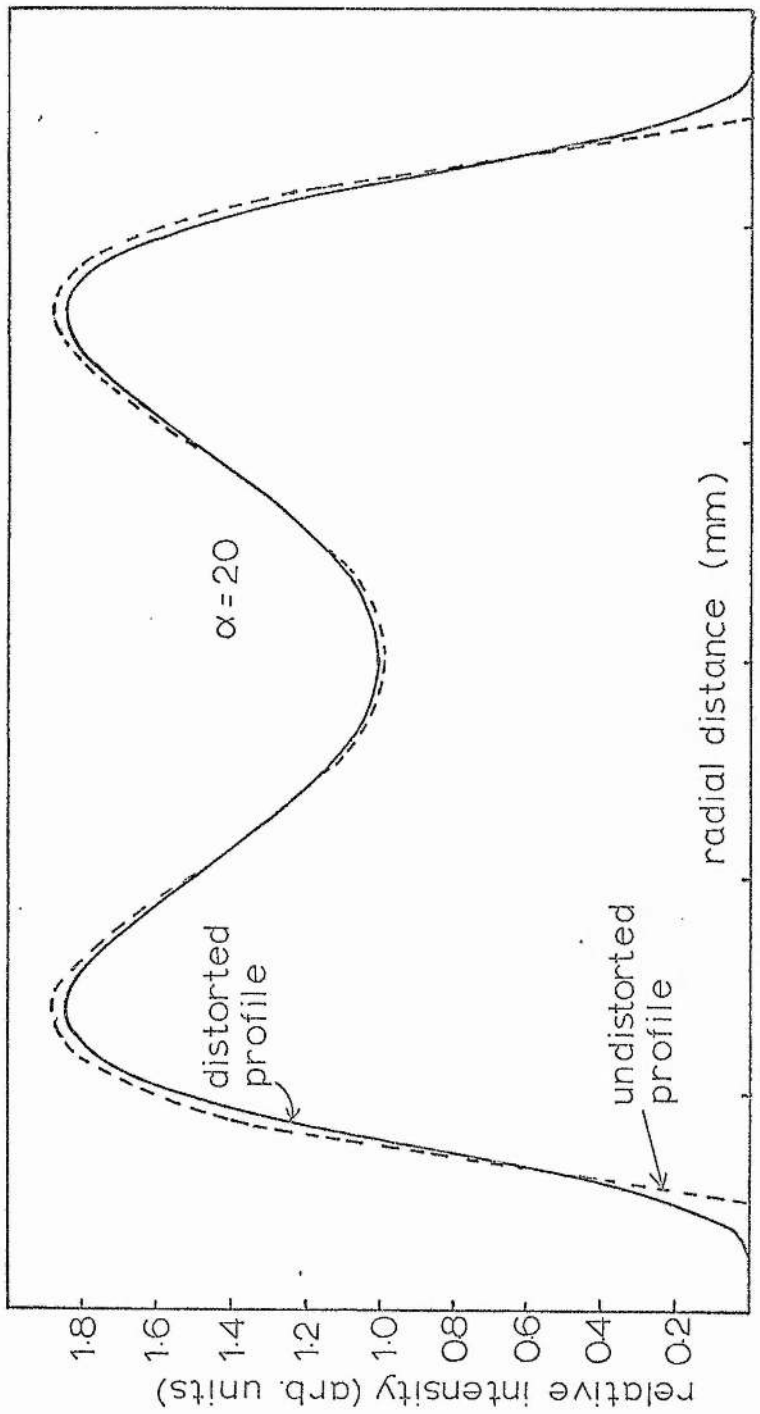

Fig. A 1.2 Comparison of a theoretical and an instrumentally distorted radial profile using computer program Fig. A 1.4.

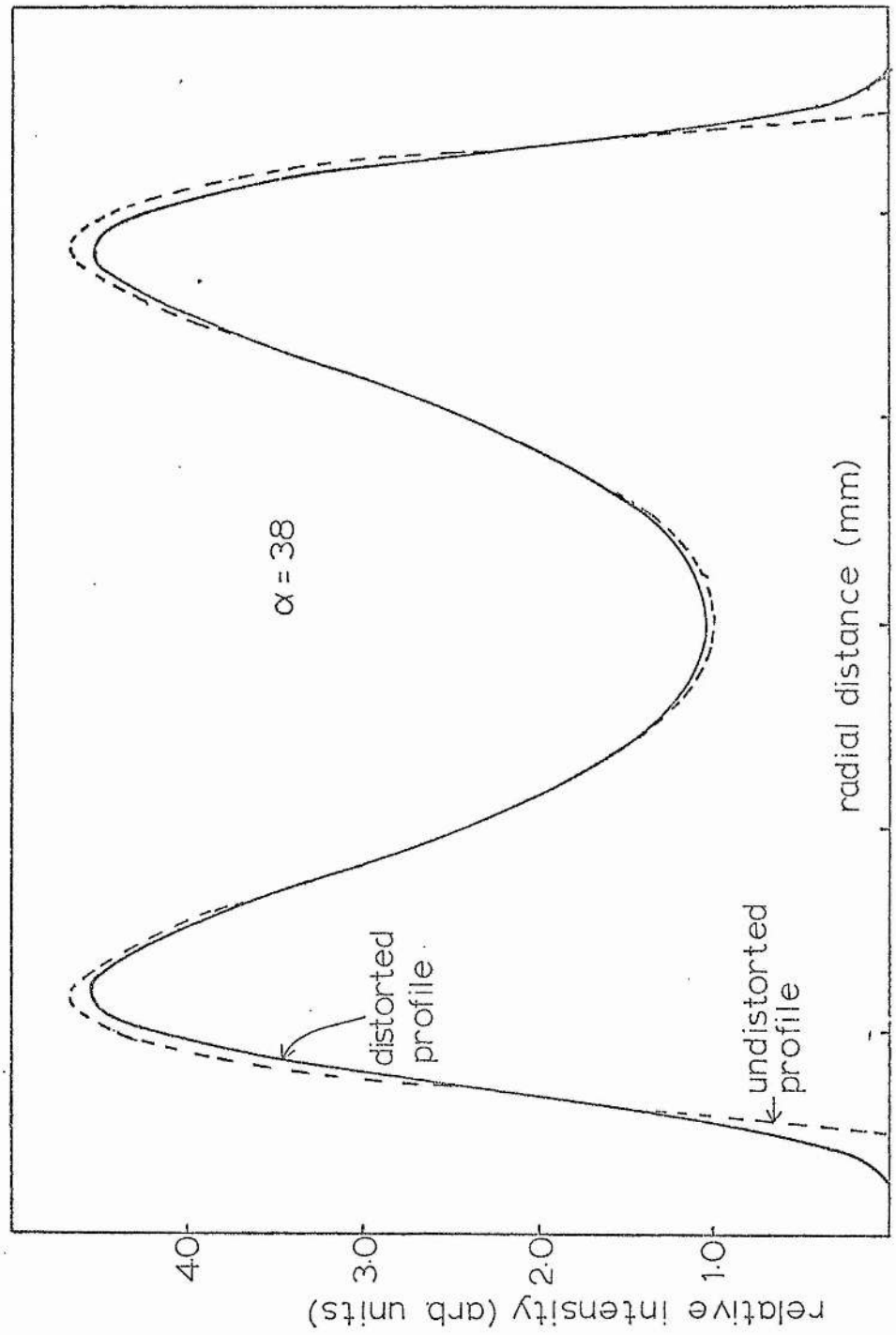

Fig. A 1.3 Comparison of a theoretical and an instrumentally distorted radial profile using computer program Fig. A 1.4

```
      DIMENSION TRULYT(1201),SUM(1201),X(1201),Y(1201),A(20)
      X(1)=0.0005
      DO 120 NUMBER=2,1201
      X(NUMBER)=X(NUMBER-1)+0.001
  120 CONTINUE
      ALPHA=20.0
      A(1)=0.0
      A(2)=ALPHA/4.0
      A(3)=0.0
      A(4)=ALPHA*(ALPHA-4.0)/64.0
      A(5)=0.0
      DO 11 JOT=6,20
      A(JOT)=ALPHA*(A(JOT-2)-A(JOT-4))/JOT**2
   11 CONTINUE
      DO 12 NUMBER=1,1000
      Y(NUMBER)=1.0
      DO 10 JOT=1,20
      Y(NUMBER)=Y(NUMBER)+A(JOT)*X(NUMBER)**JOT
   10 CONTINUE
      Y(NUMBER)=Y(NUMBER)*(1.0-1.446*X(NUMBER)**2+0.5227*X(NUMBER)**4-
     £0.0839*X(NUMBER)**6)
   12 CONTINUE
      DO 105 I=1,1201,25
      HAFSUM=0.0
      DO 104 J=1,200
      DO 104 M=1,100
      IF(M**2 .GT. 10000-(J-100)**2) GO TO 104
      NUMBER=INT(SQRT(FLOAT((I+(J-100))**2+M**2)))
      IF (NUMBER .GT. 1000) GO TO 104
      HAFSUM=HAFSUM+Y(NUMBER)
  104 CONTINUE
      SUM(I)=HAFSUM*2.0/31416.0
      TRULYT(I)=Y(I)
      WRITE(6,110) X(I),SUM(I),TRULYT(I)
  110 FORMAT(3F20.4)
  105 CONTINUE
      STOP
      END
```

Fig. A 1.4 Listing of the program to calculate instrumental distortion of profiles.

APPENDIX II

ABSORPTION OF 3889Å

The triplet structure of the He 3889Å line was examined by Gibbs and Kruger [60] with a Fabry-Perot interferometer. The term separations are shown in Fig. A2.1. This, with the theoretical relative intensities of the three transitions leads to the structure in Fig. A2.1 which is used in the computation of the absorption curve for the helium triplet metastable state.

For an optically-thin source, as used in the experiments described in Chapter III, the Doppler-broadened emission line profile is given by [54]

$$I_\nu = I_o \Sigma_m R_m \exp\left(- \frac{4 \ln 2}{\alpha^2 (\Delta\nu_D)^2} (\nu - \nu_m)^2 \right)$$

where

$$\alpha = \frac{\text{(source temperature)}}{\text{(discharge temperature)}}$$

$$= \frac{\Delta\nu_s}{\Delta\nu_D}$$

R_m is the fractional contribution to the intensity of the component with line centre at ν_m.

The intensity of the source light after absorption by the discharge with an absorption coefficient k_ν is

$$\int_\nu I_\nu \exp(-k_\nu d)\, d\nu$$

Here, d is the length of the absorption discharge. k_ν is given by

$$k_\nu = \sum_m (k_\nu)_m$$

$$= \sum_m R_m \frac{C\eta}{\Delta\nu_D} \exp\left(-\frac{4\ \ln 2}{(\Delta\nu_D)^2}\ (\nu - \nu_m)^2\right)$$

where η is the reduced number density (Chapter III):

$$\eta = N_1 \left(1 - \frac{g_1}{g_u} \frac{N_u}{N_1}\right)$$

The equation for k_ν satisfies the condition [54] that the absorption coefficients at line centre, $k_{\nu m}$, be in the ratio of the intensities, R_m. If

$$C = \frac{g_u}{g_1} A_{ul} \frac{\lambda_o^2}{8\pi} 2 \left(\frac{\ln 2}{\pi}\right)^{\frac{1}{2}}$$

the equation further satisfies the requirement [54] that

$$\sum_m \left(k_{\nu m}\right)_m = \frac{\lambda_o^2\ g_u}{8\ \pi\ g_1} \eta \frac{A_{ul}}{\Delta\nu_D} 2 \left(\frac{\ln 2}{\pi}\right)^{\frac{1}{2}}$$

Here g_u, g_1 are the upper and lower statistical weights of the transition upper and lower levels. g_u is the sum of the weights of the sublevels of the 3889Å upper level $^3P_{o,\ 1,\ 2}$; hence $g_u = 9$.

To compute the absorption, ABS, let ABSS be the intensity of the source light before absorption by the test discharge:

$$ABSS = \int_\nu I_\nu\ d\nu$$

Absorption is defined as:

(intensity of unabsorbed source light - intensity of source light after absorption)/(intensity of unabsorbed source light)

This is found from ABSD/ABSS where

$$ABSD = \int_\nu I_\nu \, d\nu \quad - \quad \int_\nu I_\nu \exp(-k_\nu \, d) \, d\nu$$

$$= \int_\nu I_\nu \quad (1 - \exp(-k_\nu \, d)) \, d\nu$$

Thus the absorption is computed from the expression

$$\int_\nu \sum_m R_m \exp\left(- \frac{4 \ln 2}{\alpha^2 \, (\Delta\nu_D)^2} \quad (\nu - \nu_m)^2\right) \times$$

$$(1 - \exp(- \sum_m R_m \frac{C \, \eta \, d}{\Delta\nu_D} \exp(- \frac{4 \ln 2}{(\Delta\nu_D)^2} \, (\nu - \nu_m)^2))) \, d\nu$$

$$\int_\nu \sum_m R_m \exp\left(- \frac{4 \ln 2}{\alpha^2 \, (\Delta\nu_D)^2} \quad (\nu - \nu_m)^2\right) d\nu$$

For the 3889Å Helium line, $C = 0.1606 \times 10^{-2}$.

If $\eta d \equiv 10^{11}$ HE

and $\Delta\nu_D \equiv 10^9$ DELNU $= 10^9 \, . \, 0.276\sqrt{T_D}$

then $\frac{C \, \eta \, d}{\Delta\nu_D} = 10^2 . C . HE/DELNU$

So, putting $A \equiv 100 \, C = 0.1606$

$$\frac{C \, \eta \, d}{\Delta\nu_D} = A . \, HE/DELNU$$

If ν and ν_m are calculated in GHz then the coefficient of $(\nu - \nu_m)^2$ may be written

$$B \equiv \frac{4 \ln 2}{(DELNU)^2} = \frac{2.77}{(DELNU)^2}$$

The integration is performed over a span of 50 GHz in increments, DHERTZ, of 0.1GHz with the spacing and relative intensity of the components as in Fig. A 2.1. The computer program prints the values of HE (10^{-11} η d) along with the corresponding values of absorption. The results are graphed in Fig. A 2.2. The program (Fig. A 2.3) was tested by changing the data so that all the components were centred at one frequency and T_D, the discharge temperature, was put equal to the source temperature T_S. In this case, the figures agreed with those given by Mitchell and Zemansky [54] for absorption by a discharge of light from a singlet transition from an optically thin source.

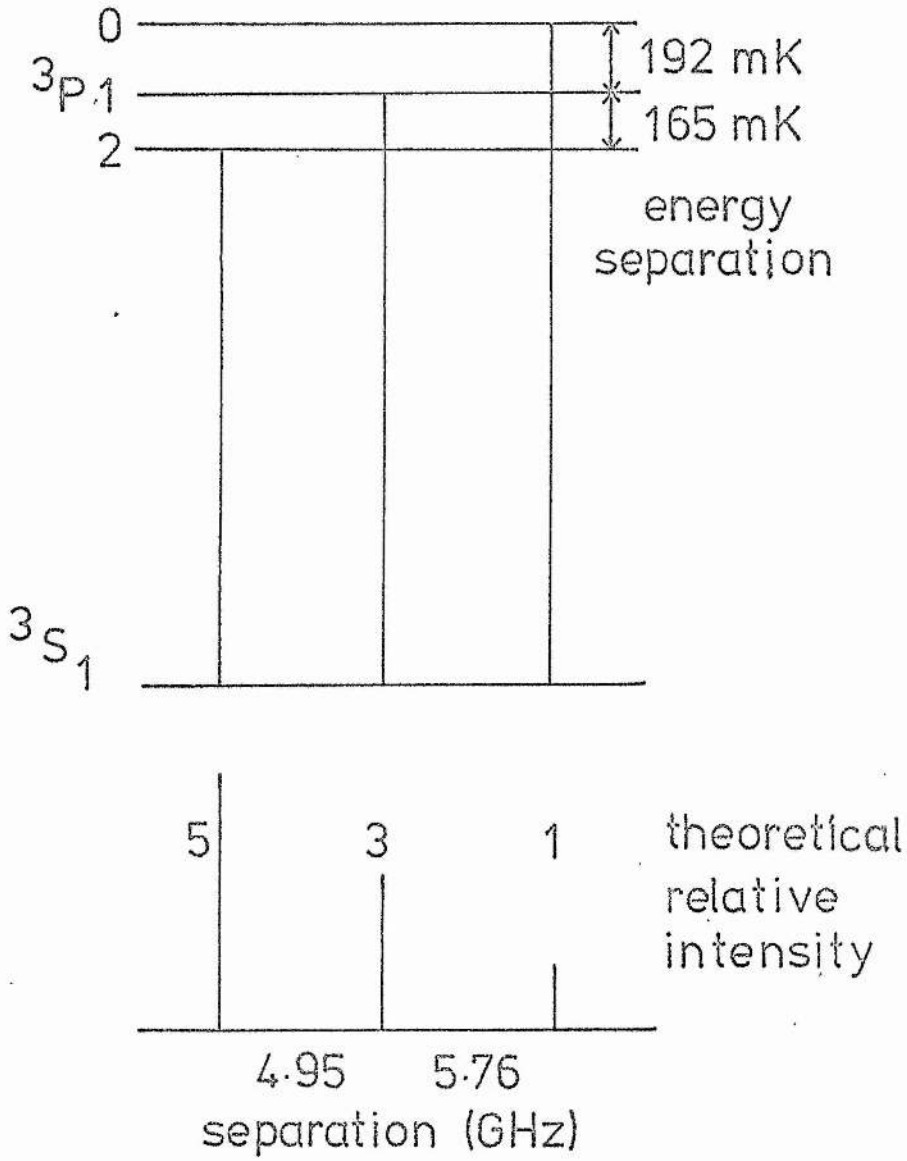

Fig. A 2.1 Structure of the He I 3889Å transition (taken from ref. 62) and the theoretical relative intensities of the components.

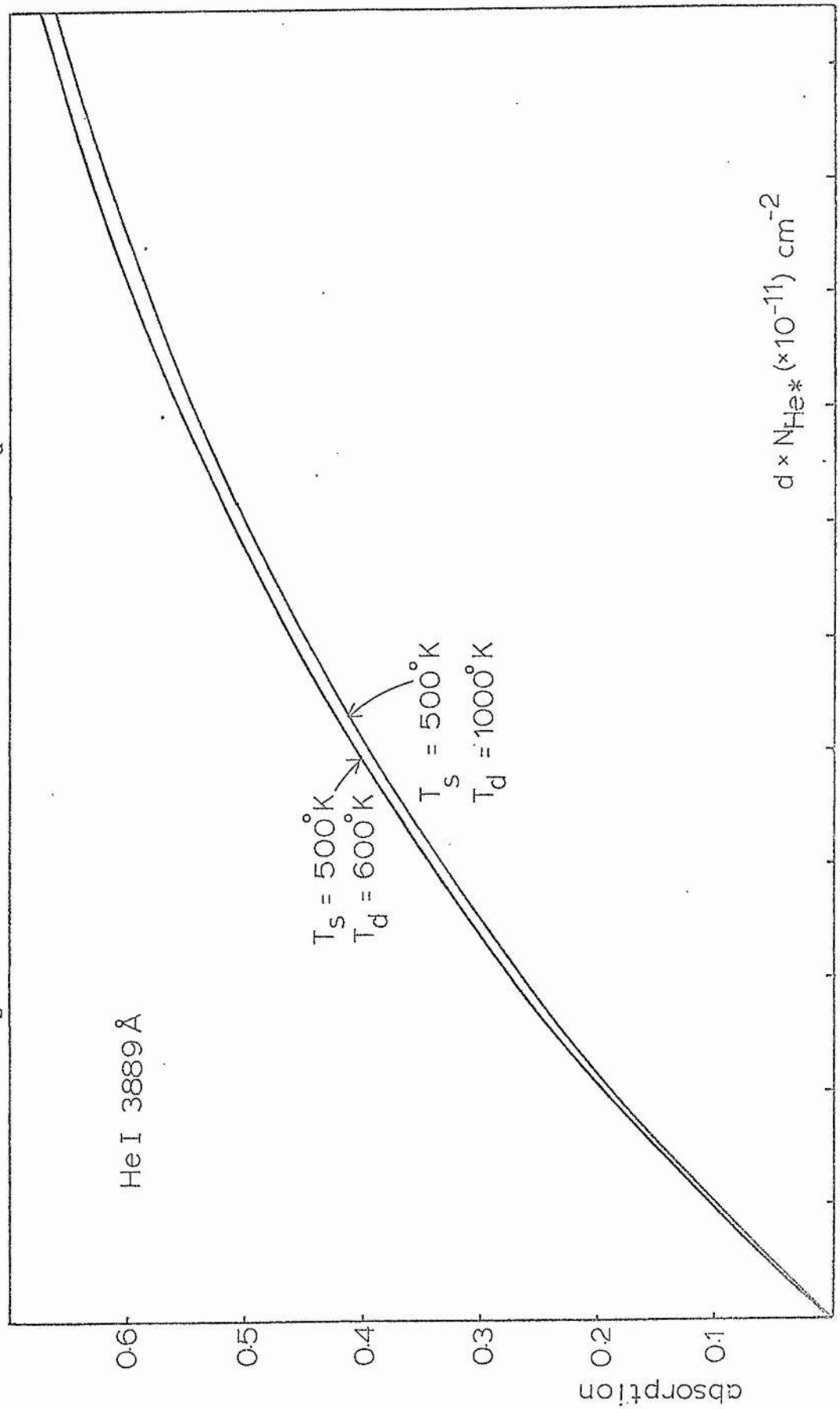

Fig. A 2.2 Computer-derived relation between absorption at 3889Å (He I) and the product of the absorption length and reduced helium triplet metastable density. Valid only for an optically-thin source, temperature T_s, and an absorption discharge of temperature T_d.

```
      DIMENSION HERTZ(500),HE(100)
      READ(5,98) TS,TD,DHERTZ,DELHE
      READ(5,99)R1,R2,R3,HZ1,HZ2,HZ3,A
   98 FORMAT(4F7.2)
   99 FORMAT(7F10.5)
      WRITE(6,100) TS,TD
  100 FORMAT(42X,3HTS=F5.0,5H, TD=F5.0//)
      ALPHA=SQRT(TS/TD)
      DELNU=0.276*SQRT(TD)
      B=2.77/DELNU**2
      HERTZ(1)=0.0
      DO 101 I=2,500
      HERTZ(I)=HERTZ(I-1)+DHERTZ
  101 CONTINUE
      HE(1)=0.0
      DO 102 J=2,100
      HE(J)=HE(J-1)+DELHE
  102 CONTINUE
      DO 104 J=1,100
      ABSS=0.0
      ABSD=0.0
      DO 103 I=1,500
      TRPS1=R1*EXP(-B*(HERTZ(I)-HZ1)**2/ALPHA**2)
      TRPS2=R2*EXP(-B*(HERTZ(I)-HZ2)**2/ALPHA**2)
      TRPS3=R3*EXP(-B*(HERTZ(I)-HZ3)**2/ALPHA**2)
      TRPS=TRPS1+TRPS2+TRPS3
      TRPD1=R1*EXP(-B*(HERTZ(I)-HZ1)**2)
      TRPD2=R2*EXP(-B*(HERTZ(I)-HZ2)**2)
      TRPD3=R3*EXP(-B*(HERTZ(I)-HZ3)**2)
      ABSS=ABSS+TRPS
      ABSD=ABSD+TRPS*(1-EXP(-A*HE(J)/DELNU*(TRPD1+TRPD2+TRPD3)))
  103 CONTINUE
      ABS=ABSD/ABSS
      WRITE(6,105) HE(J),ABS
  105 FORMAT(F50.5,F10.5)
  104 CONTINUE
      STOP
      END
```

Fig. A 2.3 Listing of the program used for relating absorption at 3889Å (HeI) to the reduced helium triplet metastable density.

APPENDIX III

STRUCTURE OF THE CADMIUM ION RESONANCE LINE 2144Å

The complete isotope-shift structure of the cadmium ion resonance line 2144Å ($5p\ ^2P_{3/2} \rightarrow 5s\ ^2S_{1/2}$) has not been published. However, enough has been reported on the structures of 4416Å and 3261Å to enable the detail to be worked out to the accuracy required for computing absorption curves.

For a relatively heavy atom such as cadmium (see for example Kopfermann [61], the principal mechanism for producing the isotope shift is the volume or field effect, where the different distributions of potential inside the nucleus for various isotopes bind penetrating orbital electrons to different degrees, the lighter isotopes of an element binding electrons more strongly than the heavier ones. This affects essentially the s electrons and, to a lesser extent, the p electrons.

Measurements of the hyperfine structure of 4416Å [62], 3261Å [55] and 2288Å [63] show that the relative positions of the isotopic components for a given transition are similar. With this assumption and the result [64] that the shift between isotopes 116 and 110 for both ion resonance lines is similar (69 mK where 1 mK $\equiv 10^{-3}$ $cm^{-1} \equiv$ 30 MHz), the structure of the 2144Å line is taken as that of the 2265Å line. The centres of gravity of isotope 113 and 111 are taken to be separated by 29 mK [65]. It is necessary to use the concept of the centre of gravity because each odd isotope gives rise to a hyperfine structure. (The even isotopes have zero nuclear moment

and so there is no hyperfine splitting.) The positions of the isotopic components of the 2144Å line are shown in Fig. A 3.1 where each odd isotope represents the weighted mean of its hyperfine components. The isotopes 106 and 108 were fixed by scaling from Kuhn and Ramsden's results [62].

The hyperfine splitting of the 5p $^2P_{3/2}$ and 5s $^2S_{1/2}$ states which are the upper and lower levels of the 2144Å transition is shown in Fig. A 3.2. The splitting of the 5p $^2P_{3/2}$ level was taken from ref. [62] and that of the 5s $^2S_{1/2}$ level is after Contreras and Kelly [65]. The relative intensities of the hyperfine components which may be deduced from the intensity rules are taken from tables by Kopfermann [61].

The total contribution of any one isotope to the observed line intensity will be in proportion to its relative abundance in the natural isotopic mixture used. From this, Fig. A 3.3 shows the final structure of the 2144Å line incorporating the hyperfine splitting. This figure is used in the ion resonance line absorption computer program (Appendix IV).

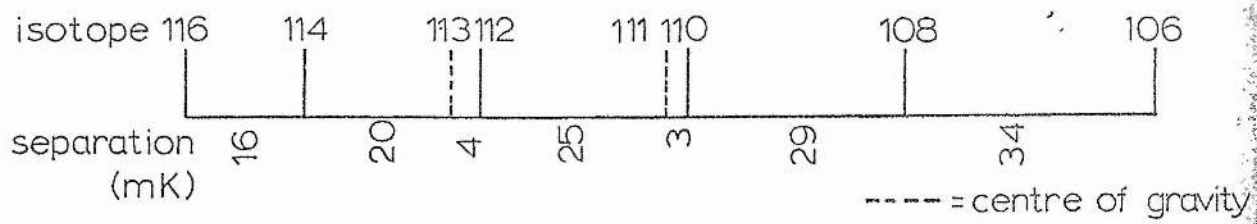

Fig. A 3.1 Isotope structure of the Cd II 2144Å transition.

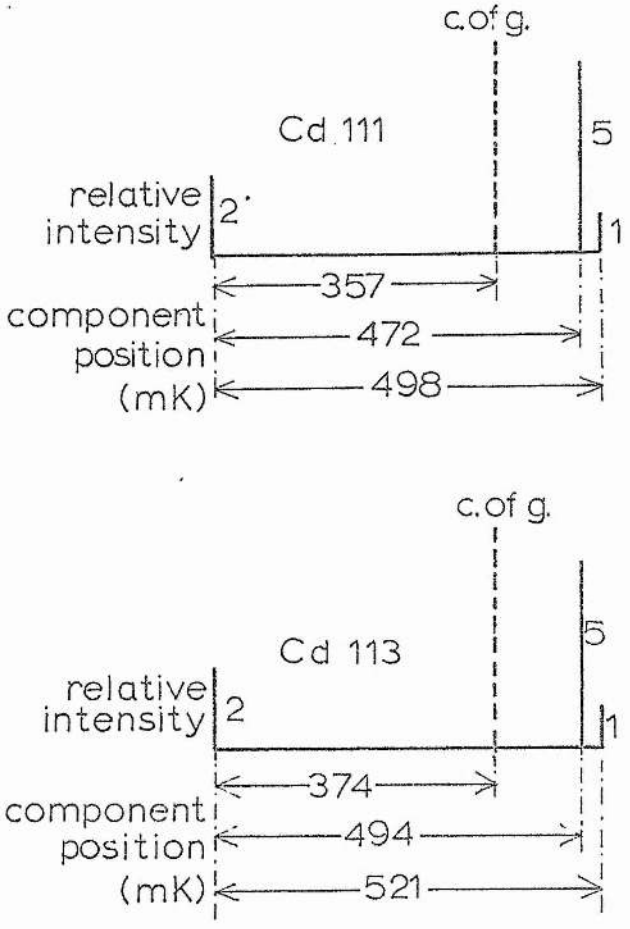

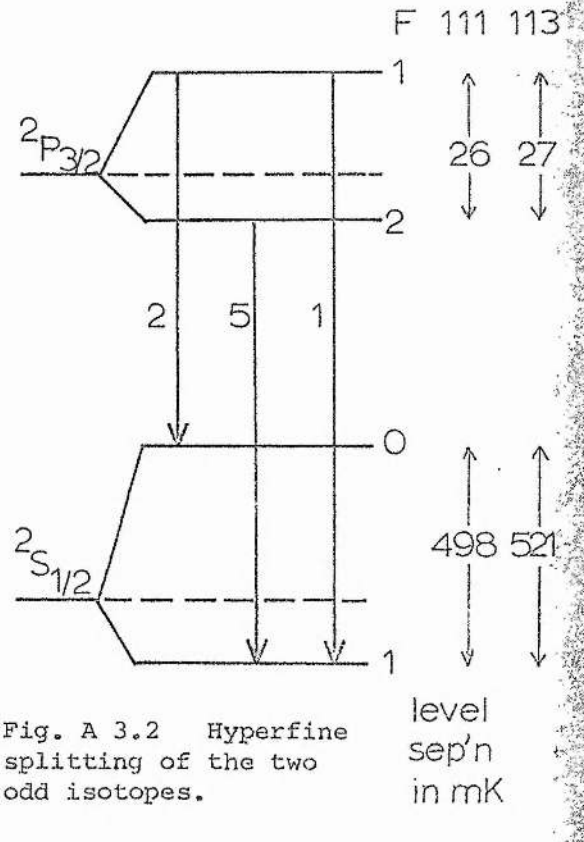

Fig. A 3.2 Hyperfine splitting of the two odd isotopes.

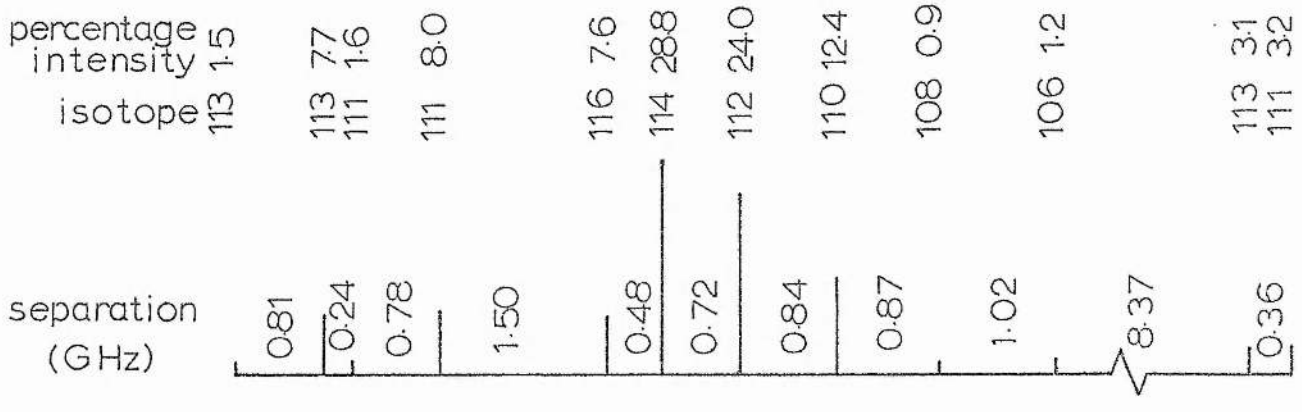

Fig. A 3.3 Final structure of the 2144Å transition.

APPENDIX IV

ABSORPTION OF 2144 Å

The computation of the absorption curve for the cadmium ion 2144Å resonance line follows the same analysis as that for the helium triplet 3889Å (Appendix II). In the present case, A = 1.01 and the integration is performed over 30 GH_z with a 0.01 GHz increment, using the structure worked out for this line in Appendix III.

The computer program (Fig. A 4.2) has been modified slightly to accommodate the additional number of components. The resulting absorption figures (Fig. A 4.1) are computed for the values of CD where $\eta d = 10^{11}$. CD in analogy with the helium case.

Fig. A 4.1 Computer-derived relation between absorption at 2144Å (Cd II) and the product of the absorption length and reduced cadmium ion ground-state density.

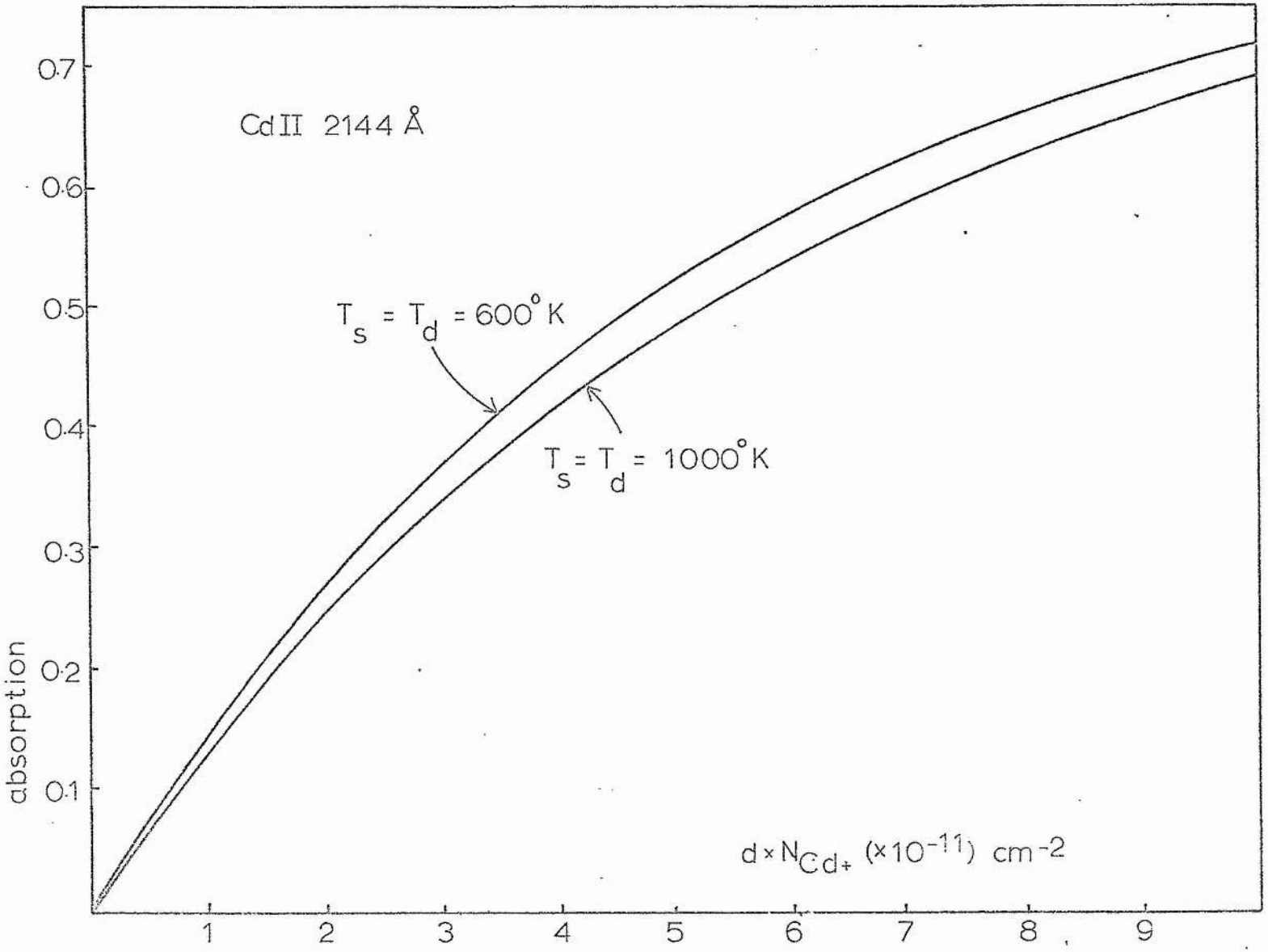

Valid only for an optically thin source, temperature T_s, and an absorption discharge of temperature T_d.

```
      DIMENSION HERTZ(3000),CD(100),R(12),HZ(12)
      READ(5,97) TS,TD,DHERTZ,DELCD,A
      READ(5,99)(R(M),M=1,12)
      READ(5,201) (HZ(M),M=1,12)
   97 FORMAT(2F7.2,3F5.2)
   99 FORMAT(12F6.3)
  201 FORMAT(12F6.2)
      WRITE(6,100)TS,TD
  100 FORMAT(42X,3HTS=F5.0,5H, TD=F5.0//)
      ALPHA=SQRT(TS/TD)
      DELNU=0.0942*SQRT(TD)
      B=2.77/DELNU**2
      HERTZ(1)=0.0
      DO 101 I=2,3000
      HERTZ(I)=HERTZ(I-1)+DHERTZ
  101 CONTINUE
      CD(1)=0.0
      DO 102 J=2,100
      CD(J)=CD(J-1)+DELCD
  102 CONTINUE
      DO 104 J=1,100
      ABSS=0.0
      ABSD=0.0
      DO 103 I=1,3000
      CDS=0.)
      DO 106 M=1,12
      IF(B*(HERTZ(I)-HZ(M))**2/ALPHA**2.GT.70.0) GO TO 106
      CDS=CDS+R(M)*EXP(-B*(HERTZ(I)-HZ(M))**2/ALPHA**2)
  106 CONTINUE
      ABSS=ABSS+CDS
      CDD=0.0
      DO 107 M=1,12
      IF(B*(HERTZ(I)-HZ(M))**2.GT.70.0) GO TO 107
      CDD=CDD+R(M)*EXP(-B*(HERTZ(I)-HZ(M))**2)
  107 CONTINUE
      ABSD=ABSD+CDS*(1-EXP(-A*CD(J)/DELNU*CDD))
  103 CONTINUE
      ABS=ABSD/ABSS
      WRITE(6,105)CD(J),ABS
  105 FORMAT(F50.5,F10.5)
  104 CONTINUE
      STOP
      END
```

Fig. A4.2 Listing of the program used for relating absorption at 2144Å (CdII) to the reduced cadmium ion ground-state density.

APPENDIX V

CORRECTION FOR SELF-ABSORPTION AT 2144Å

The spontaneous emission profiles of cadmium 2144Å emission (Chapter IV) must be corrected for self-absorption before they can indicate the relative concentrations of the $5p\ ^2P_{3/2}$ level ions. Since the number densities of the ground state ions have been measured this is achieved by computing a graph of the correction factor against the product of cadmium ion reduced number density and discharge length. The correction factor will be I_t/I_m where I_t is the intensity which would have been measured if there were no self-absorption and I_m is the actual measured intensity.

Let I_ν be the flux collected between ν and $\nu + d\nu$ by the optical detection system per unit length of discharge, neglecting absorption. Because of the linearity of the system (Chapter III) this term is constant along the column for given discharge conditions. The detected signal taking absorption into account is

$$I_m = \int_\nu \int_o^d I_\nu \exp(-k_\nu x)\, dx\, d\nu$$

$$= \int_\nu \frac{I_\nu}{k_\nu} (1 - \exp(-k_\nu d))\, d\nu$$

If (see Appendix II)

$$k_\nu = \sum_m \frac{R_m C\eta}{\Delta\nu_D} \exp\left(-\frac{4 \ln 2}{(\Delta\nu_D)^2} (\nu - \nu_m)^2\right)$$

and

$$I_\nu = I_o \sum_m R_m \exp\left(-\frac{4 \ln 2}{(\Delta\nu_D)^2} (\nu - \nu_m)^2\right)$$

then

$$I_m = \frac{I_o}{\left(\frac{C\eta}{\Delta\nu_D}\right)} \int_\nu \left(1 - \exp\left(-\sum_m R_m \frac{C\,\eta\,d}{\Delta\nu_D} \exp\left(-\frac{4\ln 2}{(\Delta\nu_D)^2}(\nu - \nu_m)^2\right)\right)\right) d\nu$$

and

$$I_t = \int_\nu \int_o^d I_\nu \, dx \, d\nu$$

$$= d \int_\nu I_o \sum_m R_m \exp\left(-\frac{4\ln 2}{(\Delta\nu_D)^2}(\nu - \nu_m)^2\right) d\nu$$

So

$$\frac{I_t}{I_m} = \frac{C\,\eta\,d}{\Delta\nu_D} \frac{\int_\nu \sum_m R_m \exp\left(-\frac{4\ln 2}{(\Delta\nu_D)^2}(\nu - \nu_m)^2\right) d\nu}{\int_\nu \left(1 - \exp\left(-\sum_m R_m \frac{C\,\eta\,d}{\Delta\nu_D} \exp\left(-\frac{4\ln 2}{(\Delta\nu_D)^2}(\nu - \nu_m)^2\right)\right)\right) d\nu}$$

This integration is performed in the computer program (Fig. A 5.2) which uses similar nomenclature to the program for Cd 2144Å absorption. The results are graphed in Fig. A 5.1. The program was tested by setting the frequencies of all the components equal to each other and the resulting graph was the same as that derived by Harrison [58] by graphical integration for a singlet transition.

Fig.A5.1 Computed graph to correct for self-absorption at 2144Å for a given reduced cadmium ion ground-state density. Curves derived for a discharge temperature of 600°K.

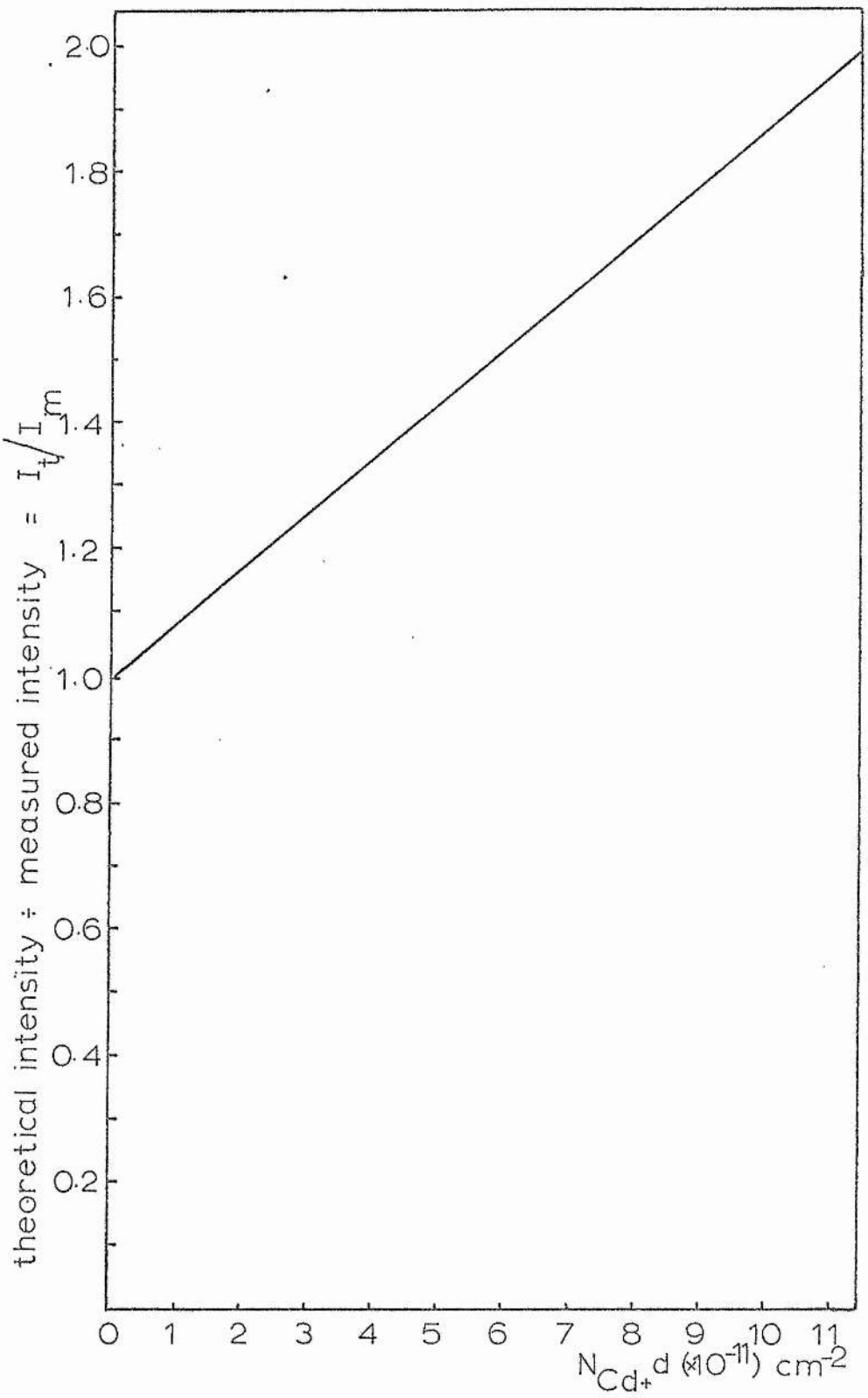

```
      DIMENSION HERTZ(3000),CD(100),R(12),HZ(12)
      READ(5,97) TD,DHERTZ,DELCD,A
      READ(5,99)(R(M),M=1,12)
      READ(5,201) (HZ(M),M=1,12)
   97 FORMAT(F7.2,3F5.2)
   99 FORMAT(12F6.3)
  201 FORMAT(12F6.2)
      WRITE(6,100)TD
  100 FORMAT(52X,3HTD=F5.0//)
      DELNU=0.0942*SQRT(TD)
      B=2.77/DELNU**2
      HERTZ(1)=0.0
      DO 101 I=2,3000
      HERTZ(I)=HERTZ(I-1)+DHERTZ
  101 CONTINUE
      CD(1)=0.0
      DO 102 J=2,100
      CD(J)=CD(J-1)+DELCD
  102 CONTINUE
      DO 104 J=2,100
      ABSS=0.0
      ABSD=0.0
      DO 103 I=1,3000
      CDD=0.0
      DO 107 M=1,12
      IF(B*(HERTZ(I)-HZ(M))**2.GT.70.0) GO TO 107
      CDD=CDD+R(M)*EXP(-B*(HERTZ(I)-HZ(M))**2)
  107 CONTINUE
      ABSS=ABSS+CDD
      ABSD=ABSD+(1-EXP(-A*CD(J)/DELNU*CDD))
  103 CONTINUE
      ABS=A*CD(J)*ABSS/DELNU/ABSD
      WRITE(6,105)CD(J),ABS
  105 FORMAT(F50.5,F10.5)
  104 CONTINUE
      STOP
      END
```

Fig. A5.2 Listing of the program used for correcting for self-absorption at 2144Å.

APPENDIX VI

CONTRIBUTION OF ELECTRON EXCITATION TO THE 5378Å TRANSITION

APPENDIX VII

COMPUTER SOLUTION OF THE CURRENT - MODULATION PROBLEM

We wish to estimate the contribution of electron excitation from the cadmium ion ground state to the pumping of the 4f levels, the upper levels of the 5378Å and 5337Å transitions.

Suppose that the pumping rate from cascade from Duffendack-excited levels at the centre of the discharge is f_{He+}. Let the additional electron pump rate be f_e at the axis. Hence the total axial pump rate of the 4f levels is $f_{He+} + f_e$.

The dip ratio of the pump rate, due to cascade from the Duffendack levels, $r_{f_{He+}}$, is found by measuring the dip ratio of the 6360Å transition, r_{6360}, assuming that this line is pumped purely by charge-exchange reactions. Hence

$$r_{f_{He+}} = r_{6360}$$

Since f_e varies as the product of the electron density and the cadmium ground-state ion density, the dip ratio of the electron pumping profile, r_{fe}, may be written

$$r_{fe} = r_e \, r_{Cd+}$$

Here r_{Cd+} is the dip ratio for the cadmium ground-state ion profile found experimentally in Chapter VI and r_e is the electron density dip ratio which is equal to 0.4 for a Bessel distribution. Thus

$$r_{fe} = 0.4 \, r_{Cd+}$$

From the definition of the dip ratio, the total pumping of the 4f levels at 0.7R must be the sum of the electron and the Duffendack contributions at 0.7R, viz $f_{He+} r_{f_{He+}} + f_e r_{fe}$. Therefore the dip ratio at 5378Å, r_{5378}, will be given by

$$r_{5378} = \frac{r_{f_{He+}} f_{He+} + r_{f_e} f_e}{f_{He+} + f_e}$$

In terms of the experimentally observed qualities this becomes

$$r_{5378} = \frac{r_{6360} f_{He+} + 0.4\, r_{Cd+} f_e}{f_{He+} + f_e}$$

Rearranging gives

$$\frac{f_e}{f_{He+}} = \frac{r_{6360} - r_{5378}}{r_{5378} - 0.4\, r_{Cd+}}$$

For example, at 10 Torr 100mA,

$$r_{6360} = 2.0$$

$$r_{5378} = 1.51$$

$$r_{Cd+} = 0.96$$

and so

$$\frac{f_e}{f_{He+}} = 0.43$$

For illustration, the profiles relating to this example are shown in Fig. 3.9. Such a value for the electron-Duffendack pumping ratio is fairly typical for a wide range of discharge conditions. However this ratio would need to be increased if electron pumping of the 6360Å transition were shown to be significant.

The equation to be solved in Chapter VII is

$$\frac{\partial x}{\partial t} = D\nabla^2 X - XN_e f$$

where X is the cadmium concentration and $N_e f$ is the ionisation rate which is modulated sinusoidally. This form of equation is not generally amenable to analytic solution and so it is reduced to a finite-difference equation for numerical solution (considering only radial dependence):

$$\Delta X = D \frac{\Delta t}{(\Delta r)^2} \left(X_{J+1} - 2X_J + X_{J-1} \right)$$

$$+ D \frac{\Delta t}{\Delta r} \frac{1}{r} \frac{1}{2} \left(X_{J+1} - X_{J-1} \right) - X_J N_e f \Delta t$$

Here X_K is the instantaneous number density at a distance $(K - 1)\Delta r$ from the axis. $\frac{D \Delta t}{(\Delta r)^2}$ must be set $\leq \frac{1}{2}$, otherwise the errors incurred by truncating the series would grow [66]. At the axis the finite-difference equation must be modified [66] so that

$$\Delta X_1 = \frac{4 D \Delta t}{(\Delta r)^2} \left(X_2 - X_1 \right) - X_1 N_e f \Delta t$$

where X_1 is the axial concentration. We divide the tube radius into ten sections.

The profile of cadmium is at first taken to be flat across the tube, and, since there would be transient oscillations when the current is first switched on in the program, the modulation of the current is not applied until 500 time increments (500 Δt) have passed to let the discharge settle down. This has been found an adequate period of time to achieve stability. The boundary condition assumed up to 500 Δt is that all the cadmium which has

been ionised appears as neutral cadmium which builds up at the boundary and which diffuses back into the plasma. Without this condition the assumed metal vapour concentration would rapidly diminish.

After 500 Δt it is recognised that the cadmium at the discharge edge will be in equilibrium with cadmium already deposited on the wall. If σ ($= \frac{N_i}{\tau_i} R^2$) is the ionisation rate per unit length of discharge, divided by π, and X_{11} is the discharge cadmium concentration at the wall, then the rate of increase of the wall population, N_w, is

$$\frac{\Delta N_w}{\Delta t} = \frac{\sigma}{2R} + X_{11} \frac{c}{4} - \frac{N_w}{\tau_w}$$

c is the average random speed of the cadmium atoms and τ_w is the wall sticking-time. This equation determines the subsequent boundary conditions. Because this rate depends on a small difference between two large quantities, the wall increase is determined in the program by summing the deviations from the equilibrium situation assumed at 500 Δt.

Fig.A 7.1 shows computed graphs of the time dependence of current, the axial cadmium neutral ground state population and excited (Duffendack-pumped) cadmium state population. Note that, while the current modulation is sinusoidal, the other two curves are obviously not. Therefore the computed average signal of the lower two curves (set arbitrarily equal to unity) does not lie symmetrically between the values of maximum and minimum signal.

The remainder of the program calculates the phase and other properties of the cadmium concentration. Since the cadmium excited and neutral ground-state densities will not be generally sinusoidal with time, the phase is determined in the same way as is done in phase-sensitive detection - the point is noted at which the signal averaged over half a period is equal to the signal averaged over one complete period. Further details of the program appear as comments in the program itself (Fig. A 7.2).

The phases of the excited and neutral cadmium signals were virtually independent of the amplitude of the current modulation. For example, at $\phi = 4 \times 10^4$, D = 110 and frequency = 1 KHz, the computed phase of the cadmium excited species was 148.8° with a peak-peak current modulation of 0.5 (ie half its average value) and 149.0° with a modulation of 0.16 peak-peak.

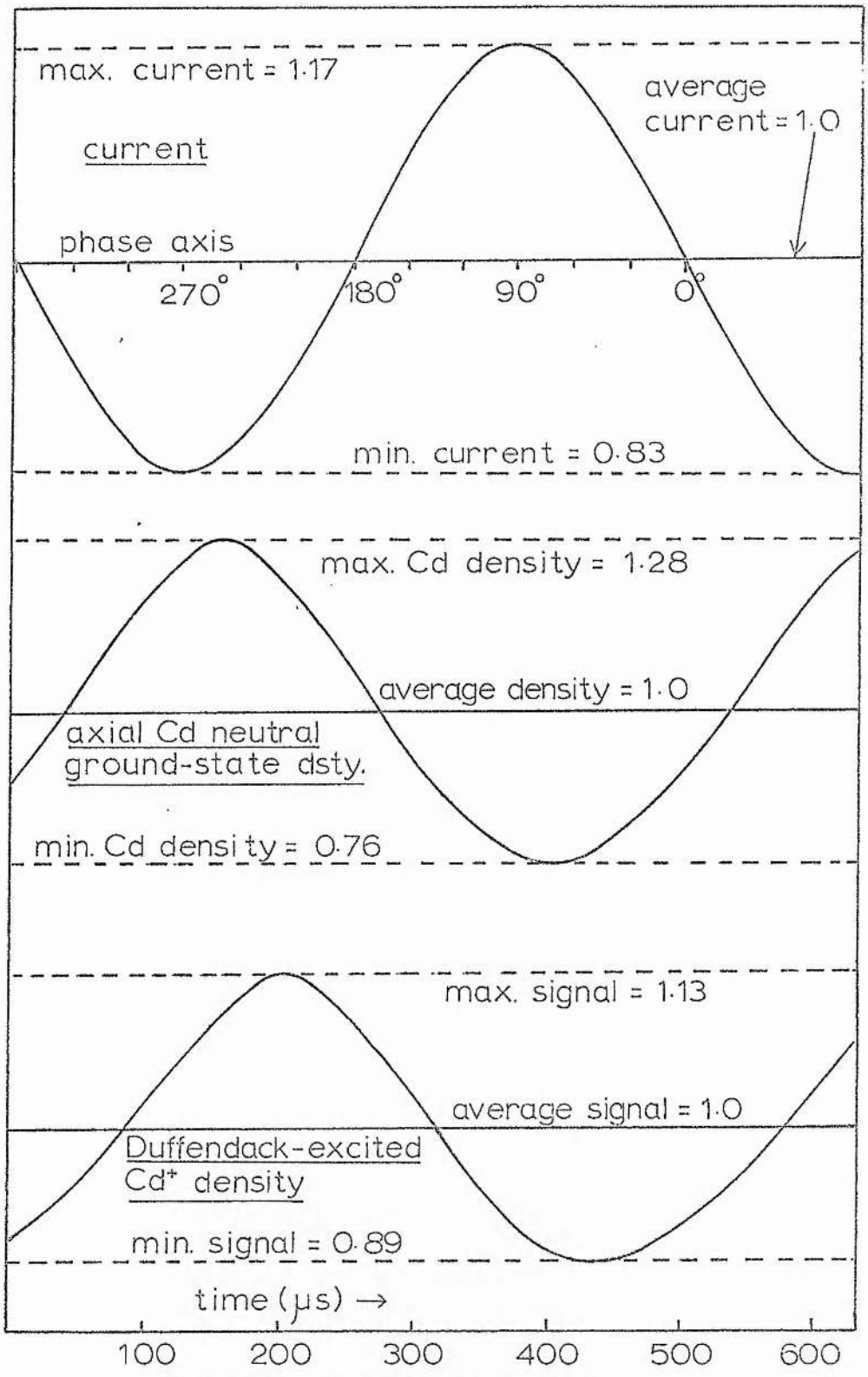

Fig. A 7.1 Computed time behaviour of current, axial cadmium neutral ground-state and axial cadmium excited-state densities. Examples shown here for current p-p modulation = 0.34, ϕ = 4×10^4 s^{-1}, D = 110 cm^2 s^{-1}, frequency = 2kHz. Computed neutral cadmium phase lead = 159°; computed excited cadmium phase lead = 126°.

```
      DIMENSION X(11),DX(11),R(11),F(11),PHI(11),D(20),FREQCY(20),VALUE(
     £7500,4),SIZE(7500)
      READ(5,10) NUMBER
   10 FORMAT (I2)
      INTEGER ALPHA,BETA,GAMMA
      REAL MODUL,NWALL
      READ(5,1) DR,DT,A,B
    1 FORMAT(4E8.1)
      READ(5,56) LAST
   56 FORMAT(I4)
      READ(5,23) TWALL
   23 FORMAT(E9.2)
      READ(5,18) (PHI(K),D(K),FREQCY(K),K=1,NUMBER)
   18 FORMAT(3F20.1)
      READ(5,900) SPEED
  900 FORMAT(E6.1)
      WRITE(6,8) DR,DT,A,B,TWALL
    8 FORMAT(1X,3HDR=E9.2,5H, DT=E9.2,4H, A=F5.3,4H, B=F5.3,8H, TWALL=F8
     £.5//)
      DO 19 K=1,NUMBER
      WRITE(6,17)PHI(K),D(K),FREQCY(K)
   17 FORMAT(1H0,1X,4HPHI=F8.1,4H, D=F5.1,9H, FREQCY=F7.1)
      PERIOD=1.0/FREQCY(K)
C
C     "LOOP 1" IS THE NUMBER OF TIME INTERVALS REQUIRED TO MAKE UP ONE
C     PERIOD.
C
      LOOP 1=INT(PERIOD/DT)
      LOOP 2=INT(PERIOD/2.0/DT)
      OMEGA=6.2832*FREQCY(K)
      ALPHA=LAST-LOOP 1
      BETA=LAST-LOOP 2
      GAMMA=ALPHA+1
      R(1)=0.0
C
C
C     THE TUBE RADIUS IS DIVIDED INTO TEN SEGMENTS.
C
      DO 2 J=2,11
```

Fig. A7.2 Listing of the program simulating current modulation of the He-Cd discharge.

```
      R(J)=R(J-1)+DR
    2 CONTINUE
C
C     "XTOTAL" IS THE INITIAL POPULATION PER UNIT LENGTH OF DISCHARGE,
C     DIVIDED BY PI. THE NUMBER DENSITY IS ARBITRARILY ASSIGNED AN
C     INITIAL VALUE OF 10.
C
      XTOTAL=10.0*R(11)*R(11)
      DO 3 J=1,11
      X(J)=10
    3 CONTINUE
      DELTA=0.0
      DELX11=0.0
      T=0.0
      DO 9 I=1,LAST
      T=T+DT
C
C     FOR STABILITY, THE DISCHARGE RUNS WITHOUT MODULATION AND WITH A
C     WALL-STICKING TIME OF ZERO FOR THE FIRST 500 TIME INCREMENTS.
C
      IF(I.GE.500) GO TO 15
      AMP=0.0
      GO TO 14
   15 TIME=T-500.0*DT
      AMP=SIN(OMEGA*TIME)
   14 CONTINUE
      DO 4 J=1,11
C
C     "F(J)" IS THE IONISATION RATE PER NEUTRAL METAL ATOM.
C
      F(J)=PHI(K)*(1.0+A*AMP)*(1.0-1.446*(R(J)/R(11))**2+0.5227*(R(J)/
     £R(11))**4-0.0839*(R(J)/R(11))**6)
    4 CONTINUE
      DO 5 J=2,10
C
C     "DX" IS THE CHANGE IN "X" IN ONE TIME INCREMENT DUE TO DIFFUSION
C     AND IONISATION.
C
      DX(J)=D(K)*DT/DR/DR*(X(J+1)-2.0*X(J)+X(J-1))+D(K)*DT/R(J)/DR*(X(J+
```

Fig. A7.2 (continued)

```
     £1)-X(J-1))/2.0-F(J)*X(J)*DT
   5 CONTINUE
     DX(1)=D(K)*DT/DR/DR*4.0*(X(2)-X(1))-F(1)*X(1)*DT
C
C      "SIGMA" COMPUTES THE TOTAL IONISATION PER UNIT LENGTH OF DISCHARGE
C      PER TIME INCREMENT,"DT", DIVIDED BY PI.
C
      SIGMA=DR*DR*F(1)*X(1)/4.0
      DO 6 J=2,10
      SIGMA=SIGMA+(R(J)*R(J)+DR*DR-R(J-1)*R(J-1))*F(J)*X(J)
   6 CONTINUE
C
C      AFTER 500 TIME INCREMENTS, A VALUE IS ASSUMED FOR THE
C      WALL POPULATION SUCH THAT THE ION FLUX AND THE NEUTRAL RANDOM FLUX
C      TO THE WALLS BALANCES THE FLUX FROM THE WALLS DETERMINED BY
C      "TWALL", THE WALL STICKING-TIME.  THIS IS TAKEN HEREAFTER AS THE
C      BOUNDARY CONDITION.
C
      IF(I.LT.500) GO TO 16
      IF(I.GT.500) GO TO 11
      SIGMA0=SIGMA
      X110=X(11)
  11  DELX11=X(11)-X110
      DNWALL=(SIGMA-SIGMA0)*DT/2.0/R(11)-DELTA*DT/TWALL+DELX11*SPEED*DT/
     £4.0
      DELTA=DELTA+DNWALL
      X(11)=X110+4.0/SPEED*(DNWALL/DT+DELTA/TWALL-(SIGMA-SIGMA0)/2.0
     £/R(11))
      DX(11)=X(11)-X(10)-DX(10)
      GO TO 20
  16  DX(11)=SIGMA*DR/R(11)/D(K)/2.0
  20  DO 7 J=1,10
      X(J)=X(J)+DX(J)
   7 CONTINUE
      X(11)=X(10)+DX(11)
C
C      "XTEMP" IS THE TOTAL INSTANTANEOUS NEUTRAL POPULATION PER UNIT
C      LENGTH OF THE DISCHARGE, DIVIDED BY PI.
C      INITIALLY, THE NUMBER DENSITY IS NORMALISED BY "RATIO" (USUALLY
```

Fig. A7.2 (continued)

```
C       UNITY TO WITHIN 0.003%) IN ORDER TO PREVENT DRIFT DUE TO ERRORS
C       INTRINSIC IN THE COMPUTATION OF SIGMA.  "FACTOR" TAKES OVER WHEN
C       THE WALL POPULATION IS ALSO CONSIDERED.
C
        XTEMP=0.0
        DO 12 J=1,10
        XTEMP=XTEMP+(X(J)+X(J+1))*(R(J)+R(J+1))*DR/2.0
   12   CONTINUE
        IF(I.GE.500) GO TO 41
        RATIO=XTOTAL/XTEMP
        DO 13 J=1,11
        X(J)=X(J)*RATIO
   13   CONTINUE
        GO TO 42
   41   FACTOR=(XTOTAL-2.0*R(11)*DELTA)/XTEMP
        DO 42 J=1,11
        X(J)=X(J)*FACTOR
   42   CONTINUE
        DIP=X(8)/X(1)
        IF (I.GE.ALPHA) GO TO 21
        GO TO 9
   21   VALUE(I,1)=X(1)*(1.0+B*AMP)
        VALUE(I,2)=DIP
        VALUE(I,3)=X(1)
        VALUE(I,4)=XTEMP
        IF(I.EQ.ALPHA) START=TIME
    9   CONTINUE
C
C       THE NEXT 34 LINES COMPUTE THE PHASE, AVERAGE SIGNAL ("AVRAGE") AND
C       THE MODULATION AMPLITUDE ("MODUL") OF THE AXIAL DENSITIES OF THE
C       NEUTRAL GROUND-STATE SPECIES AND HELIUM-ION-EXCITED SPECIES, THE
C       PI-NORMALISED DISCHARGE POPULATION AND THE DIP.
C
C
C       THE PHASE IS DETERMINED USING THE SAME CRITERIA AS PHASE-SENSITIVE
C       DETECTION, NAMELY NOTING THE POINT AT WHICH THE SIGNAL AVERAGED
C       OVER HALF A PERIOD IS EQUAL TO THE SIGNAL AVERAGED OVER ONE
C       COMPLETE PERIOD.
C
```

Fig. A7.2 (continued)

```
      PHASEB=360.0*(START/PERIOD-AINT(START/PERIOD))
      DO 29 N=1,4
      SUM=0.0
C
C     THE SIGNAL IS AVERAGED OVER ONE COMPLETE PERIOD.
C
      DO 51 I=ALPHA,LAST
      SUM=SUM+VALUE(I,N)
   51 CONTINUE
      AVRAGE=SUM*DT/PERIOD
      TOTAL=0.0
C
C     THE SIGNAL IS SUMMED OVER HALF A PERIOD.
C
      DO 52 I=ALPHA,BETA
      TOTAL=TOTAL+VALUE(I,N)
   52 CONTINUE
C
C     THE HALF-PERIOD SUMMATION IS NOW EXECUTED OVER PROGRESSIVELY
C     LATER HALF-PERIOD INTERVALS.
C
      DO 53 I=ALPHA,BETA
      INDEX=I+LOOP 2
      TOTAL=TOTAL-VALUE(I,N)+VALUE(INDEX,N)
C
C     THE NEXT 12 LINES FIND "NODE", WHICH IS THE VALUE OF "I" STARTING
C     FROM WHICH THE AVERAGE OF THE SIGNAL FOR HALF A PERIOD IS EQUAL TO
C     THE AVERAGE OF THE SIGNAL OVER ONE COMPLETE PERIOD.
C
      SIZE(I)=ABS(TOTAL-SUM/2.0)
   53 CONTINUE
      BIG=SIZE(ALPHA)
      SMALL=SIZE(ALPHA)
      DO 58 I=GAMMA,BETA
      IF(BIG.LT.SIZE(I)) BIG=SIZE(I)
      IF(SMALL.GT.SIZE(I)) SMALL=SIZE(I)
   58 CONTINUE
      DO 54 I=ALPHA,BETA
      NODE=I
```

Fig. A7.2 (continued)

```
      IF(SIZE(I).EQ.SMALL) GO TO 55
   54 CONTINUE
   55 IF(VALUE(NODE,N).LT.AVRAGE) PHASE=90.0+360.0*FLOAT(LAST-LOOP 2-NOD
     £E)/FLOAT(LOOP 1)
      IF(VALUE(NODE,N).GT.AVRAGE) PHASE=90.0+360.0*FLOAT(LAST-NODE)/FLOA
     £T(LOOP 1)
      IF(PHASE.GT.360.0) PHASE=PHASE-360.0
      PHASE1=PHASE-PHASEB
      IF(PHASE1.LT.0.0) PHASE1=PHASE1+360.0
      MODUL=2.0*BIG*DT/PERIOD/AVRAGE
      IF(N.EQ.1) WRITE(6,47)
      IF(N.EQ.2) WRITE(6,49)
      IF(N.EQ.3) WRITE(6,46)
      IF(N.EQ.4) WRITE(6,48)
   46 FORMAT(1HO,30X,21HAXIAL NEUTRAL SPECIES)
   47 FORMAT(1HO,30X,21HAXIAL EXCITED SPECIES)
   48 FORMAT(1HO,30X,24HDISCHARGE NUMBER DENSITY)
   49 FORMAT(1HO,30X,11HNEUTRAL DIP)
      WRITE(6,45) PHASE1,AVRAGE,MODUL
   45 FORMAT(10X,12HPHASE LEAD =F6.1,8H DEGREES,10X,15HAVERAGE VALUE =F8
     £.4,10X,12HMODULATION =F8.4)
      IF(MODUL .LT. 4.0/FLOAT(LOOP 1)) WRITE(6,100)
C
C     OWING TO THE DISCRETE NATURE OF THE INTEGRATION, THERE CAN BE A
C     FRACTIONAL ERROR IN THE SIGNAL EQUAL TO THE RECIPROCAL OF THE
C     NUMBER OF STEPS IN ONE PERIOD.  SINCE THE PHASE DEPENDS ON THE
C     DIFFERENCE BETWEEN THE INSTANTANEOUS SIGNAL AND THE AVERAGE
C     SIGNAL, THE PHASE IS ONLY WELL DETERMINED IF THE DIFFERENCE
C     DIVIDED BY THE AVERAGE IS MUCH GREATER THAN THE ABOVE-MENTIONED
C     FRACTION.  THIS MEANS THAT "MODUL" MUST ALSO BE LARGER THAN THE
C     RECIPROCAL OF "LOOP 1".  IF THIS CRITERION IS NOT OBEYED, THE
C     FOLLOWING IS PRINTED:-
C
  100 FORMAT(1X,49HNB:- PHASE IS SUSPECT OWING TO REDUCED MODULATION)
   29 CONTINUE
   19 CONTINUE
      STOP
      END
```

Fig. A7.2 (continued)

REFERENCES

1. Silfvast, W.T., Appl Phys Lett 13, 169 - 171, 1968.
2. Sosnowski, T.P., J Appl Phys 40, 5138 - 44, 1969.
3. Goldsborough, J.P., Appl Phys Lett 15, 159 - 161, 1969.
4. Francis, G, Handbuch der Physik, Springer-Verlag, Berlin, Vol XXII pp 53 - 208, 1956.
5. Silfvast, W.T., Appl Phys Lett 15, 23 - 25, 1969.
6. Hodges, D.T., Appl Phys Lett 18, 454 - 456, 1971.
7. Silfvast, W.T. and Klein, M.B., Appl Phys Lett 17, 400 - 403, 1970.
8. Jensen, R.C., Collins, G.J. and Bennet, W.R., Phys Rev Lett 23, 363 - 367, 1969.
9. Ferrario A, Optics Comm 7, 376 - 378, 1973.
10. Green, J.M. and Webb, C.E., J Phys B : Atom Molec Phys 7, 1698 - 1710, 1974.
11. Browne, P.G. and Dunn, M.H., J Phys B : Atom Molec Phys 6, 1103 - 1117, 1973.
12. Klein, M.B. and Silfvast, W.T., Appl Phys Lett 18, 482 - 485,
13. Griem, H.R. Plasma Spectroscopy, McGraw-Hill, New York, 1964, page 171.
14. Browne, P.G. and Dunn, M.H., J Phys B : Atom Molec Phys 7, 1113 - 1121, 1974.
15. Ferrario, A, Optics Comm 8, 333 - 335, 1973.

16. Cobine, J.D., Gaseous Conductors, Dover, New York, 1958, page 246.

17. Turner-Smith, A.R., Green, J.M. and Webb, C.E., J.Phys B : Atom Molec Phys 6, 114 - 130, 1973.

18. Turner-Smith, A.R., Ph.D. thesis, Oxford University, 1971.

19. Webb, C.E., J Appl Phys 39, 5441 - 5470, 1968.

20. Hodges, D.T., Appl Phys Lett 17, 11 - 13, 1970.

21. Geneux, E. and Wanders-Vincenz, B. Helv Phys Act 33, 185 - 220 (1960).

22. Schaefer, A.R., J Quant Spect Rad Transfer 11, 197 - 201, 1971.

23. Geneux, E. and Wanders-Vincenz, B., Phys Rev Lett 3, 422 - 423, 1959.

24. Collins, G.J., Jensen, R.C. and Bennet, W.R., Appl Phys Lett 19, 125 - 128, 1971.

25. Andersen, T and Sorensen, G., J Quant Spect Rad Transfer 13, 369 - 376, 1973.

26. Hasted, J.B., Physics of Atomic Collisions, Butterworths, London, 1964, page 417.

27. Brown, S.C., Basic Data of Plasma Physics, MIT, London, 1966.

28. Mansbach, P and Keck, J., Phys Rev 181; 275 - 289, 1969.

29. Hinnov, E, and Hirschberg, J.G., Phys Rev 125, 795 - 801, 1962.

30. Von Engel, A., Ionised Gases, Oxford, London, 1965.

31. Spenke, E, Z Phys 127, 221 - 242, 1950.

32. Silfvast, W.T. and Szeto, L.H., Appl Phys Lett 19, 445 - 447, 1971.

33. Dunn, M.H., J.Phys B : Atom Molec Phys 5, 665 - 672, 1972.

34. Schearer, L.D. and Padovani, F.A., J Chem Phys 52, 1618 - 19, 1970.

35. Riseberg, L.A. and Schearer, L.D., Phys Lett 35A, 269 - 270, 1971.

36. Phelps, A.V., Phys Rev 99, 1307 -1313, 1955.

37. Compton, K.T., Phys Rev 22, 333 - 346, 1923.

38. Crompton, R.W., Elford, M.T. and Jory, R.L., Aust J Phys 20, 369 - 400, 1967.

39. Weast, R.C.(Ed), Handbook of Chemistry and Physics, Chemical Rubber Co., Cleveland, 1973.

40. Loeb, L.B., Kinetic Theory of Gases, McGraw-Hill, London, 1934, Chapter VI.

41. Chapman, S. and Cowling, T.G., The Mathematical Theory of Non-Uniform Gases, Cambridge, London, 1952, page 245.

42. Spier, J.L., Physica 7, 381 - 384, 1940.

43. Walker, R.E. and Westenberg, A.A., J Chem Phys 29, 1139 - 1153, 1958.

44. Dalgarno, A, Atomic and Molecular Processes, ed Bates, D.R., Academic, London, 1962, page 647.

45. Grew, K.E. and Ibbs, T.L., Thermal Diffusion in Gases, Cambridge : University Press, 1952, page 6.

46. Vokaty, E and Masek, K., Czech J Phys B 22, 776 - 789, 1972.

47. Heylen, A.E.D. and Lewis, T.J., Proc Roy Soc 271, 531 - 550, 1963.

48. Smit, J.A., Physica 3, 543 - 562, 1936.

49. Reder, F.H. and Brown, S.C., Phys Rev 95, 885 - 889, 1954.

50. Savchenko, V.N., Opt Spectrosc 30, 6 - 9, 1970.

51. Penkin, N.P. and Redko, T.P., Opt Spectrosc 23, 252 - 253, 1966.

52. Ochkur, V.I. and Petrun'kin, A.M., Opt Spectrosc 245 - 248, 1963.

53. Penkin, N.P. and Redko, T.P., Opt Spectrosc 23, 353 - 354, 1966.

54. Mitchell, A.C.G. and Zemansky, M.W., Resonance Radiation and Excited Atoms, Cambridge : University Press, 1961.

55. Kelly, F.M. and Tomchuk, E., Proc Phys Soc 74, 689 - 692, 1959.

56. Phelps, A.V., Phys Rev 99, 1307 - 1313, 1955.

57. Aleskovskii, Yu M, Sov Phys JETP 17, 570 - 575, 1963.

58. Harrison, J.A., Proc Phys Soc 73, 841 - 848, 1959.

59. Mash, L.D.,Rabkin, B.M. and Rybakov, B.V., Sov Phys JETP Lett 13, 169 - 171, 1971.

60. Gibbs, R.C. and Kruger, P.G., Phys Rev 37, 1559 - 1561, 1931.

61. Kopfermann, H., Nuclear Moments (English version by Schneider, E.E.), Academic, New York, 1958.

62. Kuhn, H.G. and Ramsden, S.A., Proc Roy Soc A237, 485 - 495, 1956.

63. Kelly, F.M. and Tomchuk, E., Proc Phys Soc 78, 1304 - 1306, 1961.

64. Bishop, D.C. and King, W.H., J Phys B : Atom Molec Phys 4, 1798 - 1807, 1971.

65. Contreras, R.H. and Kelly, F.M., Canad J Phys 47, 1979 - 1982, 1969.

66. Carslaw, H.S. and Jaeger, J.C. Conduction of Heat in Solids, Clarendon, Oxford, 1959, Chapter XVIII.

67. Blaha, M., Astrophys J, 157, 473 - 477, 1969.

68. Baumann, S.R. and Smith, W.H., J Opt Soc Am, 60, 345 - 347, 1970.

69. Janossy, M., Itagi, V.V. and Csillag, L., Acta Phys Acad Sci Hung 32, 149 - 163, 1972.

70. Chanin, L.M., and Biondi, M.A., Phys Rev. 106, 473 - 479, 1957.

71. Fowler, R.G., Proc Phys Soc, 80, 620 - 625, 1962.

72. Glasstone, S., and Lovberg, R.H., Controlled Thermonuclear Reactions, Van Nostrand, Princeton, New Jersey, 1960.

73. Nielsen, R.H., Phys Rev, 50, 950 - 954, 1936.

74. Chanin and Biondi, M.A., Phys Rev. 107, 1219 - 1221, 1957.

75. Green, J.M. and Webb, C.E., J Phys B : Atom Molec Phys, 8, 1484 - 1500, 1975.